

MASTER

Natural Heat Column

A numerical study for optimizing cool thermal energy storage using groundwater as phase change material

Coppens, E.

Award date:
2019

[Link to publication](#)

Disclaimer

This document contains a student thesis (bachelor's or master's), as authored by a student at Eindhoven University of Technology. Student theses are made available in the TU/e repository upon obtaining the required degree. The grade received is not published on the document as presented in the repository. The required complexity or quality of research of student theses may vary by program, and the required minimum study period may vary in duration.

General rights

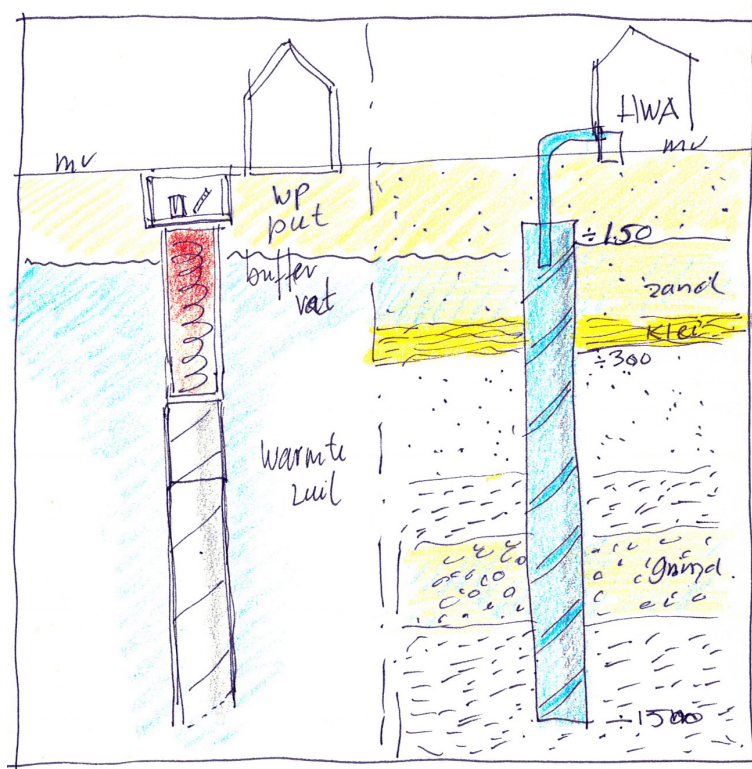
Copyright and moral rights for the publications made accessible in the public portal are retained by the authors and/or other copyright owners and it is a condition of accessing publications that users recognise and abide by the legal requirements associated with these rights.

- Users may download and print one copy of any publication from the public portal for the purpose of private study or research.
- You may not further distribute the material or use it for any profit-making activity or commercial gain

Natural Heat Column

A numerical study for optimizing cool thermal energy storage using groundwater as phase change material

Master Thesis



Natural Heat Column

A numerical study for optimizing cool thermal energy storage using
groundwater as phase change material

Master Thesis

Author	E. Coppens
IDNR	0909263
Version	3.0
Research framework	Graduation Project (4SE40)
Study	Sustainable Energy Technology
Faculty	Energy Technology — Mechanical Engineering
Tutoring	dr.ir. M.F.M. Speetjens — Eindhoven University of Technology ir. J.E.M. van Herpt — Solevo
Publication	December 2018, Eindhoven

Abstract

Natural Heat Column

A numerical study for optimizing cool thermal energy storage using groundwater as phase change material

Author E. Coppens

Tutoring dr.ir. M.F.M. Speetjens — Eindhoven University of Technology

ir. J.E.M. van Herpt — Solevo

Publication December 2018, Eindhoven

In the next decades, there will be two major challenges to overcome in the field of energy technology. The first challenge is limiting the use of fossil fuels which are running out. The second challenge is to reduce the high emission levels of carbon dioxide which is one of the major greenhouse gasses. To prevent climate change, the Ministry of Economic Affairs has published the energy agenda. This agenda presents plans for the energy transition in the Netherlands until the year 2050. One of the important pillars of this transition is the large reduction of natural gas usage. In the near future, new houses will not have a connection to the natural gas network. One of the most suitable sustainable energy sources to accomplish this is the natural heat column. This thesis will give an answer to: What is the optimal configuration of a natural heat column and how can this be analyzed with CFD?

The natural heat column is a ground source heat pump system which cools the groundwater below freeze point. Because melting ice takes as much energy as heating water from 0°C to 80°C , the specific energy is high. Therefore, a significant ground area can be saved in the built environment.

The advantage of the natural heat column is that it requires less ground volume in compare to a traditional sensible heat pump system. The disadvantage is that it uses more electrical power to drive the heat pump compressor compared to the sensible heat pump. Research shows that the advantages are significantly higher than the disadvantage. Finally, it is stated that the groundwater flow is equal to zero. By assuming this, the number of calculations is reduced significantly.

The natural heat column is with Comsol Multiphysics analyzed for water and soil surroundings. Due to the good insulating effect of frozen ground, almost no heat is being transferred to the soil. For all interfaces, the heat flux is halved within the first seven minutes of the simulation. Due to this, the glycol return temperature is 90% of its initial temperature within one day. After this, almost no heat was transferred. Here, it can be concluded that the natural heat column is not suitable for seasonal storage.

When shifting the scope of the research to daily storage with active regeneration. The glycol return temperature is strongly dependent on the inlet conditions. The morning peak generates between 0.22m^3 and 0.35m^3 of ice, in the evening this is between 0.19m^3 and 0.35m^3 . When the ice, during the afternoon, is melted by solar collectors, the optimal area of the collectors is 17m^2 . Of this area is 15.76m^2 is needed to warm the house when the natural heat column is regenerating. Furthermore, research shows that a length of six meters is sufficient for daily storage. Finally, the minimum distance for placing two columns on top of each other is four meters. The minimum distance for placing two columns next to each other is five meters. Here, the required ground circumference is far less compared to an average house in the Netherlands. In general, the results for daily storage are acceptable and the configuration is technically feasible.

Finally, with an investment cost of €30 000 and a total interest rate of 11.53%, the return on investment is larger than 100 years. When the return on investment is 100 years, the internal rate of return would be 1.63% per year. When only inflation is taken into account, the return on investment is 83 years. If there is no interest rate taken into account the payback period is 49 years. When considering the risks over the years, these return on investments can be considered high.

Based on this data, it is concluded that the concept of the natural heat column has a high potential. However, seasonal storage is not feasible. The technical results for daily storage are acceptable. To succeed in this project, the natural heat column has to be subsidized and executed by a non-governmental organization, which does not want to make a profit, but only compensates for the inflation.

Preface

In front of you lies the graduation thesis commissioned by the Eindhoven, University of Technology and written by Erik Coppens, graduating master student sustainable energy technology of the Eindhoven, University of Technology. This thesis elaborates on a numerical study for optimizing cool thermal energy storage using groundwater as phase change material.

This thesis stands not only for the graduation project itself, it also stands for the closure of my time as a student, which lasted for almost a decade. Through this way I want to thank everyone who has helped me come where I am standing today: my internship companies: Philip Morris and SUEZ ReEnergy, the GREiA institute in Lleida, who helped me studying abroad and the HZ, University of Applied Sciences and the Eindhoven, University of Technology who guided me to my bachelor and master degree.

For this thesis, I would thank everyone who helped contributing to it: the graduation commission, my friends who reviewed the thesis many times, and many others. A special thanks to my thesis supervisors: dr.ir. Michel Speetjens and ir. Jan van Herpt. Without their technical knowledge and feedback during the writing process, I would never have succeeded with this thesis as well as I did right now. I am very thankful for their time and energy.

Finally, I would like to thank my family and friends who helped me with my thesis and made sure I had enough time to relax when I was not working on my thesis. Lastly, I would like to especially thank my parents. Without their support and belief through all these years, I would never have come this far as I am now.

Erik Coppens
17 December 2018
Eindhoven

Nomenclature

Abbreviation

r^2	Coefficient of determination
APX	Amsterdam Power Exchange
CAPEX	CAPital EXpenditure
CFD	Computational Fluid Dynamics
COP	Coefficient of Performance
CTES	Cool Thermal Energy Storage
FDM	Finite Difference Method
FEM	Finite Element Method
FVM	Finite Volume Method
GSHPS	Ground Source Heat Pump Systems
LHV	Lower Heating Value
MCS	Mesh Convergence Study
NPV	Net Present Value
OPEX	OPERating EXpenditure
PCM	Phase Change Material
PV	Photovoltaic
TRT	Thermal Response Test

Dimensionless numbers

Eu	Euler number	$Eu = \frac{p}{\rho v^2}$
Pe	Péclet number	$Pe = Re \cdot Pr = \frac{\rho c_p v L}{k}$
Pr	Prandtl number	$Pr = \frac{c_p \mu}{k}$
Re	Reynolds number	$Re = \frac{\rho v L}{\mu}$

Latin

\bar{y}	average value of the known value	
A	Area	m^2
a	$\varphi \rho (\alpha_\infty - 1)$	N/m^3
b	$\frac{\mu \varphi^2}{k_0}$	N/m^3
c_p	Specific heat	J/kgK

d_{wall}	Wall thickness	m
E	Energy	J
e	Specific energy	J/kg
E_e	Average solar radiation	J/m^2
F	Force	N
$F(t, x)$	Function	
f_i	value of the trend line on position i	
F_s	Surface force	N
F_V	Volume force	N
f_{load}	Intermittency load fraction	
g	Gravitational acceleration	m/s^2
$G(t, x)$	Function	
H	Enthalpy	J
h	Specific enthalpy	kJ/kg
H_f	Heat of fusion	kJ/kg
i	Interest rate	
i	Node	
k	Thermal conductivity coefficient	W/mK
k_0	Permeability	m^2
L	Characteristic length	m
l	length	m
m	Mass flow	kg/s
n	Normal vector	
P	Power	W
p	Inflation rate	
p	Pressure	bar, Pa
Q	Heat	W
q	Flux	$m/smW/m^2$
q_0	Heat flux	W/m^2
R	Specific gas constant	J/kgK
R	Thermal resistance	K/W
r	Radius	m
r	Real rate	
R, R'	Inner, outer radius	m
T	Temperature	$^{\circ}C, K$
t	Time	s

U	Internal energy	J
U	Overall heat transfer coefficient	W/m^2K
V	Volume	m^3
v	Velocity	m/s
W	Work	W
w	Velocity	m/s
x	Distance	m
x	Vapor contents	
y	Height	m
y_i	known value on position i	

Greek

α	$-\frac{\varphi_m c_p (1 - e^{-\frac{UA}{m c_p}})}{\rho h_f}$	m^3/sK
α	Thermal diffusivity	m^2/s
α_∞	Tortuosity	
α_m	Phase transition between phase 1 and phase 2	
Δ	Difference	
η	Efficiency	
γ	Surface tension	N/m
\mathcal{O}	Order	
μ	Dynamic viscosity	$Pa \cdot s$
∇	Gradient $(\frac{\partial}{\partial x} + \frac{\partial}{\partial y} + \frac{\partial}{\partial z})$ or $(\frac{\partial}{\partial r} + \frac{1}{r} \frac{\partial}{\partial \varphi} + \frac{\partial}{\partial z})$	
ρ	Density	kg/m^3
θ	Liquid mass fraction	
φ	Porosity	

Compass rose

C	Center
E	East
N	North
NE	North-East
NW	North-West
S	South
SE	South-East
SW	South-West
W	West

Contents

1	Introduction	1
1.1	Overview sustainable energy sources	1
1.1.1	Photovoltaic cells	1
1.1.2	Underground thermal energy storage	1
1.1.3	Ice storage	3
1.1.4	Natural heat column	4
1.2	Problem definition	6
2	Problem configuration	7
2.1	Domestic data	7
2.2	Geometric data	9
3	Methodology	12
3.1	Conservation of mass	12
3.2	Conservation of momentum	13
3.2.1	Dimensionless form	13
3.2.2	Porous medium	13
3.3	Conservation of energy	15
3.3.1	Dimensionless form	15
3.3.2	Porous medium	16
3.4	Initial and boundary conditions	16
3.5	Physical properties	17
4	Numerical methods	20
4.1	Overview of numerical methods	20
4.2	Mesh convergence study	21
5	Thermodynamic analysis of the natural heat column	24
5.1	System definition	24
5.2	Heat pump definition	24
5.3	Thermodynamic model	24
5.4	Thermodynamic analysis	29
6	CFD-analysis 1: Natural heat column in water surrounding (seasonal storage)	31
6.1	Simulation results	31
6.1.1	Water temperature	31
6.1.2	Glycol return temperature	31
6.1.3	Heat flux	34
6.1.4	Ice volume	34
6.1.5	Ice layer thickness	37
7	CFD-analysis 2: Natural heat column in soil surrounding (seasonal storage)	38
7.1	Simulation results	38
7.1.1	Soil temperature	38
7.1.2	Glycol return temperature	39
7.1.3	Heat flux	41
7.1.4	Frozen ground volume	43
7.1.5	Frozen ground layer thickness	43

7.2	Optimization	46
7.2.1	Parametric study inlet temperature	47
7.2.2	Parametric study glycol mass flow	47
7.2.3	Minimum required area	50
7.2.4	Trace heating	51
8	CFD-analysis 3: Natural heat column with active regeneration (daily storage)	52
8.1	Simulation results	54
8.1.1	Boundary heat flux	55
8.1.2	Soil temperature	55
8.1.3	Glycol return temperature	56
8.1.4	Heat flux	58
8.1.5	Frozen ground volume	58
8.1.6	Frozen ground layer thickness and height	59
8.2	Optimization	61
8.2.1	Parametric study inlet temperature	61
8.2.2	Parametric study mass flow	63
8.2.3	Parametric study regeneration	64
8.2.4	Minimum required area	65
9	Business Case	66
9.1	Alternatives	66
9.2	Advantages	66
9.3	Risks	66
9.4	Cashflow	67
9.5	Project plan	67
9.6	Investment	68
9.7	Scenario 2	69
10	Conclusion and recommendations	70
10.1	Conclusion	70
10.2	Recommendations	72
	Bibliography	73
A	TU/e code of scientific conduct	75
B	Cause-consequence analysis of background	79
C	Derivation equation ice melting due to thermal losses	81
D	Temperature distribution CFD-analysis 1	82
E	Derivation equation ice growing	87
F	Mesh convergence study CFD-analysis 2	89
G	Temperature distribution CFD-analysis 2	91
H	Derivation parametric study glycol mass flow	96
I	Mesh convergence study CFD-analysis 3	97
J	Temperature distribution CFD-analysis 3	99
K	Temperature distribution CFD-analysis 3 (detailed)	104
L	Derivation cylinder height	109

Chapter 1

Introduction

1.1 Overview sustainable energy sources

In the next decades, there will be two major challenges to overcome in the field of energy technology. The first challenge is limiting the use of fossil fuels which are running out. The second challenge is to reduce the high emission levels of carbon dioxide which is one of the major greenhouse gasses. To prevent climate change, 195 countries have signed the Paris Agreement in December 2015. In which governments agreed that the increase in the global average temperature should stay below 2°C [1]. To execute this plan in the Netherlands, the Ministry of Economic Affairs has published the energy agenda [2]. This agenda presents plans for the energy transition in the Netherlands until the year 2050. One of the important pillars of this transition is the large reduction of natural gas usage. In the near future, new houses will not have a connection to the natural gas network. Furthermore, local governments are investigating the possibilities to modify households to zero natural gas households. The expected CO₂ reduction of this measure is represented in Figure 1.1 [2]. In this first chapter, different sustainable energy sources will be discussed, to see if they are suitable to accomplish the plans in the energy agenda. Here will be concluded that the natural heat column has the highest potential, however, more research to this has to be done. In Section 1.2 the problem definition to this research will be elaborated.

1.1.1 Photovoltaic cells

A sustainable alternative for natural gas is solar energy. Solar energy is easy to adapt in the built environment and it is not causing global warming. However, the downside of this is that silicon photovoltaic (PV) cells have a maximum efficiency of 31%. The rest of the energy is lost due to fundamental recombination (13%) and spectral mismatch (56%) [3]. Because of its low efficiency, a better alternative is to use thermal solar collectors. For a black absorber, the theoretical efficiency is 100%. In reality, the efficiency is around 40% for hot tap water and up to 70% for low heat purposes (e.g. heat pumps) [4]. The different costs, efficiency and payback period of the PV cells are shown in Table 1.1 [4]. Due to its low efficiency, PV cells alone are not the ideal solution to reach the Paris Agreement.

1.1.2 Underground thermal energy storage

The energy agenda states that the Dutch government is committed to strongly decrease the heat demand of households by requiring houses to have a minimum energy label. Furthermore, the Dutch government is obligated to subsidize energy-saving measures [2]. A second sustainable alternative which could contribute to reach the challenges stated in the energy agenda is underground thermal energy

Table 1.1: Development of important characteristic data for PV cells in the Dutch climate

	1980	2007	2015	2030	Long term
Costs complete system in $\text{€}/W_p$ (excl. tax)	>30	5	2.5	1	0.5
Production costs electricity in $\text{€}/\text{kWh}$ (2007)	>3	0.50	0.25	0.10	0.05
Typical efficiency commercial module	<8%	15%	20%	25%	40%
Energy payback time in year (complete system)	>10	3	1.5	<1	<0.5

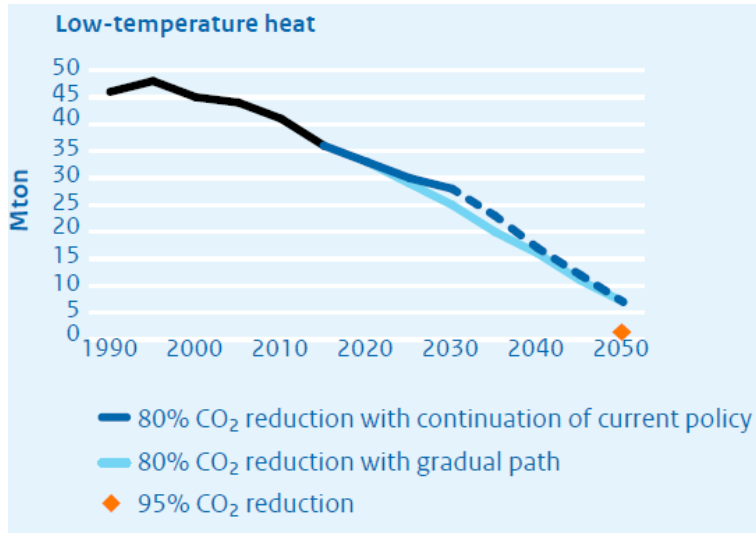


Figure 1.1: Transition of CO₂ reduction

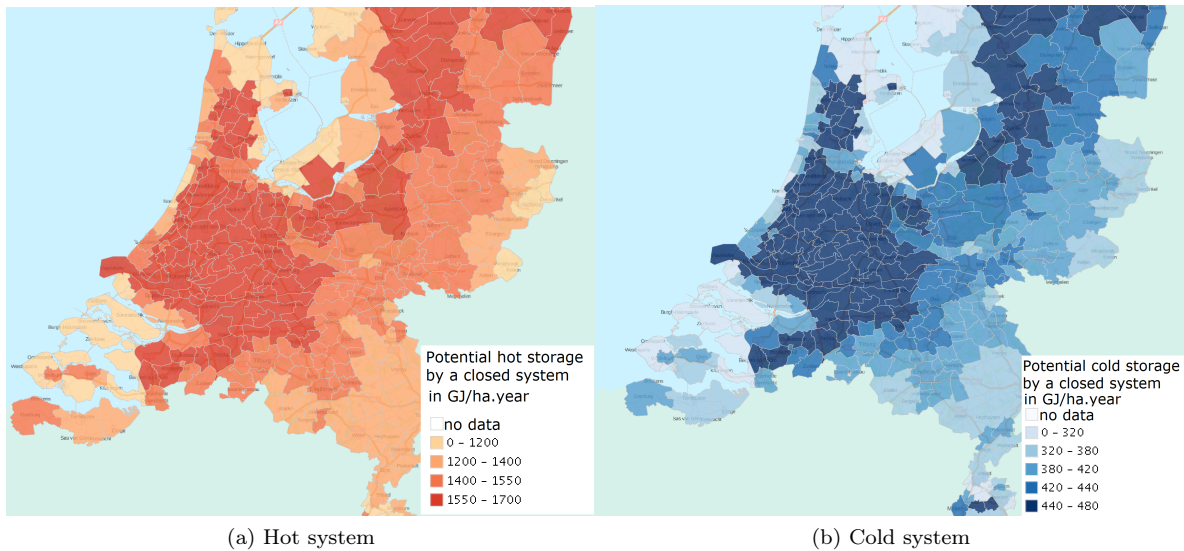


Figure 1.2: Potential annual storage by a closed system in GJ/ha

storage (UTES). Here, houses in the Netherlands can be cooled in the summer months and heated in the winter months by a small heat pump. This in contrast with an electrical system where only heating is possible. Figure 1.2 shows the potential of seasonal storage in the Netherlands is high, especially the west [5]. A large disadvantage of UTES is the depth of the system. There it can be considered that the minimum depth of such system is fifty meters. Here, the following threats could happen [6]:

- Short circuit of water layers
- Temperature changes in soil
- Groundwater height changes
- Soil fouling with chemicals

Although UTES systems have a high potential to reach the challenges in the energy agenda, however, due to the threats, this system has significant uncertainties.

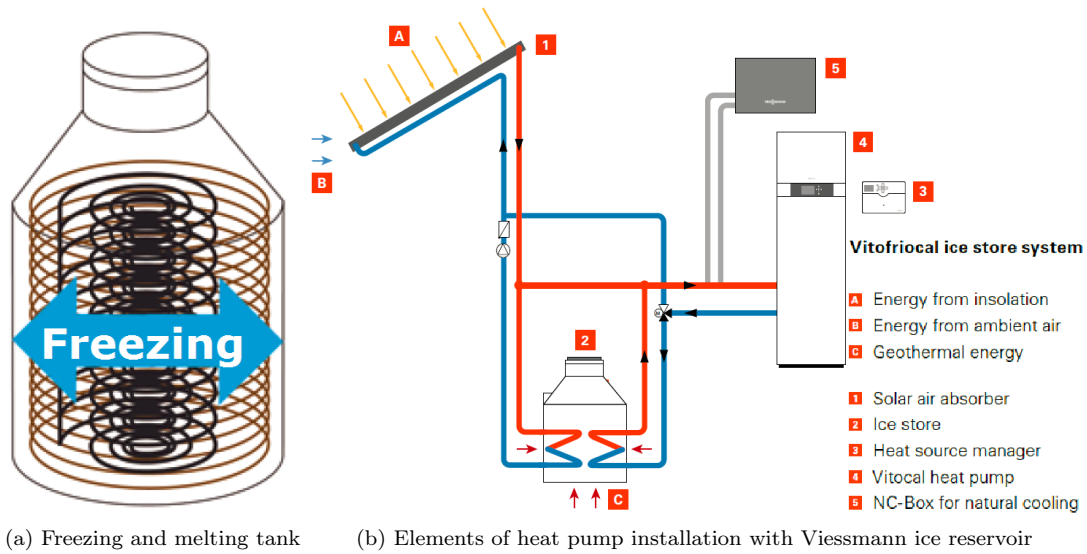


Figure 1.3: Viessmann ice storage system

1.1.3 Ice storage

Although modern houses are well insulated nowadays, the space in a typical Dutch house for generating its own sustainable energy is limited. A solution to this problem is to store energy in ice. Due to the high latent heat capacity of ice, a large amount of heat in a small temperature range: the latent heat of ice is equal to the energy of heating water from 0°C to 80°C . Furthermore, the thermal conductivity of ice is relatively high compared to other inorganic phase change materials (PCM). In general, the use of PCM is extremely suitable for seasonal storage. In a simple example, as will be mentioned in Chapter 5, is assumed that ice in the winter is used to heat a building (from 5°C to 20°C). With the use of the heat pump, heat is extracted from the system and the water will freeze. During the summer months, the ice is used to cool the building (from 30°C to 20°C). In a balanced system, the ice will melt in the summer as much as it grows during the winter months. As mentioned before, ice PCM is very compact, therefore the disadvantages of the deep boreholes are not necessary here.

A practical example of seasonal ice storage is the ice storage system of Viessmann B.V. This system uses two 20 kW ice reservoirs of 2.5 meter in diameter and 3.56 meter in height. A visual representation of the reservoirs can be found in Figure 1.3 a. As seen in Figure 1.3 b, the system can be connected to a thermal solar collector. Besides generating extra heat, it can regenerate the ice when the system is not demanding energy, as will be discussed later on in Chapter 5. This total system could replace 120 liters of oil and the different components are well coordinated by a smart controlled system [7].

Although the ice storage system of Viessmann is a new concept cool thermal energy storage (CTES) plays a significant role in demand-side managing for many years. There are three main classifications for CTES: sensible (chilled water storage), latent (ice storage) and thermal chemical (eutectic salt storage). The main disadvantage of chilled water storage is that it needs a large storage tank to meet the demand. The advantage of this is that, due to stratification, water with different temperatures can be extracted. In general, chilled water systems are used for seasonal storage. Ice storage systems have a significantly smaller storage tank. By using the latent heat, water is transferred to ice. In most cases, this is done by feeding the storage tank with a glycol or brine solution, typically 3°C to 5°C below zero [8]. Although research has shown that an ice storage air conditioning could save 55% of the electricity costs [9], the majority of these systems do not reach this amount of savings due to improper design. Oversized and undersized chillers, as well as a poor choice of the storage tank, are the main results of high costs. Therefore, designing an ice reservoir air conditioning system should be done with care [10]. Another advantage of ice reservoir air conditioning is that it plays an important role in demand-side managing. Ice storing not only saves significant operational costs, it also maintains the balance in the national electricity grid [11]. Eutectic salt storage systems have the advantage that the energy density is five times higher compared to latent storage and even ten times higher energy density compared to latent storage [12]. However, these systems are too expensive to adapt in practice.

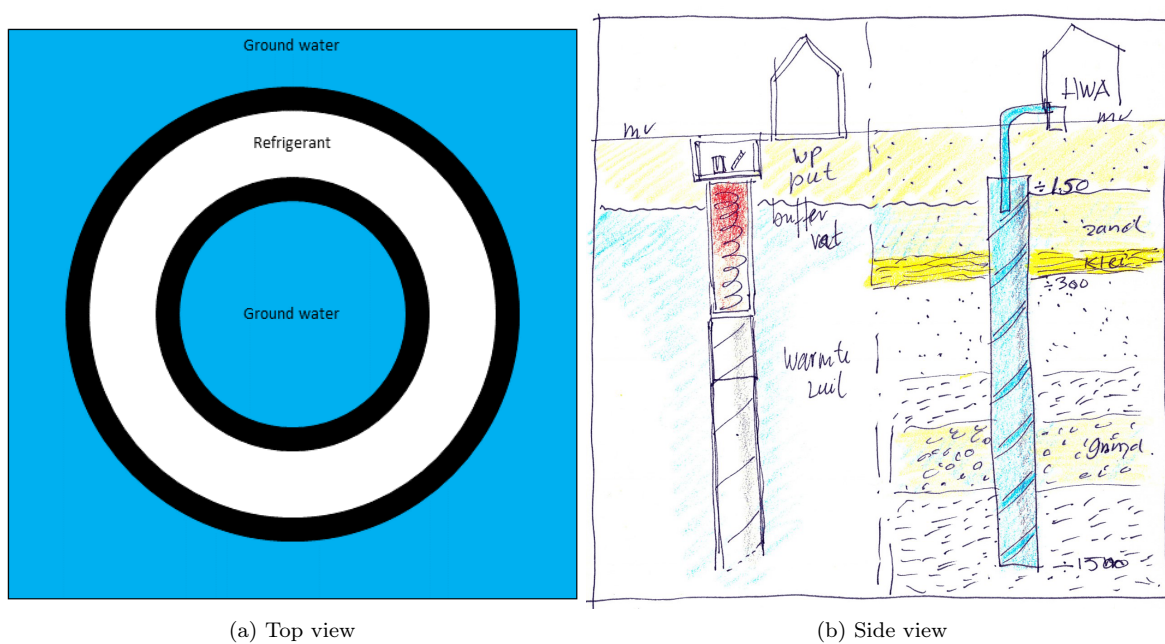


Figure 1.4: Visual representation of a natural heat column

1.1.4 Natural heat column

The big advantage of the ice storage system is that it is a simple proven technique which can save a significant amount of money. The disadvantage is the volume: the reservoir is partly built above the ground (which requires a significant amount of space) and partly underground (which results in a cost barrier for digging). To avoid this disadvantage, Solevo has developed the natural heat column. The natural heat column is a hollow cylinder which transfers its heat through the wall to the groundwater (see Figure 1.4 a). As a result, the installation costs of digging and required area are significantly reduced. On top of the natural heat column, a heat pump is placed, which is located below ground level in the garden. This is graphically shown in Figure 1.4 b. A natural heat column has a typical length of three meters and is with a price of €30 000 sufficient enough to realize a net natural gas energy household [13]. Although this technique seems promising, further analysis is necessary to verify the natural heat column technically. This will be done in this thesis. In Appendix B is a cause-consequence analysis executed for this problem definition.

Although the natural heat column is a new concept, other ground source heat pump systems (GSHPs) are becoming more popular for the heating and cooling of buildings. A typical GSHPs is represented in Figure 1.5, which shows a U-shaped borehole freezing the groundwater [14]. When GSHPs are used to freeze the ground, as in the case of the natural heat column, complex effects will occur. The downside of freezing the ground is that the soil will expand and could cause damage to the system. Furthermore, freezing groundwater has numerous hydrogeological and biological effects. Predicting the freezing and melting of the water process in the pores in interaction with the groundwater is, however, a difficult process, and the mathematical models need to be of a high standard to calculate this [15].

The first mathematical model was developed in 1988 by Lunardini [16]. In this model is suggested to split the frozen soil problem into three regions and solve each region one dimensional. In the first region the soil contains water and ice and there is no phase change. In the second region the soil contains water and ice, however, there is a phase change. Finally, there is the thawed zone. Although there are no analytical solutions for this problem, Lunardini developed a model to solve this problem numerically.

Afterwards, this model is improved along others. For example, in 2007 McKenzie used the three-dimensional program SUTRA-ICE [17], which is developed by the United States Geological Survey, to evaluate the temperature in a large peat bog [15]. Although SUTRA-ICE provided accurate results, which were validated against other data, it seems that the model applied numerous simplifications and is therefore not suitable for complex systems.

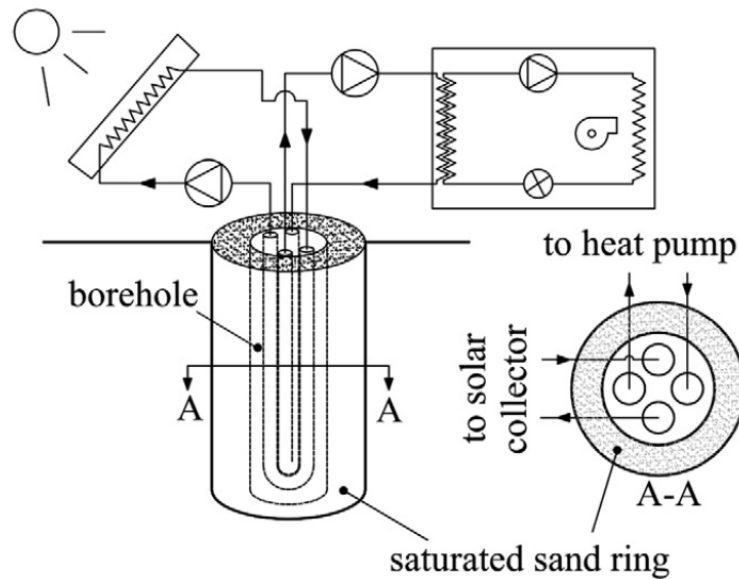


Figure 1.5: System configuration for a ground source heat pump system

In 2007 the computer program FEFLOW (Finite Element subsurface FLOW system) became available [18]. FEFLOW is a program for simulating groundwater flow, mass transfer and heat transfer in a porous media. The program uses finite element analysis to solve the equations for different scenarios. The program is in development since 1979 by the institute for water resources planning and systems research Inc. of Berlin. FEFLOW is used by many researchers and its results are considered accurate.

When operating below freezing point, the GSHPS can be compressed by freezing soil. This pipe deformation will not only shorten the service life of the system but also influence the system efficiency and safety. One of the first investigations of the damage done to the ground in combination with GSHPS was done by Wang in 2013 [19]. Wang performed experiments and concluded that when using a U-shaped borehole pipe, the soil will freeze asymmetrically. This will lead to a decrease in the lifetime for the GSHPS. Furthermore, Wang concluded that in a ground layer with a finer material the freezing process will be faster than in a ground layer with a courser material.

In 2013, using these experiments, Yang developed a one-dimensional mathematical model with phase change to simulate the heat transferred in the soil around the boreholes [20]. The method which was used is called the backward calculating time step method. This resulted in the same conclusions as Wang has found.

In 2016 Zheng used the scientific open-source software OpenGeosys [21] to investigate the heat pump efficiency in relation to the outlet temperature when groundwater and the surrounding soil is frozen [22]. This was done by comparing two boreholes with different lengths for a single household in the northern part of Europe. The simulation revealed that a longer borehole resulted in a higher heat pump efficiency. However, this does not always lead to better financial performances. For this investigation, the optimal financial diameter was 86 meters, although this is very location dependent.

Lastly, an important side effect of the GSHPS are the high initial costs. In order to not overestimate the borehole diameter, pipe size, and configuration, the soil thermal conductivity, and borehole thermal resistance need to be determined carefully. When there is a 10% error in the soil thermal conductivity, calculations show a 4.5% to 5.8% error in the design of the system [23]. These thermal properties are measured with a thermal response test (TRT) (see Figure 1.6) [24]. In this test, a borehole heat exchanger is inserted and heating fluid is circulated through a heat exchanger.

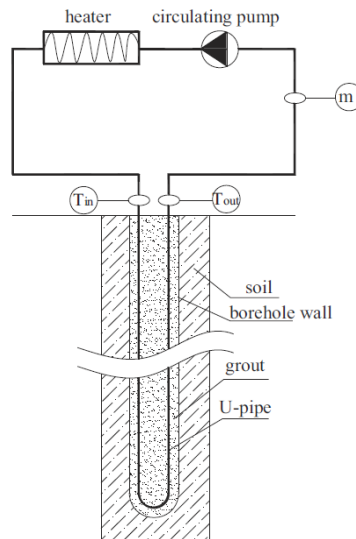


Figure 1.6: Typical borehole test setup

1.2 Problem definition

The main question of this thesis will be: What is the optimal configuration of a natural heat column in different types of ground and how can this be analyzed with Computational Fluid Dynamics (CFD)?

For this main question, the following subquestions are defined:

1. Which type of household needs to be simulated?
2. What is the structure of the ground and what type of effect has this on the natural heat column?
3. How does a thermal solar collector effect the system?
4. What is the minimum required space of the natural heat column?
5. What is the effect of multiple sources on top of each other?
6. What is the return on investment of the natural heat column?

After this introduction, the problem definition and its configuration will be elaborated in Chapter 2. In Chapter 3 will the methodology be discussed and in Chapter 4 the numerical methods. The results of the different analyses, as described in the subquestions are evaluated and discussed in Chapter 5 until 8. In Chapter 9 the different analyses are economically evaluated by a business case. Finally, the conclusion can be found in Chapter 10. As requested by the TU/e, the scientific code of conduct is added to this thesis and it can be found in Appendix A.

Chapter 2

Problem configuration

This chapter will elaborate on Section 1.2 and will define the problem definition more specific. To do this the domestic data of the Netherlands will be analyzed first. When the house data, types of ground and energy consumption are known, a definition can be made of the simulation parameters. In the second part of this chapter, the proper geometry for simulating will be defined. This simulation will be close to reality, but still, have an acceptable computational time for solving.

2.1 Domestic data

To decide what the initial parameters of the simulation are, the domestic data of the Netherlands is investigated. Figure 2.1[25] shows that most people in the Netherlands live in a terraced house, which is built in the second part of the 20th century and is owned by its occupants. The average Dutch house has four to five rooms, and the usable area of the house is between fifty and a hundred square meters (incl. garden). An average terrace house consumes $1500m^3$ natural gas on annual basis, which cost €100 a month[26]. Based on the average of four to five rooms per house, it can be assumed that the household consists of four occupants. This will result in an average electricity usage of $4155kWh$ on annual basis, which will cost around €67 a month [26].

When investigating the soils in the Netherlands, there are four main categories: bog ground, sand ground, clay ground, and loam ground (see Figure 2.2). Because these types of ground are mixtures, only the substances of types of ground are simulated, namely: sand, clay, silt, and gravel. The physical properties of these types of ground can be found in Table 2.1, note that the thermal diffusivity is equal to $\alpha = \frac{k}{\rho c_p}$ [27] [28]. Finally, it is assumed that on annually base, the natural heat column is used to cool the house for six months and heat the house the other six months. This will be done for eight hours per day.

Table 2.1: Physical properties of the soil

	Gravel	Sand	Silt	Clay
Density (kg/m^3)	1950	1950	1500	1500
Thermal conductivity (W/mK)	2.0	2.0	1.5	1.5
Specific heat (J/kgK)	1045	1045	2085	2085
Thermal diffusivity (m^2/s)	9.81e-7	9.81e-7	4.80e-7	4.80e-7
Porosity (%)	32.5	37.5	42.5	55.0



Figure 2.1

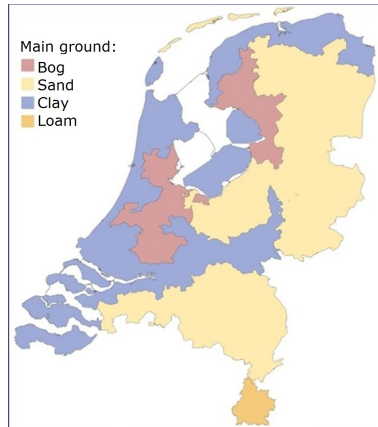
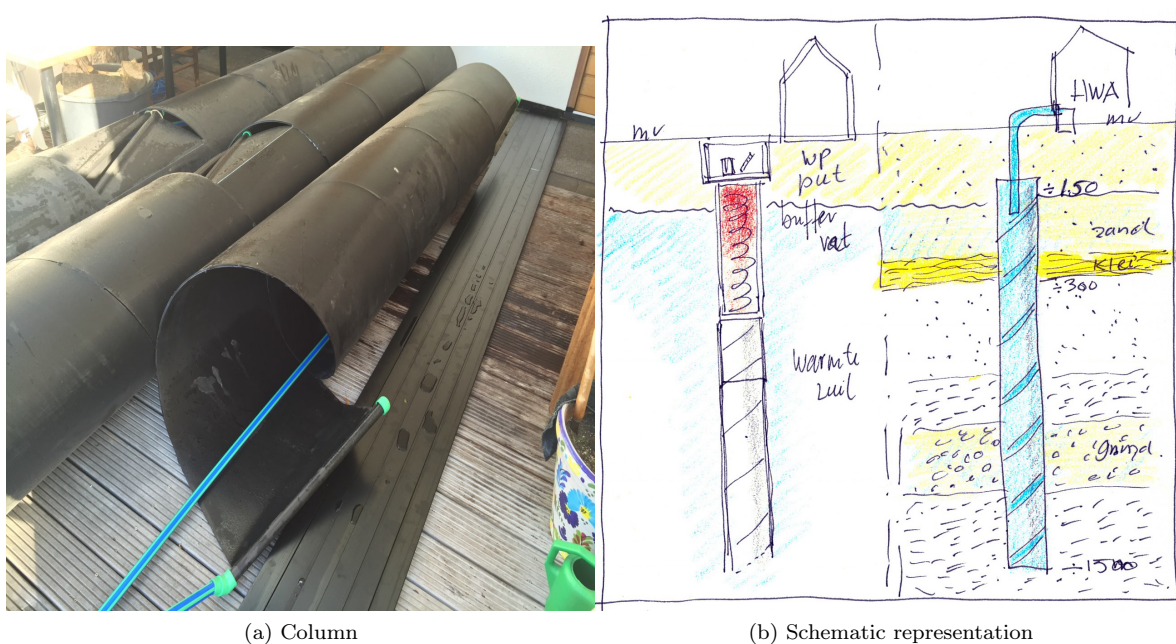


Figure 2.2: Schematic representation of the ground types in the Netherlands



(a) Column

(b) Schematic representation

Figure 2.3: Original design of the natural heat column

2.2 Geometric data

When performing a CFD-analysis, it is important to choose an optimal geometry. This geometry must have an acceptable computational time for solving the analysis, while still it must be close to reality. The original geometry, as proposed by creator of the natural heat column, is shown in Figure 2.3. This geometry has to be translated to a geometry which is suitable for CFD-analysis. For example, the rotated channels inside the annulus, as shown in Figure 2.3 a, are an important part of the natural heat column. However, due to its complex geometry, this would give a large computational time. Therefore, the trade-off is made to simulate this channels as straight tubes.

This study initially decided to start with a three-dimensional geometry, where the connection pipes are placed in a so-called tube-in-tube configuration (see Figure 2.4). Here, the glycol enters the system by the 25mm diameter outer tube and flows into the cylinder through a distribution plate, which is placed ten meters below the surface on top of the cylinder. The cylinder itself is the main component of the natural heat column. Here, the glycol give its cold energy, through a 0.5mm thick wall, to the surroundings. The cylinder has the geometric shape of an annulus, with an outer radius of 0.26m and an inner radius of 0.255m. At the bottom of three meters long cylinder, a collection plate sends the glycol back, along the inner tube, outside the system.

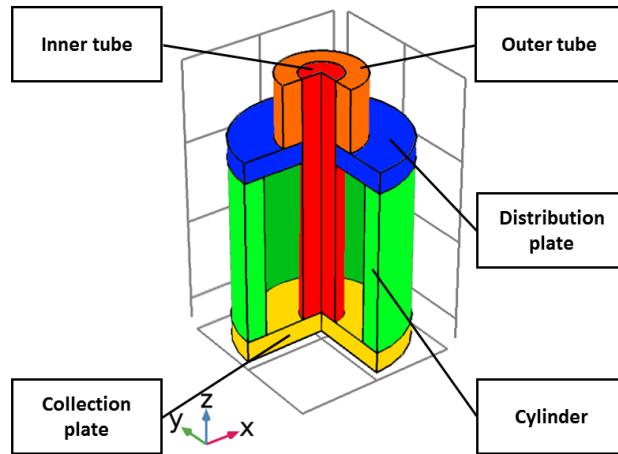


Figure 2.4: Schematic representation of the different components of the natural heat column

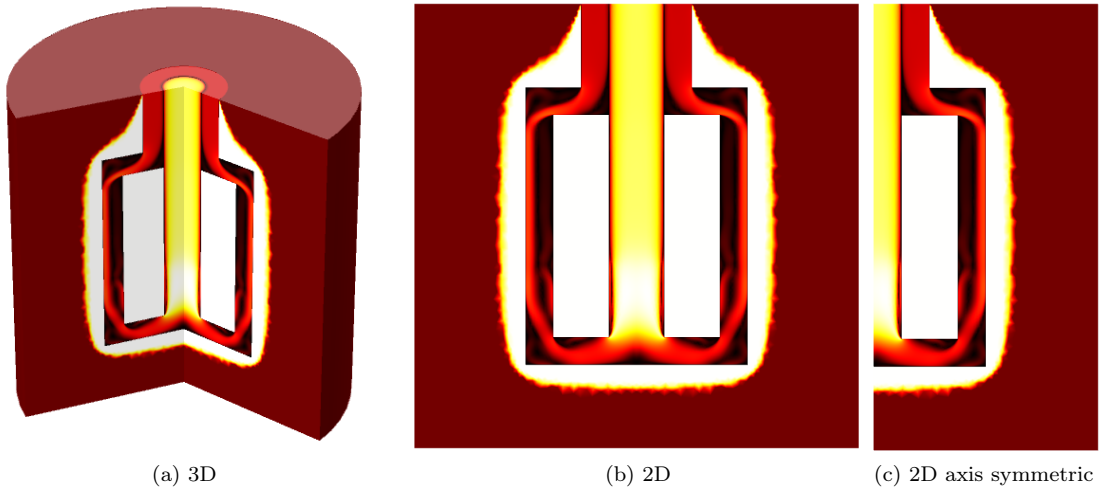


Figure 2.5: Overview of different dimensions geometry

When the geometry of Figure 2.4 would be solved with CFD-analysis. A possible solution can be found in Figure 2.5 a. Here, the glycol enters the outer tube as a Poiseuille flow. The flow is zero at the walls and in the middle of the tubes at its maximum. When the flow enters the cylinder, it starts giving its cold energy from the glycol interface, trough the wall, to the soil interface. This soil interface will freeze. In Figure 2.5 the white colored area represents frozen soil and the red area represent soil which is still containing groundwater. Because the geometry is for all rotation angles the same, there can be assumed that the simulation only variates in the r and z dimension. To save a significant amount of computational time, the geometry is modified from three-dimensional to two-dimensional, as shown in Figure 2.5 b. To reduce the computational time further, an axis-symmetrical line is added through the middle of the geometry. Here, the parameters left of the line are equal to the values right of this line. This final geometry is represented in Figure 2.5 c.

To investigate the geometry in more detail (see left side of Figure 2.6), the diameter of the connection pipes and the cylinder diameter where varied. Table 2.2 shows that simulating the natural heat column for one hour a large amount of computational time is needed. In this table case 1 represent pipes with a large diameter and case 10 represents the original pipes, with a small diameter. Although this geometry is close to reality, the computational time is far too large and needs to be reduced. The exact physics and data of this analysis will be elaborated later-on in this thesis.

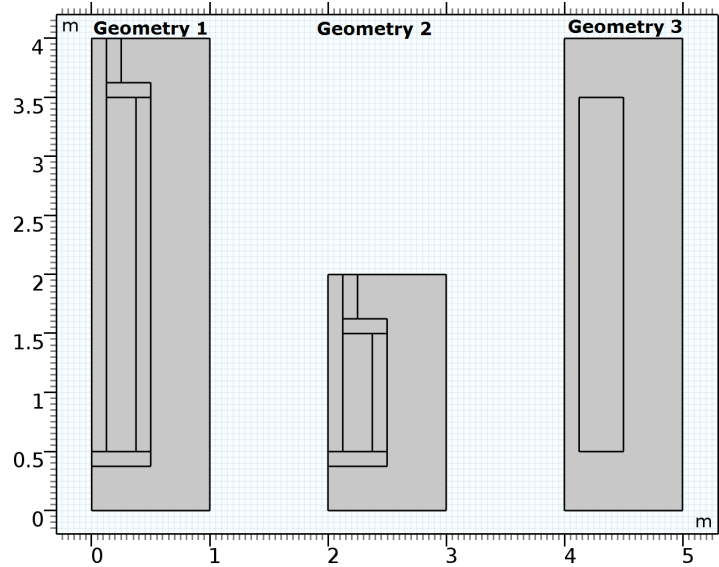


Figure 2.6: Overview of different analysis geometry

Table 2.2: Computational time in seconds of different geometries for simulating one hour

Case	Geometry 1	Geometry 2	Geometry 3
01	471	133	35
02	51 584	1120	87
03		227	56
04		522	45
05		1477	45
06		3249	51
07		6115	66
08		177 189	146
09			259
10			2021

To realize this, the height of the cylinder is decreased from three meters to one meter, as it can be seen in the middle of Figure 2.6. From Table 2.2 it can be concluded that for the cases with a large pipe diameter, the computational time is acceptable. However, when simulating the natural heat column for one hour with a geometry close to the reality the computational time almost equals fifty hours. Therefore, this geometry is not suitable for simulating as well.

The third geometry, located at the right side of Figure 2.6, is reduced to only the cylinder itself. Although this geometry is a very simplified version of the original model, the computational times in Table 2.2 show acceptable values for all cases. Despite this geometry is far from the original natural heat column, the heat is mostly transferred by the cylinder itself and the ice will only form at this place. With this conclusion and the acceptable computational times, the third geometry of Figure 2.6 is the geometry which is going to be investigated for the simulation.

The next chapter will define the physics that is applied to this geometry.

Chapter 3

Methodology

In the previous chapter, the problem configuration is explained. In this chapter, the methodology will be explained to solve the problem configuration. In the first three sections, the governing equations of mass, momentum and energy equations will be elaborated. Each of these equations will be solved to its dimensionless form and the equations will be rewritten for a porous medium. Making equations dimensionless is extremely helpful in analyzing a thermodynamic problem. When grouping variables into smaller numbers of dimensionless parameters, the analyzing work is considerably reduced [29]. When the governing equations are elaborated, the initial and boundary conditions, which make the problem specific for solving, will be discussed. Finally, the physical properties of the different materials which are used will be elaborated.

During this methodology there are two questions which will be answered during this thesis:

- What will be the refrigerant return temperature as a function over time?
- What will be the ice layer thickness after a period of a hundred days?

3.1 Conservation of mass

The first fundamental law of fluid mechanics is the conservation of mass. Simply saying, the conservation of mass is [29]:

$$\left\{ \begin{array}{c} \text{rate of mass} \\ \text{efflux from} \\ \text{control} \\ \text{volume} \end{array} \right\} - \left\{ \begin{array}{c} \text{rate of mass} \\ \text{flow into} \\ \text{control} \\ \text{volume} \end{array} \right\} + \left\{ \begin{array}{c} \text{rate of} \\ \text{accumulation} \\ \text{of mass within} \\ \text{control volume} \end{array} \right\} = 0 \quad (3.1)$$

This can be rewritten in the integral equation for the conservation of mass, which is defined as:

$$\frac{\partial}{\partial t} \iiint \rho dV + \iint \rho(\vec{v} \cdot \vec{n}) dA = 0 \quad (3.2)$$

When differentiating the conservation of mass, the equation becomes:

$$\nabla \cdot \rho \vec{v} + \frac{\partial \rho}{\partial t} = 0 \quad (3.3)$$

Furthermore, it is assumed that the fluid is incompressible, so:

$$\nabla \cdot \vec{v} = 0 \quad (3.4)$$

This equation is known as the so-called continuity equation (First derived by Leonhard Euler (1707 – 1783)). When substituting $\vec{v}^* = \vec{v}/v_\infty$ and $\nabla^* = L\nabla$ the conservation of mass can be rewritten in its dimensionless form, which is:

$$\nabla^* \cdot \vec{v}^* = 0 \quad (3.5)$$

3.2 Conservation of momentum

The second fundamental law of fluid mechanics is the conservation of momentum. Again, this law can simply be defined as [29]:

$$\left\{ \begin{array}{c} \text{sum of} \\ \text{forces acting} \\ \text{on control} \\ \text{volume} \end{array} \right\} = \left\{ \begin{array}{c} \text{rate of} \\ \text{momentum} \\ \text{out of control} \\ \text{volume} \end{array} \right\} - \left\{ \begin{array}{c} \text{rate of} \\ \text{momentum} \\ \text{into control} \\ \text{volume} \end{array} \right\} + \left\{ \begin{array}{c} \text{rate of} \\ \text{accumulation} \\ \text{of momentum} \\ \text{within control} \\ \text{volume} \end{array} \right\} \quad (3.6)$$

The deriving this equation further, the integral equation for the conservation of momentum is defined as:

$$\sum \vec{F} = \frac{\partial}{\partial t} \iiint \rho \vec{v} dV + \iint \rho \vec{v} (\vec{v} \cdot \vec{n}) dA \quad (3.7)$$

When differentiating the conservation of momentum, the equation becomes:

$$\rho \frac{\partial \vec{v}}{\partial t} + \rho \vec{v} \cdot \nabla \vec{v} = \mu \nabla^2 \vec{v} - \nabla p \quad (3.8)$$

This is the so-called Navier-Stokes equation (named after Claude-Louis Navier (1785 – 1836) and George Gabriel Stokes (1819 – 1903)).

3.2.1 Dimensionless form

When substituting $\vec{v}^* = \vec{v}/v_\infty$, $t^* = tv_\infty/L$, $\nabla^* = L\nabla$ and $\nabla^{2*} = L^2\nabla^2$. The dimensionless form of the Navier-Stokes equation is:

$$\left(\frac{\partial}{\partial t^*} + \vec{v}^* \cdot \nabla^* \right) \vec{v}^* = \frac{\mu}{L\rho v_\infty} \nabla^{2*} \vec{v}^* - \frac{\nabla^* p}{\rho v_\infty^2} \quad (3.9)$$

Introducing Reynolds number, which in this research has a typical value of 10^5 :

$$Re = \frac{\text{Inertial force}}{\text{Viscous force}} = \frac{Lv_\infty\rho}{\mu} \sim \frac{\mathcal{O}(-3) \cdot \mathcal{O}(-1) \cdot \mathcal{O}(3)}{\mathcal{O}(-6)} \sim \mathcal{O}(5) \quad (3.10)$$

Where L is the diameter of the column, and v_∞ the glycol inlet velocity.

Furthermore introducing Eulers number, which in this research has a typical value of 10^5 :

$$Eu = \frac{\text{Pressure force}}{\text{Inertial force}} = \frac{p}{\rho v_\infty^2} \sim \frac{\mathcal{O}(5)}{\mathcal{O}(3) \cdot 2\mathcal{O}(-1)} \sim \mathcal{O}(5) \quad (3.11)$$

Where p is the inlet pressure. The final form of the dimensionless Navier-Stokes equation becomes:

$$\left(\frac{\partial}{\partial t^*} + \vec{v}^* \cdot \nabla^* \right) \vec{v}^* = \frac{1}{Re} \nabla^{2*} \vec{v}^* - \nabla^* Eu \quad (3.12)$$

3.2.2 Porous medium

The momentum balance can be rewritten for a linearized porous medium. For the liquid the equation this is:

$$\varphi\rho_f \frac{\partial \vec{w}}{\partial t} = -\varphi\nabla p + F_s + F_V \quad (3.13)$$

In 1956, Biot assumed that the volume forces for the liquid are zero and the surface forces are equal to [30]:

$$F_s = b(\vec{v} - \vec{w}) + a \frac{\partial(\vec{v} - \vec{w})}{\partial t} \quad (3.14)$$

Where, \vec{v} is the velocity of the solid particles and \vec{w} the velocity of the liquid particles. Furthermore:

$$b = \frac{\mu\varphi^2}{k_0} \quad (3.15)$$

And

$$a = \varphi\rho(\alpha_\infty - 1) \quad (3.16)$$

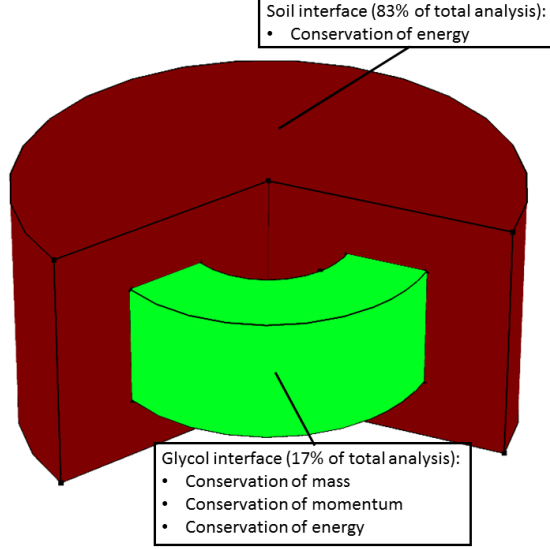


Figure 3.1: Schematic overview of interfaces

The equation becomes:

$$\varphi \rho_f \frac{\partial \vec{w}}{\partial t} = -\varphi \nabla p + \frac{\mu \varphi^2}{k_0} (\vec{v} - \vec{w}) + \varphi \rho (\alpha_\infty - 1) \frac{\partial (\vec{v} - \vec{w})}{\partial t} \quad (3.17)$$

Furthermore, it is assumed that the total system is stationary $\frac{\partial}{\partial t} = 0$ and that there is a rigid porous medium (the solid particles cannot change form shape ($\vec{v} = 0$)), therefore:

$$0 = -\varphi \nabla p - \frac{\mu \varphi^2}{k_0} \vec{w} \quad (3.18)$$

When knowing that a flux has a form of:

$$q = \varphi \vec{w} \quad (3.19)$$

The final equation becomes:

$$q = \varphi \vec{w} = -\frac{k_0}{\mu} \nabla p \quad (3.20)$$

This is the so-called Darcy equation, which is used to determine the groundwater fluid mechanics for a steady state, saturated porous medium [31]. The Darcy equation is firstly experimentally determined by Henry Darcy (1803 – 1858).

When the assumption is made that the main driver for the pressure difference is the capillary pressure, the Darcy equation becomes:

$$v = \frac{k_0}{\mu \Delta L} \frac{2\gamma}{r} = \frac{2k_0 \gamma \pi r}{V \mu} \quad (3.21)$$

The surface tension for water is $75.64 \cdot 10^{-3} N/m$ [32] and the viscosity is $1 \cdot 10^{-3} Pa \cdot s$. The permeability for very open gravel ground has a maximum value of $10^{-7} m^2$ [28]. Furthermore, when assuming that the pore radius is one millimeter and the volume of the ice is approximately three hundred cubic meters (see later-on in Chapter 5), the groundwater velocity is $1.58 \cdot 10^{-10} m/s = 0.014 mm/day$. Therefore, it is concluded that, in the rest of this thesis, the velocity of the groundwater in the soil is $0 m/s$.

This assumption not only implies that there is no movement in groundwater, but it also results in a huge saving of computational time. For the porous medium, which contains significantly more nodes compared to the glycol area, only the energy equation has to be calculated. Which means the number of calculations is significantly decreased. This is schematic represented in Figure 3.1

3.3 Conservation of energy

The third and last governing equation is the conservation of energy. This is simply defined as [29]:

$$\left\{ \begin{array}{l} \text{rate of addition} \\ \text{of heat to control} \\ \text{volume from} \\ \text{its surroundings} \end{array} \right\} - \left\{ \begin{array}{l} \text{rate of work done} \\ \text{by control volume} \\ \text{on its surroundings} \end{array} \right\} = \left\{ \begin{array}{l} \text{rate of energy} \\ \text{out of control} \\ \text{volume due to} \\ \text{fluid flow} \end{array} \right\} \quad (3.22)$$

$$- \left\{ \begin{array}{l} \text{rate of energy into} \\ \text{control volume due} \\ \text{to fluid flow} \end{array} \right\} + \left\{ \begin{array}{l} \text{rate of accumulation} \\ \text{of energy within} \\ \text{control volume} \end{array} \right\}$$

In the mathematical form, the integral equation for the conservation of energy is defined as:

$$\frac{\delta Q}{dt} - \frac{\delta W}{dt} = \frac{\partial}{\partial t} \iiint e \rho dV + \iint (e + \frac{p}{\rho})(\vec{v} \cdot \vec{n}) dA \quad (3.23)$$

In differential form this is:

$$\rho c_p \frac{\partial T}{\partial t} + \rho H_f \frac{\partial \alpha_m}{\partial T} \frac{\partial T}{\partial t} + \rho c_p \vec{v} \cdot \nabla T + \rho H_f \frac{\partial \alpha_m}{\partial T} \vec{v} \cdot \nabla T = \nabla \cdot k \nabla T \quad (3.24)$$

Where α_m represents the phase transition between phase one and phase two and is defined as:

$$\alpha_m = \frac{1(1-\theta)\rho_{ice} - \theta\rho_{water}}{2\theta\rho_{water} + (1-\theta)\rho_{ice}} \quad (3.25)$$

Where:

$$\theta = \frac{m - m_{ice}}{m_{water} - m_{ice}} \quad (3.26)$$

3.3.1 Dimensionless form

If: $\vec{v}^* = \vec{v}/v_\infty$, $t^* = tv_\infty/L$, $\nabla^* = L\nabla$, $H_f^* = c_p T/H_f$ and $T^* = \frac{T-T_0}{T_\infty-T_0}$. The dimensionless equation becomes:

$$\left(\frac{\partial}{\partial t^*} + \vec{v}^* \cdot \nabla^*\right)T^* + \frac{\partial \alpha_m}{\partial H_f^*} \left(\frac{\partial}{\partial t^*} + \vec{v}^* \cdot \nabla^*\right)T^* = \nabla^* \cdot \frac{k}{\rho c_p v_\infty L} \nabla^* T^* \quad (3.27)$$

Introducing Prandtl number, which in this research has a typical value of 10^{-2} :

$$Pr = \frac{\text{Momentum diffusivity}}{\text{Thermal diffusivity}} = \frac{\mu c_p}{k} \sim \frac{\mathcal{O}(-6) \cdot \mathcal{O}(3)}{\mathcal{O}(-1)} \sim \mathcal{O}(-2) \quad (3.28)$$

The dimensionless conservation of energy equation is:

$$\left(\frac{\partial}{\partial t^*} + \vec{v}^* \cdot \nabla^*\right)T^* + \frac{\partial \alpha_m}{\partial H_f^*} \left(\frac{\partial}{\partial t^*} + \vec{v}^* \cdot \nabla^*\right)T^* = \nabla^* \cdot \frac{1}{RePr} \nabla^* T^* \quad (3.29)$$

Which is sometimes written as:

$$\left(\frac{\partial}{\partial t^*} + \vec{v}^* \cdot \nabla^*\right)T^* + \frac{\partial \alpha_m}{\partial H_f^*} \left(\frac{\partial}{\partial t^*} + \vec{v}^* \cdot \nabla^*\right)T^* = \nabla^* \cdot \frac{1}{Pe} \nabla^* T^* \quad (3.30)$$

With the Péclet number, which has a typical value of 10^3 :

$$Pe = \frac{\text{Advective transport rate}}{\text{Diffusive transport rate}} = Re \cdot Pr = \frac{\rho c_p v_\infty L}{k} \sim \mathcal{O}(5) \cdot \mathcal{O}(-2) \sim \mathcal{O}(3) \quad (3.31)$$

This dimensionless form of the energy equation is valid in the general analysis. However, in the previous section is elaborated that the velocity in the soil interface is zero. Here, the reduced, dimensionless energy equation is:

$$\left(\frac{\partial}{\partial t^*} + \vec{v}^* \cdot \nabla^*\right)T^* + \frac{\partial \alpha_m}{\partial H_f^*} \left(\frac{\partial}{\partial t^*} + \vec{v}^* \cdot \nabla^*\right)T^* = \nabla^* \cdot \frac{1}{Pe} \nabla^* T^* \quad (3.32)$$

$$\frac{\partial T^*}{\partial t^*} + \frac{\partial \alpha_m}{\partial H_f^*} \frac{\partial T^*}{\partial t^*} = \nabla^* \cdot \frac{1}{Pe} \nabla^* T^* \quad (3.33)$$

3.3.2 Porous medium

As mentioned before, the energy equation for a porous medium is:

$$\rho(c_p + H_f \frac{\partial \alpha_m}{\partial T}) (\frac{\partial}{\partial t} + \vec{v} \cdot \nabla) T = \nabla \cdot k \nabla T \quad (3.34)$$

When splitting this for a solid part and a fluid part and assume a porous rigid ($\vec{v} = 0$), the energy equations for a porous medium are [33]:

$$(1 - \varphi) \rho_s c_{ps} \frac{\partial T}{\partial t} = \nabla \cdot (1 - \varphi) k_s \nabla T \quad (3.35)$$

And:

$$\varphi \rho_f (c_{pf} + H_f \frac{\partial \alpha_m}{\partial T}) \frac{\partial T}{\partial t} = \nabla \cdot \varphi k_f \nabla T \quad (3.36)$$

For the fluid energy equation the physical properties will be modified for the phase change, so:

$$\rho = \theta \rho_{water} + (1 - \theta) \rho_{ice} \quad (3.37)$$

$$c_p = \frac{1}{\rho} (\theta \rho_{water} c_{pwater} + (1 - \theta) \rho_{ice} c_{pice}) \quad (3.38)$$

$$k = \theta k_{water} + (1 - \theta) k_{ice} \quad (3.39)$$

3.4 Initial and boundary conditions

In the previous sections, the governing equations are discussed. These equations are valid for each heat and flow problem. Only when there are specific initial and boundary conditions applied to these governing equations, the problem can be solved for the natural heat column.

In Subsection 3.2.2 is stated that the groundwater flow inside the soil is equal to zero. Therefore, only the energy equation has to be solved for the soil. However, the conservation of mass and momentum needs to be solved for the glycol inside the cylinder. To avoid solving the mass and momentum equation for the soil interface, both interfaces are completely decoupled and it can be seen as two different simulations. The glycol interface inside the cylinder and the porous medium interface outside the cylinder are connected through the polypropylene wall. In the simulation, this wall is a numerical boundary condition of an ultra-thin wall with a finite thickness. Therefore, the wall can be approached to the linear correlation:

$$q = -k \frac{dT}{dx} = -k_{wall} \frac{T_{inside} - T_{outside}}{d_{wall}} \quad (3.40)$$

Here $T_{outside}$ is an external temperature, taken from outside the cylinder. The heat transfer problem outside the cylinder calculates the heat flux through this wall, by:

$$-\vec{n} \cdot \vec{q} = q_0 \quad (3.41)$$

This q is already known from the first equation. Furthermore, there is assumed that the wall has no slip, so the velocity at the wall is equal to zero. This is schematically represented in Figure 3.2.

In the initial condition is defined that the temperature of the soil is $15^\circ C$. The temperature of the refrigerant is at the initial condition $-1.8^\circ C$, which is equal to the inlet temperature of glycol. The fluid is initially not moving.

When the simulation starts, the glycol enters at a source well at the top of the cylinder with a velocity of $0.21 m/s$, this is equal to meet the demand as described in Section 2.1 (assuming a return temperature of $15^\circ C$). The glycol leaves the cylinder as a normal flow in a sink at the bottom. Both the inlet source as the outlet sink are infinity well insulated, the heat is only transferred through the walls of the cylinder.

Finally, the outer walls of the soil are defined as an open boundary. This implies that the soil domain is infinite. The initial temperature of the soil at this boundary is $15^\circ C$. In Figure 3.3 is a schematic representation illustrated for the used initial and boundary conditions.

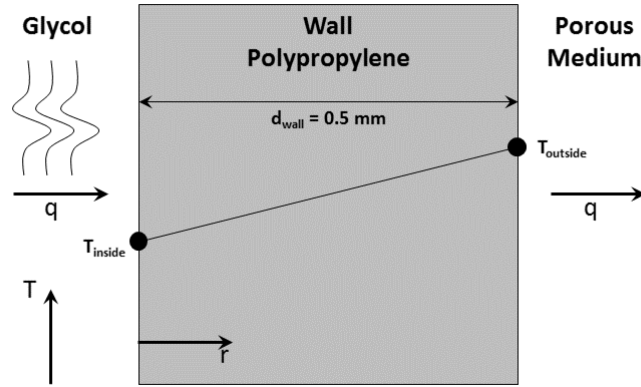


Figure 3.2: Schematic representation of the wall interface, which couples both interfaces

3.5 Physical properties

The natural heat column, which is elaborated in Chapter 2 has, according to the technical definitions which are given, an aqueous solution of 20Vol% monoethylenglycol with a freezing temperature of $-10^{\circ}C$. The glycol enters an annulus with a temperature of $-1.8^{\circ}C$ and has the following physical properties:

$$\rho(kg/m^3) = AT^2(^{\circ}C) + BT(^{\circ}C) + C \quad (3.42)$$

$$k(W/mK) = AT^2(^{\circ}C) + BT(^{\circ}C) + C \quad (3.43)$$

$$c_p(J/kgK) = AT^2(^{\circ}C) + BT(^{\circ}C) + C \quad (3.44)$$

$$\mu(Pa \cdot s) = AT^2(^{\circ}C) + BT(^{\circ}C) + C \quad (3.45)$$

The cylinder is entirely made of polypropylene which has the physical properties:

$$\rho(kg/m^3) = A \quad (3.46)$$

$$k(W/mK) = AT^2(^{\circ}C) + BT(^{\circ}C) + C \quad (3.47)$$

$$c_p(J/kgK) = AT(^{\circ}C) + B \quad (3.48)$$

While the glycol mixture flows down the cylinder it will transfer energy through the wall with the surroundings. The surrounded groundwater has an initial temperature of $15^{\circ}C$. When the analysis starts, the temperature will reduce and the water will be transformed into ice. This ice will grow slowly around the cylinder. The physical properties of ice are:

$$\rho(kg/m^3) = AT(^{\circ}C) + B \quad (3.49)$$

$$k(W/mK) = AT(^{\circ}C) + B \quad (3.50)$$

$$c_p(J/kgK) = A \quad (3.51)$$

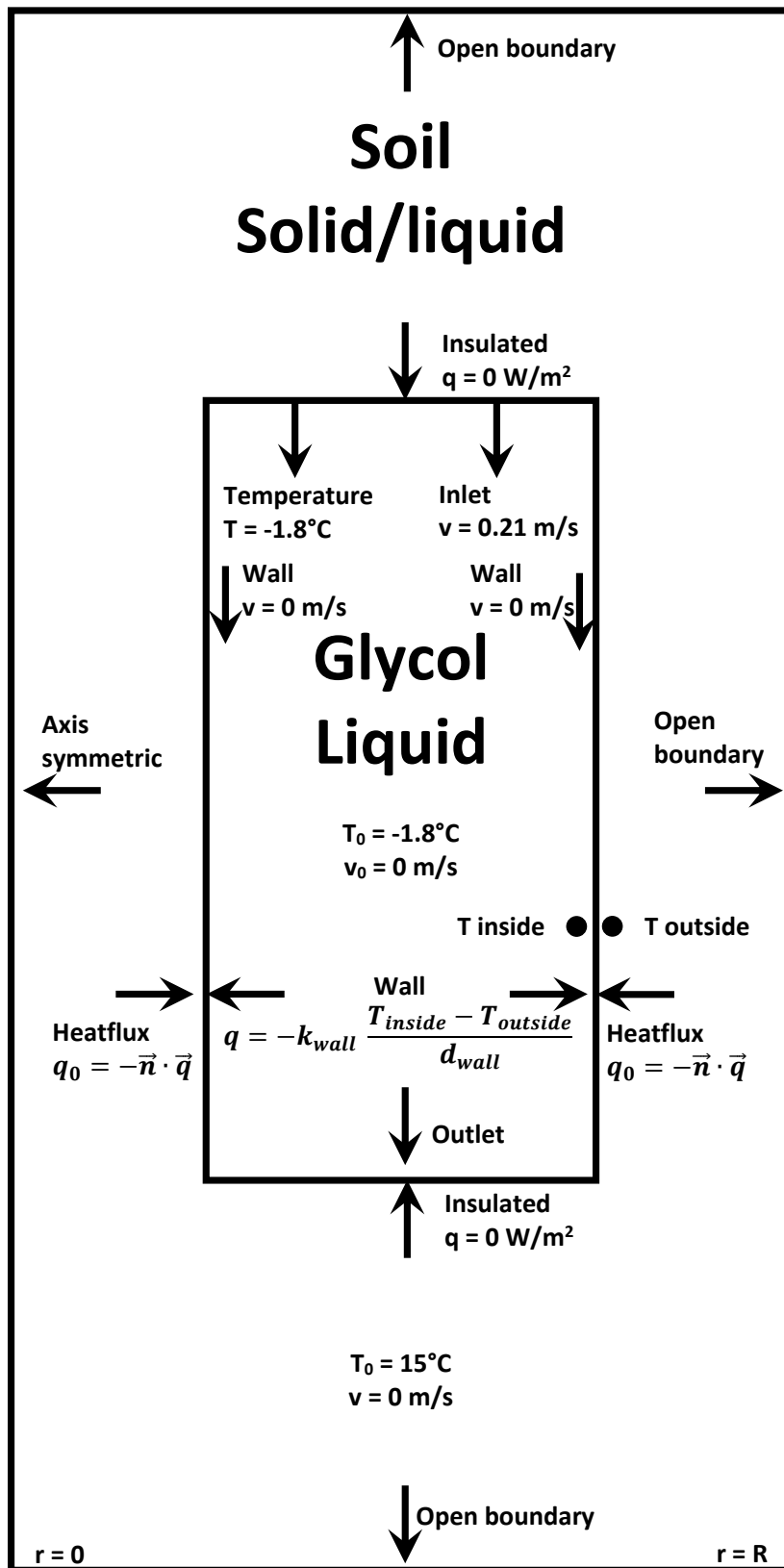


Figure 3.3: Schematic representation of the used initial and boundary conditions

Table 3.1: Physical property coefficients

		A	B	C	D	E	F
Water	Density	1094.0233	-1813.2295	3863.9557	-2479.8130		
	Thermal cond.	-2.4149	2.45165e-2	-0.73121e-4	0.99492e-7	-0.53730e-10	
	Specific heat	0.2399	12.8647	-33.6392	104.7686	-155.4709	92.37726
	Viscosity	0.45047	1.39753	613.181	63.697	6.896e-5	
Ice	Density	-2	900				
	Thermal cond.	-0.01	2.2				
	Specific heat	2000					
Glycol	Density	-0.003	-0.2333	1036			
	Thermal cond.	3e-6	4e-4	0.502			
	Specific heat	-0.0167	1.8333	3870			
	Viscosity	4.5e-9	-1.63e-7	3.11e-6			
Poly-propylene	Density	910					
	Thermal cond.	-2e-6	1e-4	0.22			
	Specific heat	6.4	1590				

And for water:

$$\rho(kg/m^3) = \rho_c(kg/m^3) + A\left(1 - \frac{T(K)}{T_c(K)}\right)^{0.35} + B\left(1 - \frac{T(K)}{T_c(K)}\right)^{2/3} + C\left(1 - \frac{T(K)}{T_c(K)}\right) + D\left(1 - \frac{T(K)}{T_c(K)}\right)^{4/3} \quad (3.52)$$

$$k(W/mK) = A + BT(K) + CT^2(K) + DT^3(K) + ET^4(K) \quad (3.53)$$

$$c_p(J/kgK) = R(J/kgK)\left(\frac{A}{1 - \frac{T(K)}{T_c(K)}} + B + C\left(1 - \frac{T(K)}{T_c(K)}\right) + D\left(1 - \frac{T(K)}{T_c(K)}\right)^2 + E\left(1 - \frac{T(K)}{T_c(K)}\right)^3 + F\left(1 - \frac{T(K)}{T_c(K)}\right)^4\right) \quad (3.54)$$

$$\mu(Pa \cdot s) = E \cdot \exp\left(A\left(\frac{C - T(K)}{T(K) - D}\right)^{1/3} + B\left(\frac{C - T(K)}{T(K) - D}\right)^{4/3}\right) \quad (3.55)$$

In the above equations: the critical temperature of water is $T_c = 647.10K$, the critical density of water is $\rho_c = 322kg/m^3$ and the specific gas constant of is water $R = 461.52J/kgK$. The coefficients of the physical properties which are used in the simulation can be found in Table 3.1[27].

In the next chapters, this methodology will be applied in different simulations to find an answer on the two questions, stated at the beginning of this chapter and see what the overall performances of the natural heat column are.

Chapter 4

Numerical methods

The final step of performing a CFD-analysis is to find the most optimal mesh. The mesh has to give results close to the analytic solution. In this chapter, an overview of the different numerical methods is given. Furthermore, a mesh convergence study will be executed to see what the mesh performances are.

4.1 Overview of numerical methods

For theoretical heat and flow problems, the conservation laws for mass, momentum, and energy are described in Chapter 3. However, these equations can not be solved analytically. To use the results of these second order partial differential equations, they can be approached by using a numerical method. The three most used methods are: the finite difference method (FDM), the finite volume method (FVM), and the finite element method (FEM).

The finite difference method is the most straightforward easiest to adapt to the three methods. It applies the main difference theory on the differential equation, therefore no integrating methods are used. The main difference theory is defined as:

$$\frac{\partial F(t, x)}{\partial t} + \frac{\partial G(t, x)}{\partial x} = \frac{F(t, x) - F(t - \Delta t, x)}{\Delta t} + \frac{G(t, x + \Delta x) - G(t, x)}{\Delta x} \quad (4.1)$$

The advantage of the finite difference method is that the calculations are straightforward. The mesh has a rectangular shape, which makes the process simpler to model. When the limit of Δt and Δx goes to zero, the approximation becomes more accurate. For large systems, this is a significant problem, because more accurate results mean a higher computational time [34]. Because the value of G on position $(t, x + \Delta x)$ is initially not known, an assume has to be made. Firstly, one can assume that the time step Δt is so small that $G(t, x + \Delta x) = G(t - \Delta t, x + \Delta x)$ (explicit method). Secondly, there can be assumed a map of G and G on position $(t, x + \Delta x)$ is solved iterative (implicit method). The advantage of the implicit method is that the error is being controlled. The disadvantage of this model is the iterative process which takes a large computational time [35].

The finite volume method is similar to the finite difference method, only here each node represents a small volume. Over this volume, the average value is obtained by integrating:

$$\overline{F(x)} = \frac{1}{x_{i+\frac{1}{2}} - x_{i-\frac{1}{2}}} \int_{x_{i-\frac{1}{2}}}^{x_{i+\frac{1}{2}}} F(x) dx \quad (4.2)$$

The finite volume method has become increasingly popular over the last ten to fifteen years. The biggest advantage is that this method only needs to evaluate a flux for the cell boundaries. However, the biggest disadvantage is that it cannot be easily made of higher order [34].

The finite element method is the most elaborate and most used of the three models. It works in the same way as the finite volume method, only the properties are calculated for different cells instead of nodes. These cells have different sizes. Areas with a high fluctuation are represented by small cells and areas with a low fluctuation are represented by large cells. Furthermore, to save computational time, the cells are not rectangular, but triangular. The big advantage of the finite element method is that it is a very general method and the number of cells can easily be increased which makes the mesh finer. The

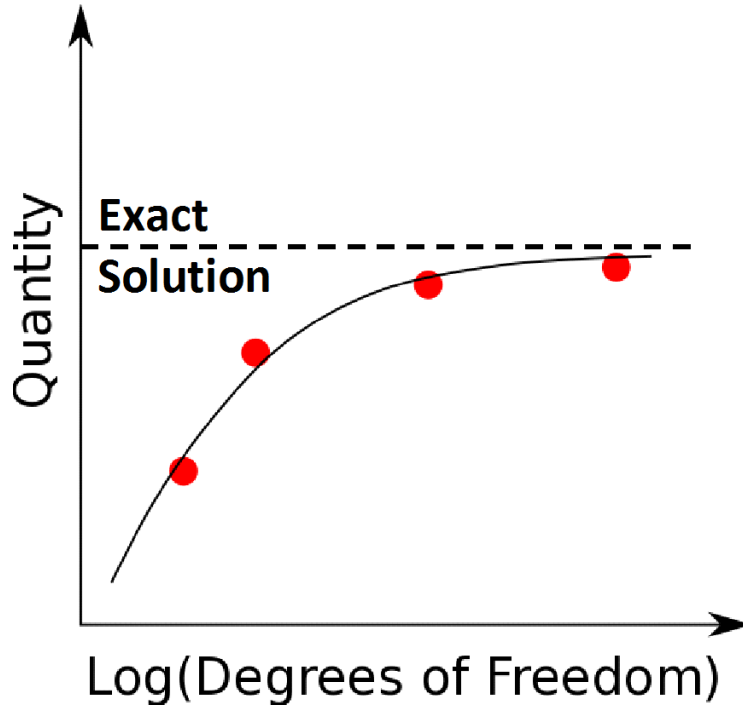


Figure 4.1: Convergence of quantity with an increase in degrees of freedom

disadvantage of the finite element method is that it contains quite advanced mathematics and is difficult to apply at first sight [34].

The research of this thesis will be simulated with Comsol Multiphysics. This software uses the finite element method to calculate its mesh. Because this method is the most accurate, the finite element method will be used in this thesis.

4.2 Mesh convergence study

When a mesh is built from a small number of elements, the computational time is low, however, the results are not physical. When a mesh contains an infinite number of elements, the result is the same as when the problem would be solved analytically, however, the computational time would be infinitely large. To find the optimum, a Mesh Convergence Study (MCS) is executed. In the Mesh Convergence Study, the mesh will be made finer and finer. This will be done until the results are not fluctuating anymore. If two subsequent mesh refinements do not change the result substantially, it can be assumed that the result has converged (see Figure 4.1).

In CFD-analysis 1 (see Chapter 6) there is chosen to use two meshes. One for the glycol interface inside the cylinder and one for the water/ice interface outside the cylinder. In the mesh inside the cylinder, the number of elements changes as a function over the width of the cylinder. In the mesh outside the cylinder, the number of elements changes as a function over the ground radius. In Table 4.1 the statistics of the mesh are represented. Knowing that the cylinder diameter is five millimeters the minimum number of elements for the width of the cylinder are: 4, 5, 9, 10 and 12. In this mesh convergence study, the water/ice temperature outside the cylinder (see Figure 4.2) and the glycol velocity inside the cylinder are evaluated for a period of one week. The results are shown in Figure 4.3.

Figure 4.3 shows that the temperatures in the mesh almost direct converge. However, this is not the case for the velocities inside the cylinder. Until mesh 3 or mesh 4, the meshes are dependent on their mesh size. Because mesh 4 runs smoothly this mesh will be chosen to analyze in the next chapters. Furthermore, the setup of this mesh convergence study is used in the other simulations to perform their mesh convergence study.

Table 4.1: Mesh convergence study – statistics

	Mesh 1	Mesh 2	Mesh 3	Mesh 4	Mesh 5
Min. size cylinder [m]	1.25e-3	1.00e-3	5.56e-4	5.00e-4	4.17e-5
Min. size ground [m]	0.3250	0.2600	0.1444	0.1300	0.1083
Min. element quality	0.08782	0.1342	0.1346	0.07601	0.06616
Avg. element quality	0.8870	0.9241	0.9269	0.8922	0.8934
Triangular element	420 205	428 224	843 582	1 155 000	1 414 214
Quadrilateral elements	19 508	24 306	43 506	48 308	57 910
Edge elements	5241	6450	11 266	12 472	14 882
Vertex elements	8	8	8	8	8

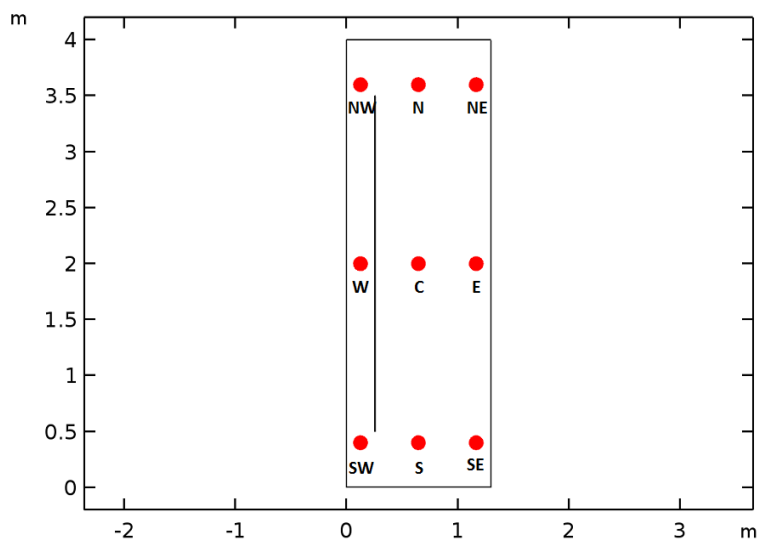


Figure 4.2: Overview of mesh convergence study points

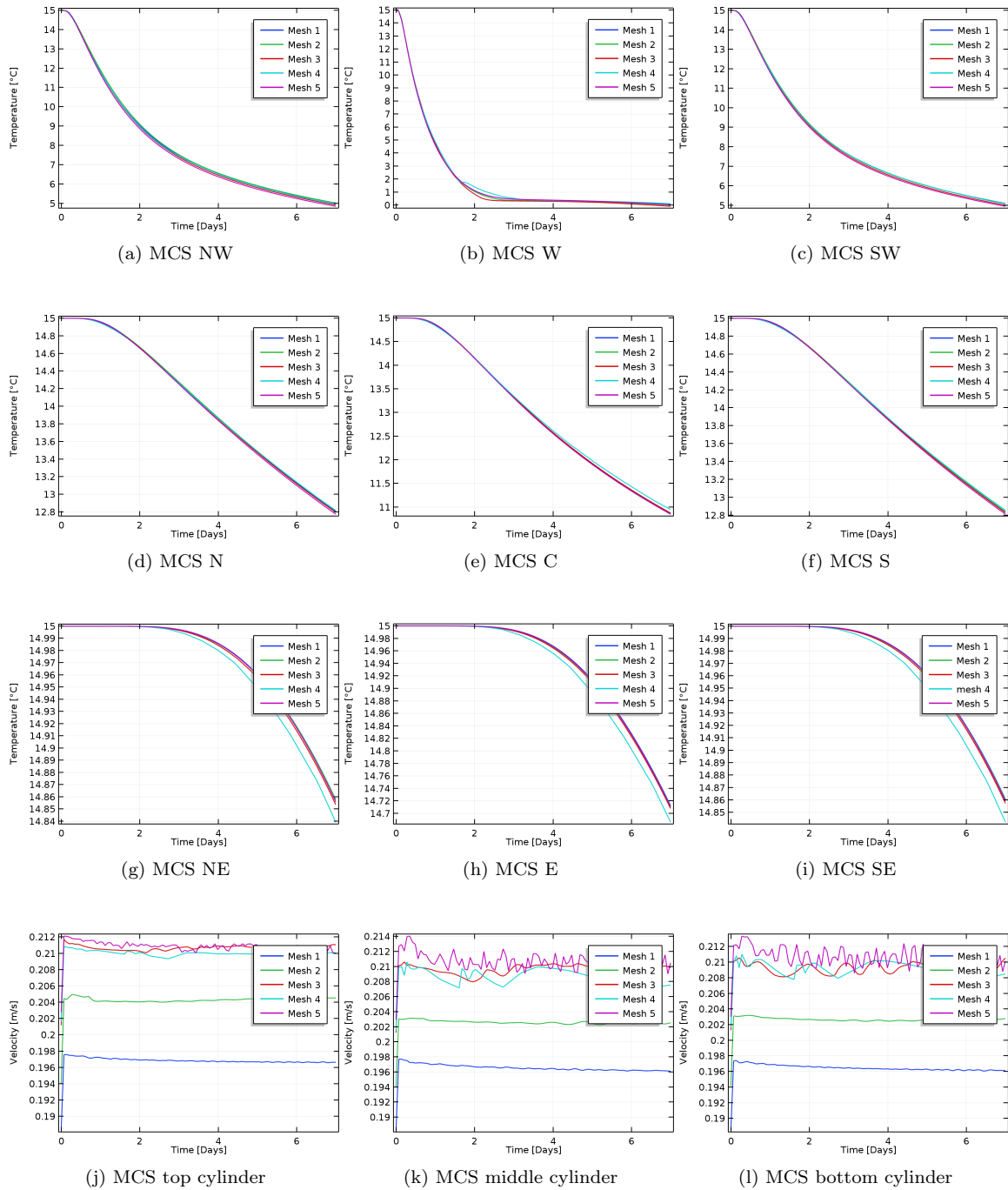


Figure 4.3

Chapter 5

Thermodynamic analysis of the natural heat column

Before applying CFD-analysis to the natural heat column, there need to be defined a system and a thermodynamic model first. With these definitions, a first thermodynamic analysis can be made to determinate what the performance, losses, and volumes of the system are.

5.1 System definition

The natural heat column is divided into two system regimes: a winter regime and a summer regime. During winter, the house needs to be heated. This will be done by displacing heat from the soil to the house. By using a heat pump the heat can be lifted up from a low soil temperature to a higher room temperature. Because the heat is subtracted from the soil, the soil temperature will decrease and eventually, the groundwater will starts freezing.

During summer, the opposite is true. Here the house needs to be cooled. Therefore, the heat is displaced from the house to the ground. Although this is possible without a heat pump, the heat pump is used to accelerate and control the process. Because energy is added to the soil, the temperature in the soil will increase and the frozen groundwater (which was formed during winter), will starts melting.

In an ideal system, the frozen ground will freeze in the winter, as it will melt during summer. When the system is in unbalance, thermal solar collectors on the roof of the house can regenerate the system by adding or subtracting heat to the ground. The total system is connected by a smart network of valves and tubes. A process flow diagram of a possible network is represented in Figure 5.1.

5.2 Heat pump definition

To define the heat pump, this heat pump (refrigerant: R134a) is connected to outside air. During the winter months, an outside temperature of $5^{\circ}C$ is heated to a room temperature of $20^{\circ}C$. This will be done by freezing the ground at $0^{\circ}C$. In the summer months, an outside temperature is $30^{\circ}C$, is cooled to a room temperature of $20^{\circ}C$. This will be done by melting the ground at $0^{\circ}C$. The mass flow of the condenser (at winter mode) and the evaporator (at summer mode) is $0.603kg/s$. This is equivalent to the annual natural gas usage of an average Dutch household ($1500m^3$, see Section 2.1). Furthermore, there is assumed that there is no temperature difference between the condenser (for winter mode) and the evaporator (for summer mode). The complete calculation of the heat pump for both the summer and winter period can be found in Table 5.1 and Table 5.2. The numbers correspond with Figure 5.2.

5.3 Thermodynamic model

In Section 3.3 is stated that the integral equation for the conservation of energy is defined as:

$$\frac{\delta Q}{dt} - \frac{\delta W}{dt} = \frac{\partial}{\partial t} \iiint e \rho dV + \iint (e + \frac{p}{\rho})(\vec{v} \cdot \vec{n}) dA \quad (5.1)$$

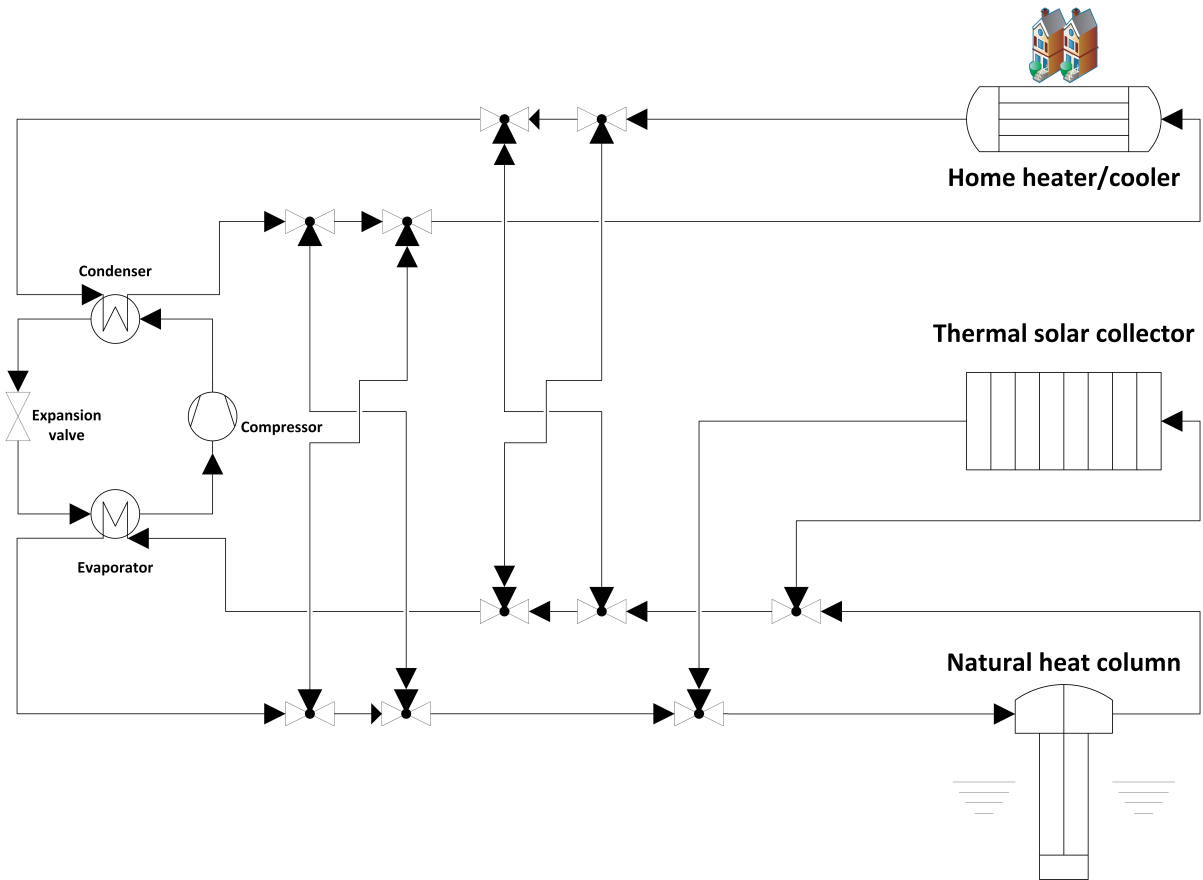


Figure 5.1: Process flow diagram of the system

Table 5.1: Calculations of the heat pump in winter mode

NO	Medium	m kg/s	p bar	T °C	h kJ/kg	s kJ/kgK	x
1	R134a	0.05	5.72	20.00	227.23	1.10	0.00
2	R134a	0.05	2.93	0.00	227.23	1.10	0.14
3	R134a	0.05	2.93	0.00	397.20	1.72	1.00
4	R134a	0.05	5.72	22.52	410.92	1.72	>1.00
101	Air	0.60	1.00	5.00			
102	Air	0.60	1.00	20.00			
103	H2O	0.03	1.00	0.00	0.00		
104	H2O	0.03	1.00	0.00	-333.55		

Table 5.2: Calculations of the heat pump in summer mode

NO	Medium	m kg/s	p bar	T °C	h kJ/kg	s kJ/kgK	x
1	R134a	0.04	5.72	20.00	227.23	1.10	0.00
2	R134a	0.04	2.93	0.00	227.23	1.10	0.14
3	R134a	0.04	2.93	0.00	397.20	1.72	1.00
4	R134a	0.04	5.72	22.52	410.92	1.72	>1.00
101	H2O	0.02	1.00	0.00	-333.55		
102	H2O	0.02	1.00	0.00	0.00		
103	Air	0.60	1.00	30.00			
104	Air	0.60	1.00	20.00			

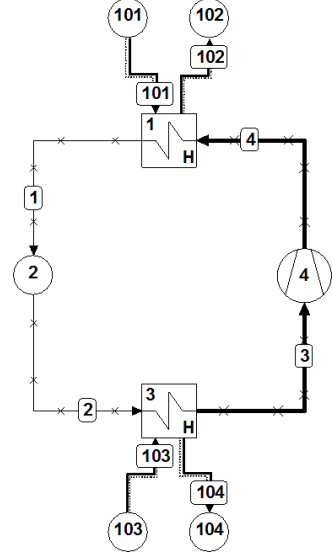


Figure 5.2: Schematic representation of the heat pump with corresponding numbers

When there is assumed that the system is steady, incompressible, and inviscid, the energy equation becomes:

$$Q - W = \iint (e + \frac{p}{\rho})(\vec{v} \cdot \vec{n})dA \quad (5.2)$$

Or:

$$Q - W = dU + mg(y_2 - y_1) + \frac{1}{2}m(v_2^2 - v_1^2) + \frac{m}{\rho}(p_2 - p_1) \quad (5.3)$$

By definition the enthalpy is:

$$H_2 - H_1 = dH = dU + Vdp \quad (5.4)$$

When this definition is applied to the energy equation, and the assumption is made that there is no difference in height ($mg(y_2 - y_1) = 0$) or velocity ($\frac{1}{2}m(v_2^2 - v_1^2) = 0$), the equation of energy is:

$$Q - W = H_2 - H_1 = m(h_2 - h_1) \quad (5.5)$$

In this equation is defined that when Q is positive, heat is charged to the system and when W is positive, work is discharged from the system. The final reduced energy equation for each of the components, shown in Figure 5.2, are:

1. For the condenser only heat is discharged to the system:

$$Q = m(h_4 - h_1) \quad (5.6)$$

2. For the expansion valve no change in heat or work occurs:

$$h_2 = h_1 \quad (5.7)$$

3. For the evaporator only heat is charging to the system:

$$Q = m(h_3 - h_2) \quad (5.8)$$

4. For the compressor only work is charging to the system:

$$W = m(h_4 - h_3) \quad (5.9)$$

With this new reduced definitions, the performance of a heat pump can be calculated. This performance is graphically shown in Figure 5.3. Here, the temperature differences of the inlet and outlet of the evaporator and condenser are plotted over the transferred heat of evaporator and condenser. From Figure 5.3 it can be concluded that during winter the heat of the latent heat pump is larger compared to the sensible heat pump. Therefore more energy is needed to store underground. During summer the opposite is true. Here, the latent heat pump is smaller compared to the sensible heat pump. In this case, the latent heat pump extracts less heat from the ground. Furthermore, it can be concluded that when the outside of the evaporator or condenser has reached the temperature inside the evaporator or condenser, the evaporator or condenser has reached its maximum heat transfer. When looking to Figure 5.3, this is true in most cases.

Finally, the performance of a heat pump is calculated. This performance is expressed in a coefficient of performance (COP), which is, by definition, the total useful heat divided by the electric energy added by the compressor. The higher the COP, the better the performance of the heat pump. For the winter mode, the COP of the heat pump is defined as:

$$COP = \frac{Q_{cond}}{W_{pump}} = \frac{m(h_4 - h_1)}{m(h_4 - h_3)} = \frac{h_4 - h_1}{h_4 - h_3} = \frac{410.92 - 227.23}{410.92 - 397.20} = 13.39 \quad (5.10)$$

For the summer mode the COP of the heat pump is:

$$COP = \frac{Q_{evap}}{W_{pump}} = \frac{m(h_3 - h_2)}{m(h_4 - h_3)} = \frac{h_3 - h_1}{h_4 - h_2} = \frac{397.20 - 227.23}{410.92 - 397.20} = 12.39 \quad (5.11)$$

When subtracting both coefficients, the result will always be equal to one, because:

$$COP_1 - COP_2 = \frac{h_4 - h_1}{h_4 - h_3} - \frac{h_3 - h_1}{h_4 - h_2} = \frac{h_4 - h_3}{h_4 - h_2} = 1 \quad (5.12)$$

The results for both modes are summarized in Figure 5.4 and the log(p)h-diagram of the described system can be found in Figure 5.5.

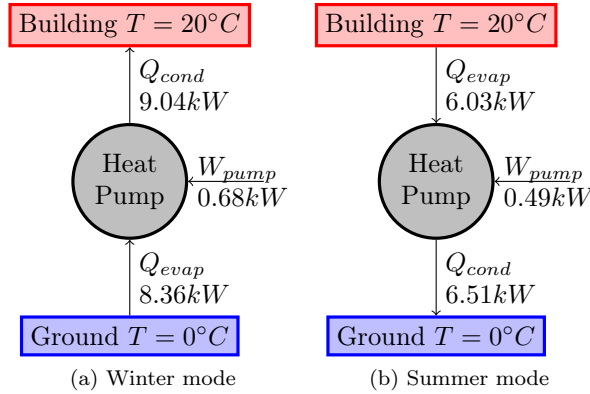


Figure 5.4: Heat pump calculations

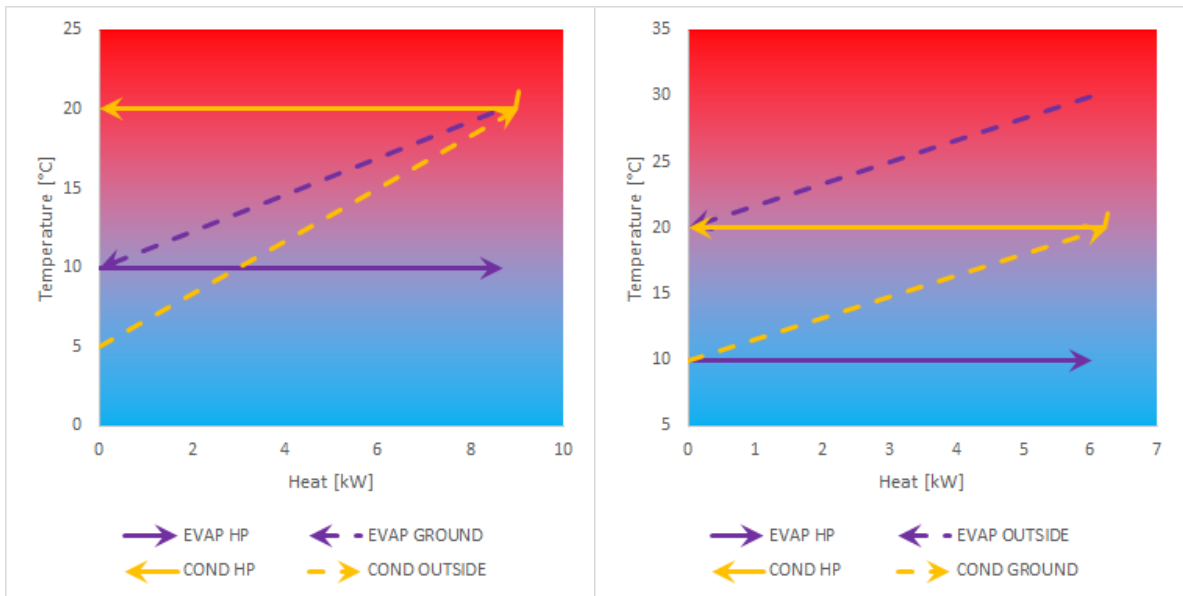
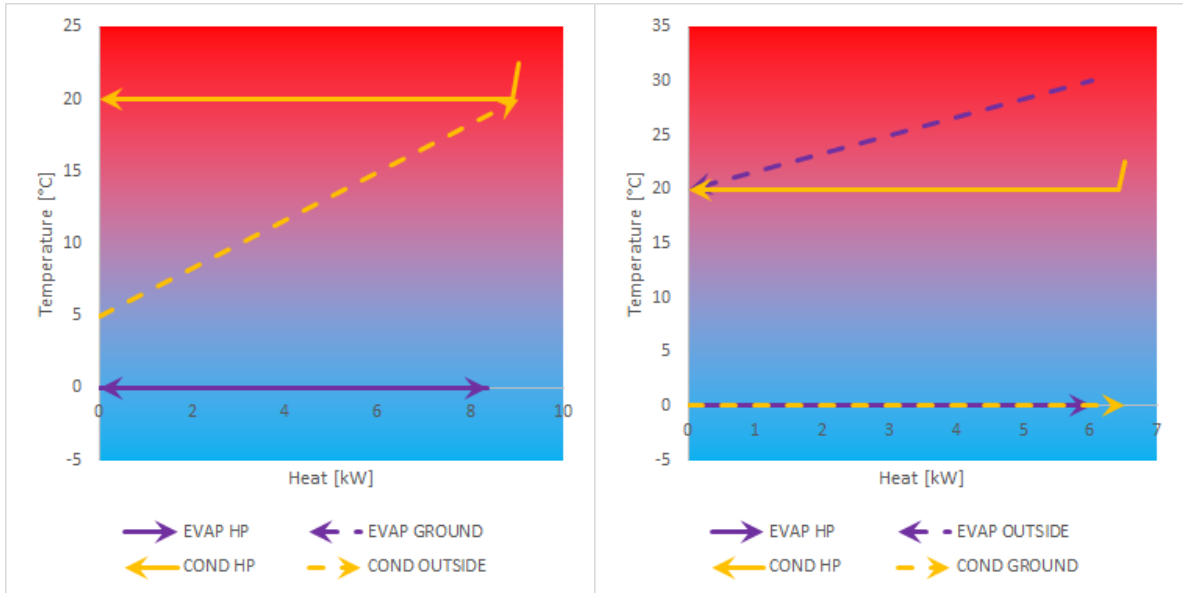


Figure 5.3: QT diagrams of the defined system

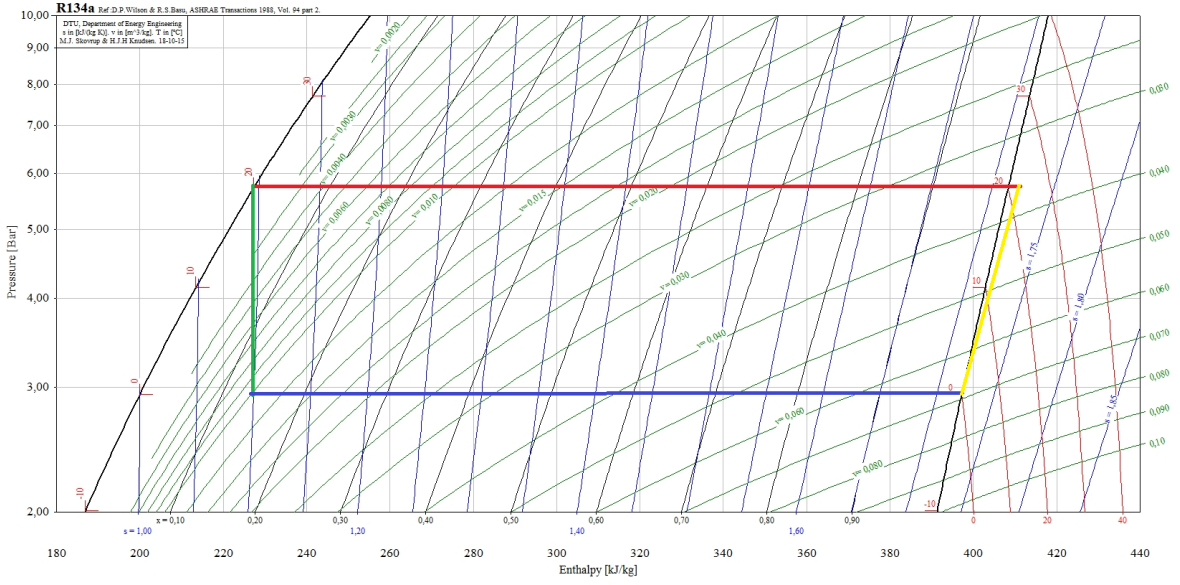


Figure 5.5: Log(p)h-diagram of the heat pump

5.4 Thermodynamic analysis

Now the system and the thermodynamic model are defined, a thermodynamic analysis can be made. In order to do this, there will be calculated which volume of ice needs to be stored underground. This is calculated by:

$$V_{ice} = \frac{Qt}{\varphi\rho H_f} \quad (5.13)$$

When the heat pump provides heat for a half year, with an average of eight operating hours a day, the volume of the ice grows $359.59m^3$ during winter and shrinks $279.83m^3$ during the summer months (according to above equation with a power of $8.36kW$ during winter and $6.51kW$ summer). This means that $79.76m^3$ of ice must be melted by solar collectors. When these volumes are being compared with a traditional heat pump, where the refrigerant is displaced from $10^\circ C$ ($h = 42.12kJ/kg$) to $20^\circ C$ ($h = 84.01kJ/kg$), there is calculated how much volume in saved:

$$\eta_{ground} = 1 - \frac{V_{lat}}{V_{sens}} = 1 - \frac{[\frac{Qt}{\varphi\rho\Delta H}]_{lat}}{[\frac{Qt}{\varphi\rho\Delta H}]_{sens}} = 1 - \frac{[Q/H_f]_{lat}}{[Q/\Delta h]_{sens}} \quad (5.14)$$

During summer, using Figure 5.3 for Q , this is:

$$\eta_{ground} = 1 - \frac{6.51/333.55}{6.25/41.89} = 86\% \quad (5.15)$$

And during winter, using Figure 5.3 for Q , this is:

$$\eta_{ground} = 1 - \frac{8.36/333.55}{8.71/41.89} = 87\% \quad (5.16)$$

However, the trade-off of using the natural heat column is that pumping a refrigerant from $0^\circ C$ to $20^\circ C$, consumes $1.16kW$ of electrical power. With a traditional heat pump, where the refrigerant is displaced from $10^\circ C$ to $20^\circ C$, this only is $0.55kW$ of electrical power. It seems that with an APX price of $\text{€}40/\text{MWh}$, the electric costs for the pump are $\text{€}67.82$ a year, for the traditional heat pump the costs are yearly $\text{€}32.24$. Although the operational costs of a latent heat pump are higher, the area needed is significantly lower. Therefore, a latent heat pump can have a high potential in areas where limited space is available.

Finally, it can be calculated how long the ice will take to melt, due to thermal losses. This is done by using the following equation (see Appendix C):

$$t(m_{ice} = 0) = \frac{m_{ice0}^{2/3}}{\left(\frac{3}{4\pi\rho\varphi}\right)^{1/3} \frac{k_{ground}6\pi}{H_f} (T_{ground} - T_{ice})} \quad (5.17)$$

With a ground temperature of $10^\circ C$, it will take seventeen months until the total volume of ice ($111.93m^3$) has been melted (see Figure 5.6). During the operational time of six months, only $58m^3$ has been melted due to the thermal losses. Because this melted volume due to thermal losses is a significant number, it has to be taken into account when designing the natural heat column. In the next chapters, the results in this chapter will be used for the different CFD-analyses. And the exact results of the system will be simulated in Comsol.

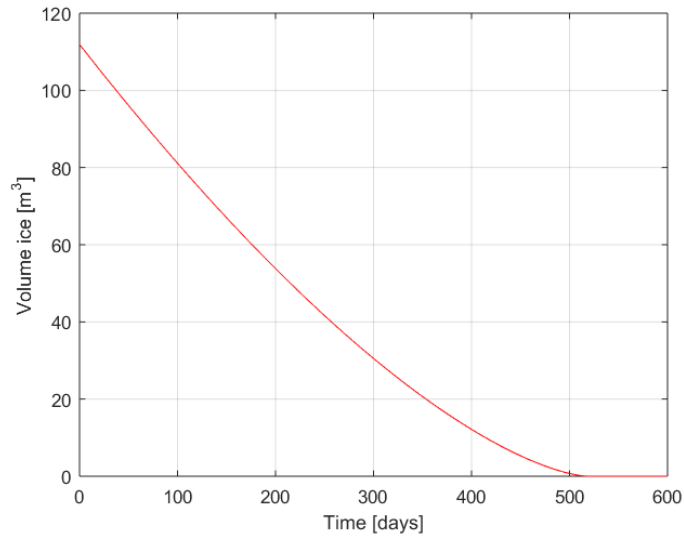


Figure 5.6: Volume of ice over time during summer by $10^\circ C$ ground temperature

Chapter 6

CFD-analysis 1: Natural heat column in water surrounding (seasonal storage)

In this first analysis, there is assumed that the soil interface only contains a water/ice mixture. When the methodology, described in Chapter 3, and the mesh, described in Chapter 4, are applied, the simulation can be solved. In this chapter the results are represented and will be discussed by the research questions, stated at the beginning of Chapter 3:

- What will be the refrigerant return temperature as a function over time?
- What will be the ice layer thickness after a period of a hundred days?

The geometry of this analysis is graphically represented in Figure 6.1.

6.1 Simulation results

When the model is applied to Comsol Multiphysics, the governing equations can be solved. Because the seasonal effects are investigated, there is chosen to run the analysis for a hundred days with a time step of one day. To cover the start-up effects: the first hour of the simulation is solved, with a time step of sixty seconds. It took Comsol 1 hour, 7 minutes and twenty seconds to solve the calculations with the solver PARDISO.

6.1.1 Water temperature

In Figure 6.2 the temperature distribution is shown for multiple days and in Figure 6.3 the three-dimensional temperature plot after a hundred days is represented. There it can be concluded that the water/ice mixture shows a significant drop in temperature. The maximum water temperature after a hundred days is 3.5°C . More temperature plots for different times are presented in Appendix D.

When plotting the different temperatures over time, the results in shown Figure 6.4 are obtained. Here, the different temperatures correspond to Figure 4.2. From these results, it concludes that the west points show a faster drop in temperature compared to the east points. This is due to the fact that the cylinder is located the closest to this west points. The small horizontal part in the west temperature line indicates the point where the first water transforms into ice. In the start-up plot, represented in Figure 6.4 b, the decrease in temperature starts very slowly during the first hours.

6.1.2 Glycol return temperature

The return temperature, shown in Figure 6.5, represents the temperature located at the bottom sink of the cylinder, and has a initial condition of -1.8°C . This initial condition is equal to the glycol inlet temperature which will reduce the computational time of the simulation significantly. In reality, the initial condition is equal to the ground temperature -15°C . Furthermore, Figure 6.5 shows that within one day the temperature reaches a value of 90% of its final temperature and 99% within twenty days.

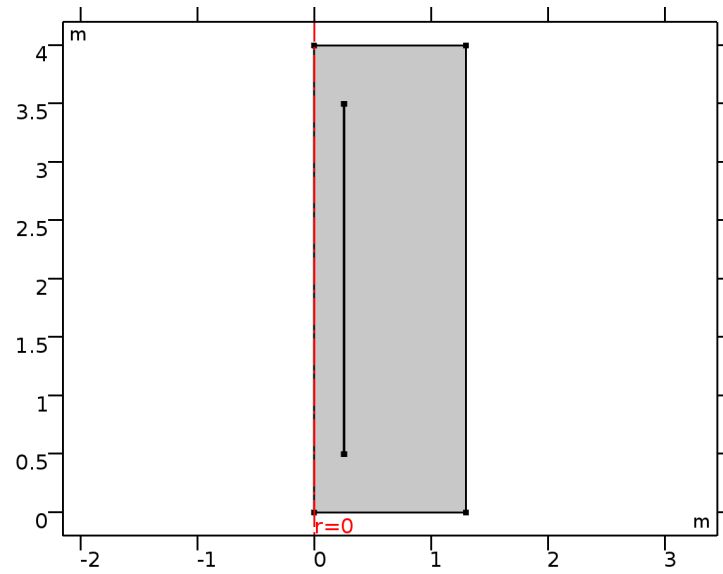


Figure 6.1: Geometry of analysis 1

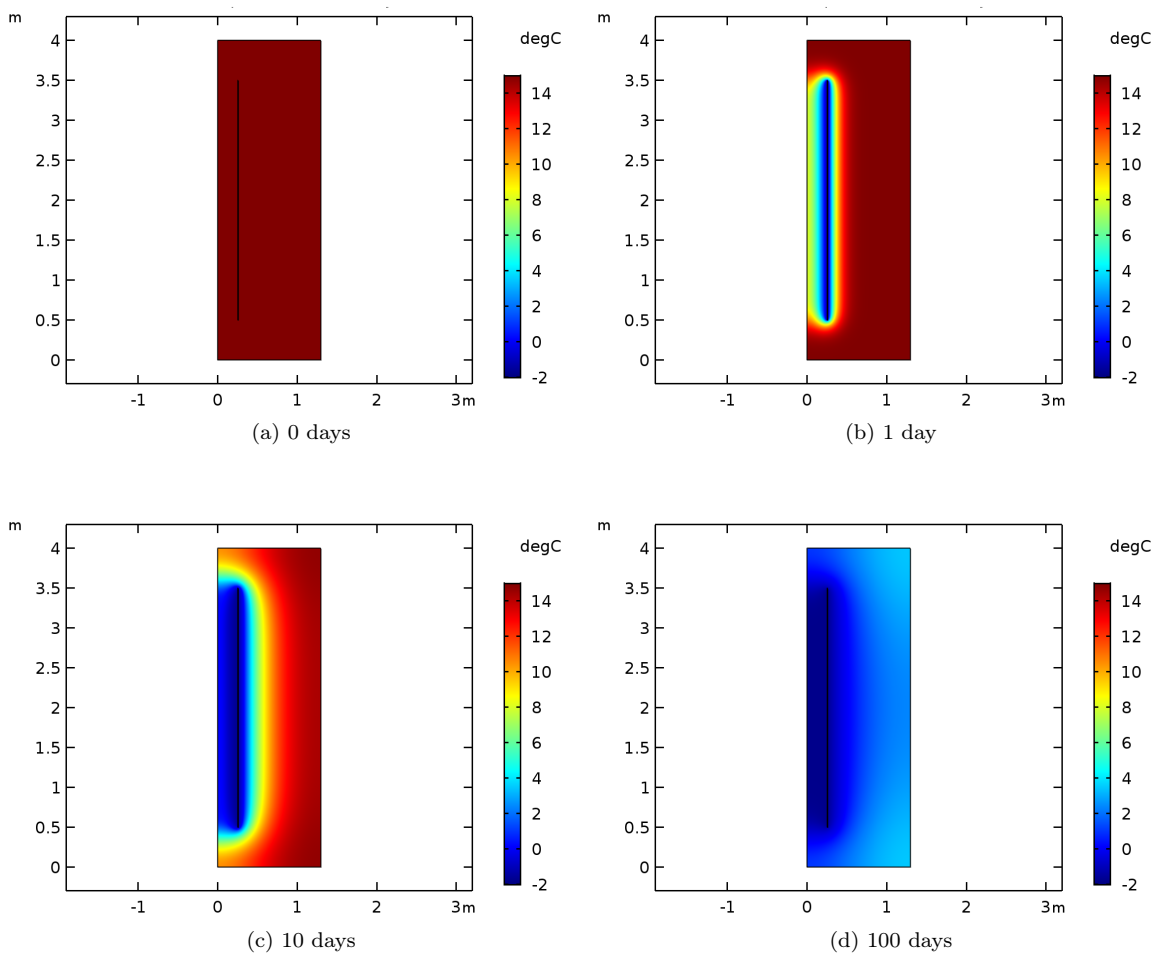


Figure 6.2: 2D plot of temperature

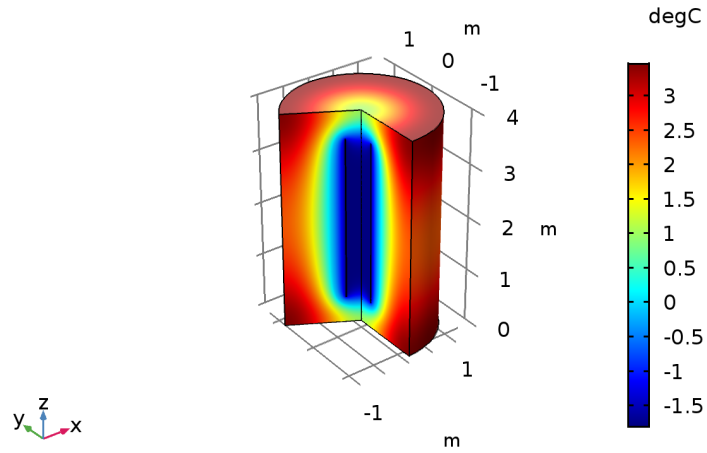


Figure 6.3: Temperature plot after a hundred days – 3D

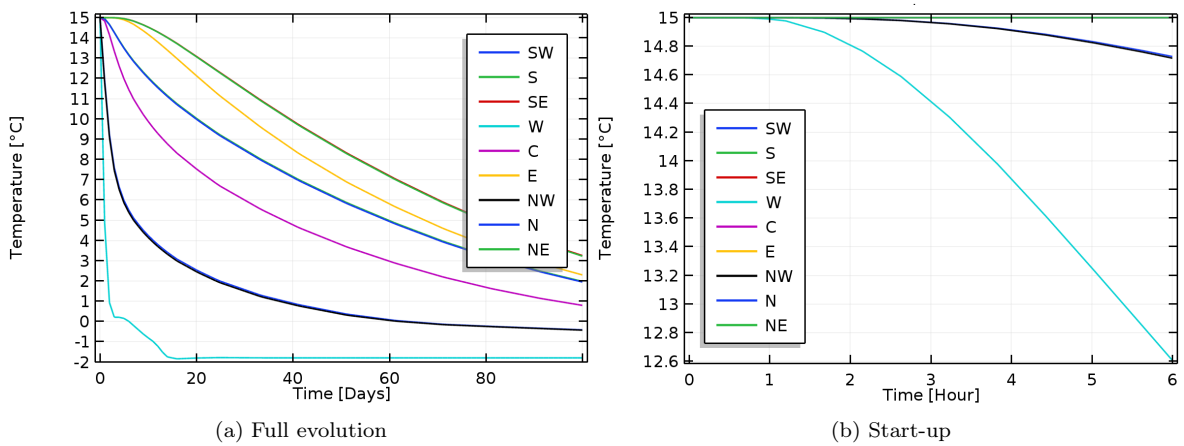


Figure 6.4: Water/ice temperature over time

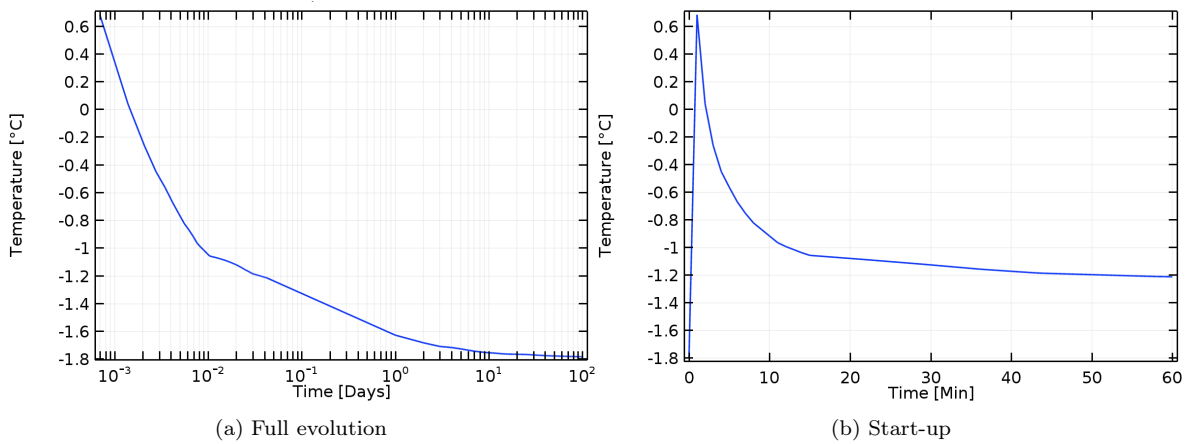


Figure 6.5: Return temperature over time

6.1.3 Heat flux

A direct effect of this fast decrease of temperature is shown in Figure 6.6. Here, the heat flux through the wall is plotted against time. After six minutes the heat flux will be halved, and within an hour almost no heat will be transferred through the wall. Which is calculated with the equation:

$$Q = UA\Delta T_{ln} \quad (6.1)$$

With the thermal resistance:

$$R = \frac{1}{UA} = \frac{\ln(r_{wall}/r_0)}{2\pi k_{wall}l} + \frac{\ln(r_{ice}/r_{wall})}{2\pi k_{ice}l} \quad (6.2)$$

And the logarithmic temperature difference:

$$\Delta T_{ln} = \frac{(T_{ice} - T_{in}) - (T_{ice} - T_{out})}{\ln\left(\frac{T_{ice}-T_{in}}{T_{ice}-T_{out}}\right)} \quad (6.3)$$

When calculating the ratio of the thermal resistance over the initial resistance this becomes:

$$\begin{aligned} \frac{R}{R_0} &= \frac{\frac{\ln(r_{wall}/r_0)}{2\pi k_{wall}l} + \frac{\ln(r_{ice}/r_{wall})}{2\pi k_{ice}l}}{\frac{\ln(r_{wall}/r_0)}{2\pi k_{wall}l}} \\ &= 1 + \frac{k_{wall}}{k_{ice}} \frac{\ln(r_{ice}/r_{wall})}{\ln(r_{wall}/r_0)} \\ &= 1 - \frac{k_{wall}}{k_{ice}} \frac{\ln(r_{wall})}{\ln(r_{wall}/r_0)} + \frac{k_{wall}}{k_{ice}} \frac{1}{\ln(r_{wall}/r_0)} \ln(r_{ice}) \\ &= 71 + 52\ln(r_{ice}) \end{aligned} \quad (6.4)$$

As a result, one meter of ice, the thermal resistance will be 83 times higher than the initial thermal resistance. This is a significant problem for the system's performance.

6.1.4 Ice volume

The volume of the ice is plotted against time in Figure 6.7 and graphically shown in Figure 6.8 for multiple days. This can almost perfectly be simplified by two trend lines: one before twelve days, and one after twelve days. For the first twelve days this is done by:

$$V(t) = 0.2706t + 0.5607 \quad (6.5)$$

And after twelve days:

$$V(t) = 0.0263t + 3.6845 \quad (6.6)$$

Therefore, the volume of the ice increases with $0.27m^3/day$ for the first twelve days and after twelve days the volume of the ice increases with $0.026m^3/day$. The reason for this decrease is explained by the ice, which grows to the middle of the cylinder, reaching the center line, after which it can only grow towards the outside. The results of these trend lines are plotted in Figure 6.9. The trend line has a coefficient of determination of $r^2 = 0.9810$. This so-called coefficient of determination is a standard for the variance in numbers. The coefficient of determination is calculated by:

$$r^2 = 1 - \frac{\sum_i (y_i - f_i)^2}{\sum_i (y_i - \bar{y})^2} \quad (6.7)$$

Where y_i is the known value on position i , \bar{y} the average value of the known value and f_i the value of the trend line on position i . When r^2 is larger than 0.81, it can be concluded that there is a very strong correlation between the data and the trend line [36]. Which is true in this case.

When the ice volume over time is calculated analytically, the following equation is used (see full derivation in Appendix E):

$$t = e \frac{\pi r_{out}^2}{v} \quad (6.8)$$

It will take 12.3 days until the water inside the cylinder is fully frozen. This is close to the twelve days, which is found by the least square regression analysis method.

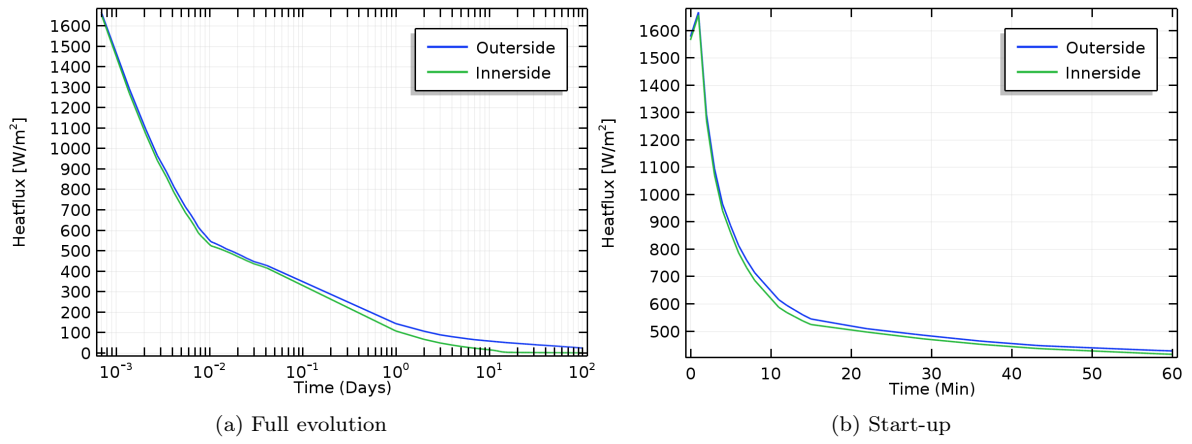


Figure 6.6: Heat flux through the wall over time

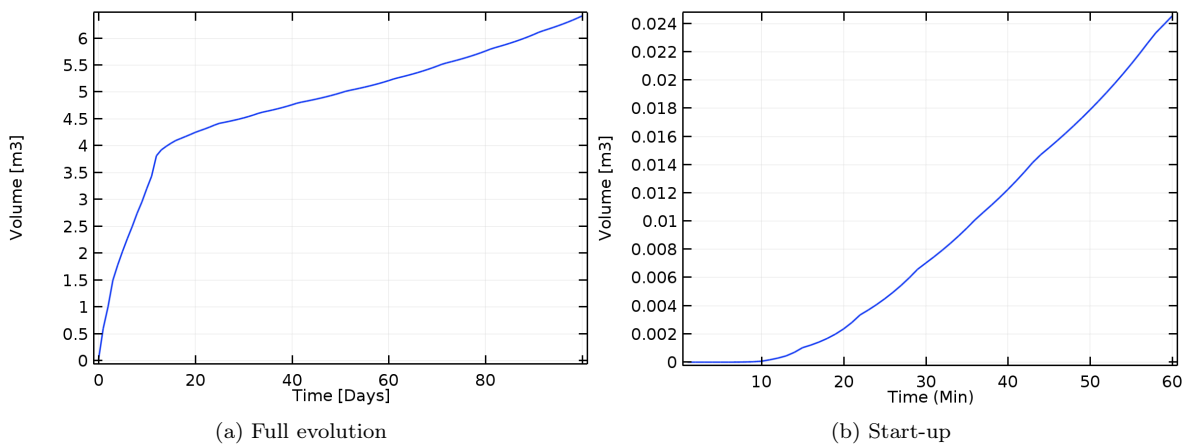


Figure 6.7: Ice volume over time

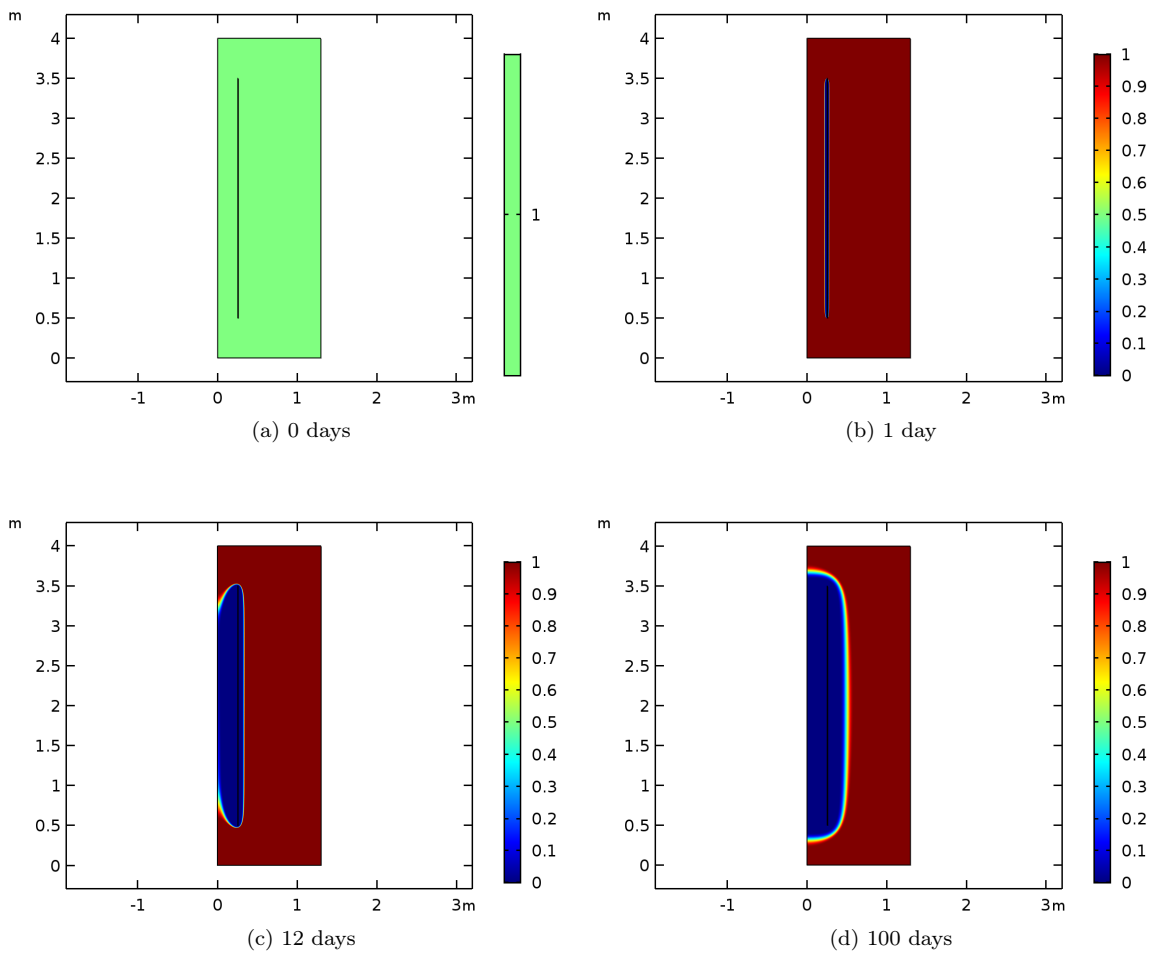


Figure 6.8: 2D plot of phase change ($0 = ice$)

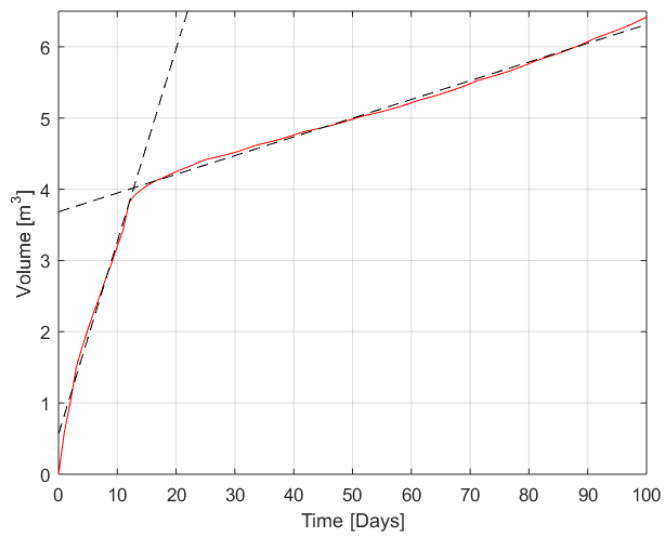


Figure 6.9: Ice volume over time with trend line

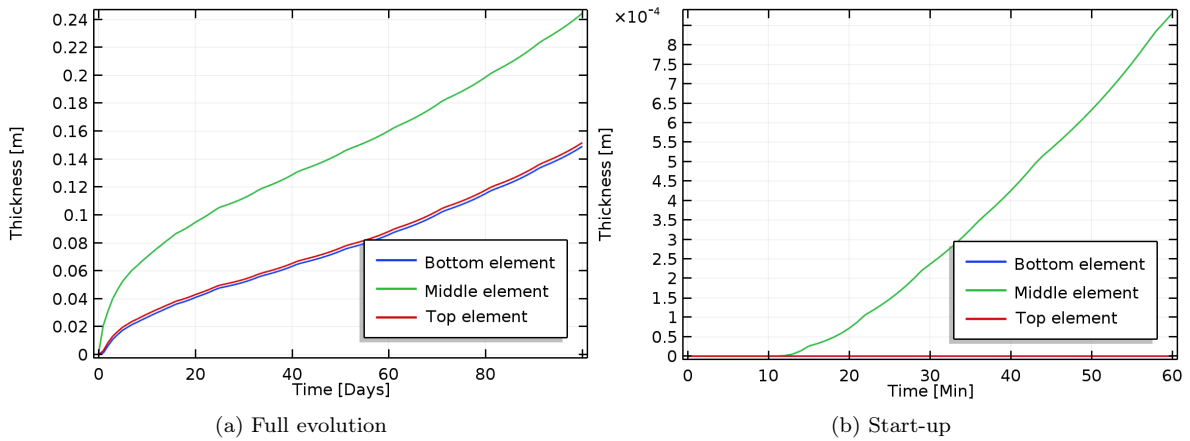


Figure 6.10: Ice layer thickness (measured from outside cool element) over time

6.1.5 Ice layer thickness

Finally, the ice layer thickness at the top, middle and bottom of the cylinder is plotted against time in Figure 6.10. From this it can be concluded that the ice layer grows similar to an oval, with the largest thickness in the middle of the cylinder.

The goal of this analysis is to find the refrigerant temperature as a function over time. The answer to this question can be found in Figure 6.5. This figure shows that the return temperature after a hundred days is 0.02°C higher with respect to the inlet temperature. Furthermore, the ice layer thickness is investigated after a hundred days. Figure 6.10 illustrates the ice layer thickness in the middle of the cylinder of 0.24 meter. The volume of the ice increases with $0.026\text{m}^3/\text{day}$. This is significantly less than the $3.94\text{m}^3/\text{day}$ expected in Chapter 5. The difference in numbers can be explained by the assumptions made in Chapter 5. Here, the return temperature remains constant over time at 15°C . As shown in Figure 6.6, the heat transfer is almost immediately zero. This is due to the high thermal resistance: R/R_0 . For one meter of ice, the thermal resistance will be 83 times higher than the initial resistance. From this, it can be concluded that the results of this first CFD-analysis are not yet sufficient in comparison with the reality. In the next CFD-analysis, as will be discussed in Chapter 7, the focus will be on investigating what the possibilities are for applying a porous ground medium instead of a water/ice mixture. Furthermore, the effects of regenerating will be investigated.

Chapter 7

CFD-analysis 2: Natural heat column in soil surrounding (seasonal storage)

In this second analysis, the surrounding outside the cylinder interface contains ground with a water/ice mixture instead of only water and ice (which is described in Chapter 6). The types of ground which are investigated are sand, gravel, clay, and silt. The mesh of this simulation consists of minimal ten elements over the width of the cylinder and minimal ten elements over the width of the surrounding. This mesh is constructed in the same way as described in Chapter 4. The detailed results of the mesh convergence study are presented in Appendix F. In this chapter, the results of the second CFD-analysis will be discussed. Furthermore, the effect of the different types of ground will be investigated. Again this will be done by finding an answer to the research questions stated in Chapter 3.

- What will be the refrigerant return temperature as a function over time?
- What will be the ice layer thickness after a period of a hundred days?

7.1 Simulation results

In the same way as CFD-analysis 1, this simulation lasted for a hundred days with a time step of one day. To cover the start-up effects: the first hour of the simulation is solved, with a time step of sixty seconds. It took Comsol 5 hours, 32 minutes and 20 seconds to solve the calculations. Again the solver PARDISO is used.

7.1.1 Soil temperature

In Figure 7.1, the temperature distribution over time is plotted for sand. When plotting the soil temperature of sand at different places over time (see Figure 4.2), the results of Figure 7.2 are obtained. Here it can be found that temperatures located at the west side show a faster drop in temperature compared to the temperatures at the east side, which stay above $0^{\circ}C$. When the temperature at the west location is colder than $0.5^{\circ}C$ it decreases slower. At this point, the simulation starts with the freezing of the soil. This will continue until $-0.5^{\circ}C$. When the temperature of the different types of soil are compared (e.g. the east temperature in Figure 7.3) it can be concluded that the temperature of sand reduces first, followed by gravel and clay. Silt has the slowest drop in temperature. This can be explained by the thermal diffusivity of the soils:

$$\frac{\partial T}{\partial t} = \nabla \cdot \alpha \nabla T \quad (7.1)$$

A high thermal diffusivity through the frozen ground means a high drop in temperature. The thermal diffusivity for a porous medium is:

$$\alpha_{soil} = (1 - \varphi)\alpha_{ground} + \varphi\alpha_{ice} \quad (7.2)$$

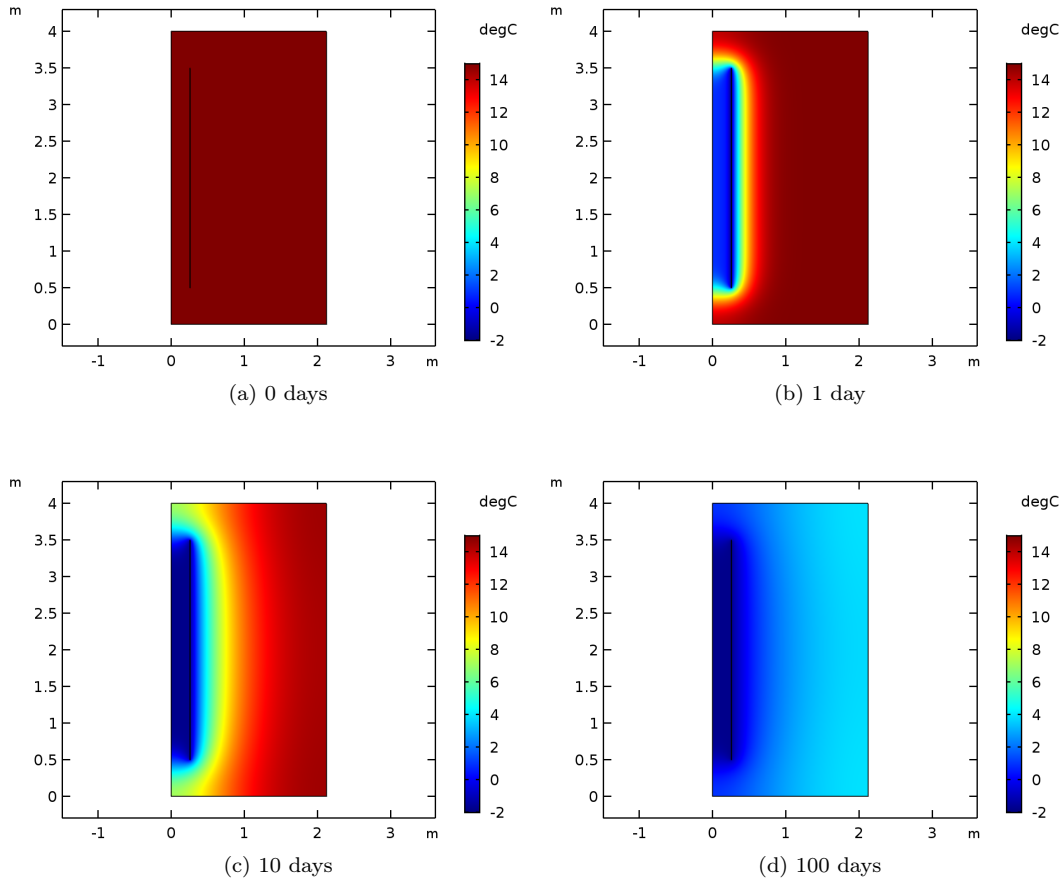


Figure 7.1: 2D plot of temperature (sand)

When using the data of Table 2.1, the thermal diffusivities are:

- $\alpha_{sand} = (1 - 0.375)9.81 \cdot 10^{-7} + 0.375 \cdot 1.22 \cdot 10^{-6} = 1.07 \cdot 10^{-6} m^2/s$
- $\alpha_{gravel} = (1 - 0.325)9.81 \cdot 10^{-7} + 0.325 \cdot 1.22 \cdot 10^{-6} = 1.06 \cdot 10^{-6} m^2/s$
- $\alpha_{clay} = (1 - 0.55)4.80 \cdot 10^{-7} + 0.55 \cdot 1.22 \cdot 10^{-6} = 8.88 \cdot 10^{-7} m^2/s$
- $\alpha_{silt} = (1 - 0.425)4.80 \cdot 10^{-7} + 0.425 \cdot 1.22 \cdot 10^{-6} = 7.96 \cdot 10^{-7} m^2/s$

In Figure 7.3 is shown that the maximum temperature after a hundred days for sand is $3.90^\circ C$, for gravel $4.46^\circ C$, for clay $4.81^\circ C$, and for silt $6.13^\circ C$. Because the sequence of these temperatures is equal to the sequence of the thermal diffusivities, there it can be concluded that there is a correlation between the temperature decrease and the thermal diffusivity. How higher the thermal diffusivity of the soil, how faster the decrease in temperature. All these temperatures are significantly higher than the maximum temperature for water, which was $3.5^\circ C$ (see Chapter 6). This is due to the high thermal conductivity of water and ice. Finally, the start-up phase, shown in Figure 7.2 b, concludes that the maximum temperature drop at the first hour is less than $1^\circ C$. More temperature plots for different times can be found in Appendix G.

7.1.2 Glycol return temperature

When comparing the return temperature in Figure 7.4 with the return temperature in CFD-analysis 1, the results are similar. Although the return temperature in this simulation does not reach 99% of its final value, 90% of its final value is reached within one day. When comparing different types of soils in Figure 7.5, it is shown that all the soils reach 90% of its final value within one day. Again, the direct effect of this is the fast decrease of heat flux through the wall. Because of this fast decrease, changing the soil does not influence the return temperature.

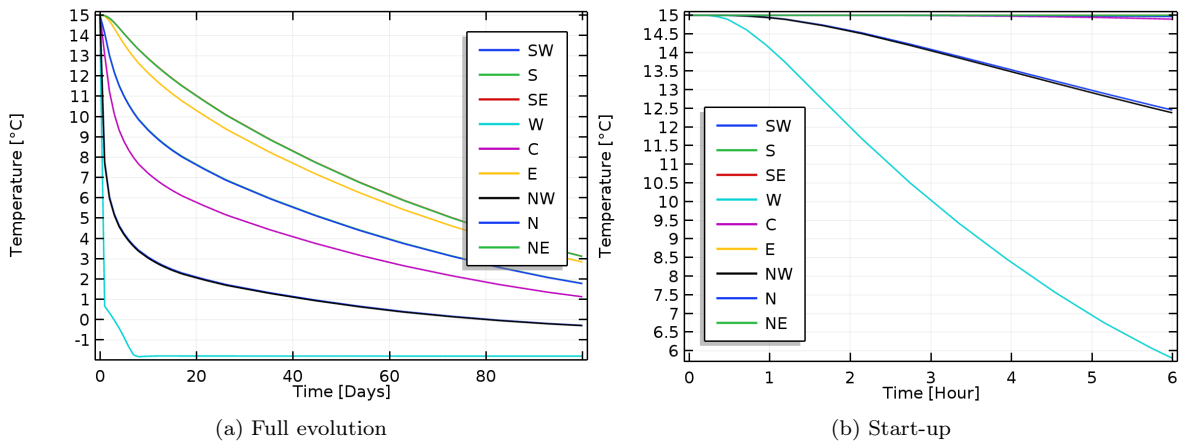


Figure 7.2: Soil temperature (sand) over time

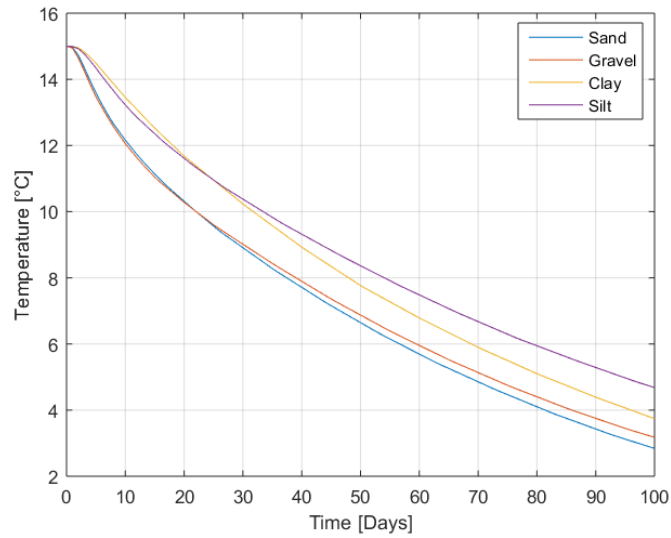


Figure 7.3: Different east soil temperatures over time

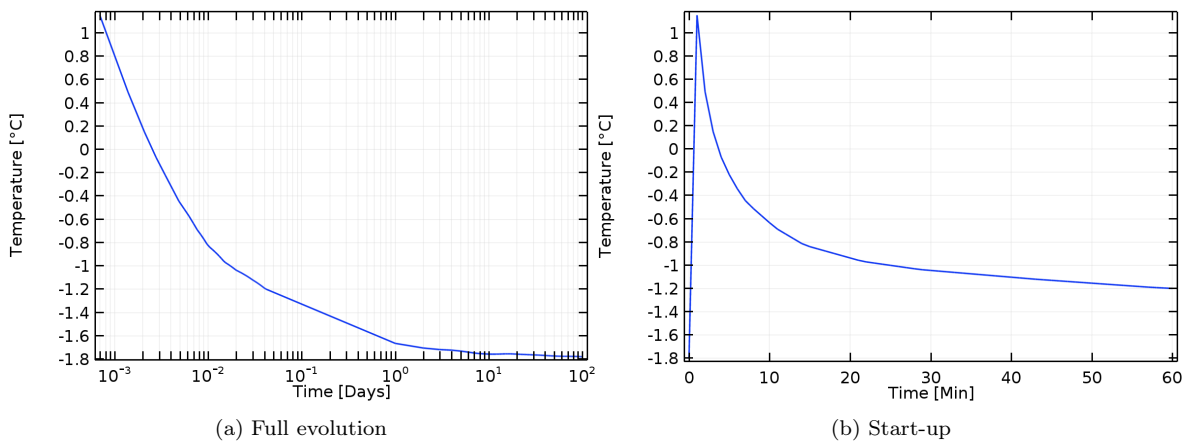


Figure 7.4: Return temperature (sand) over time

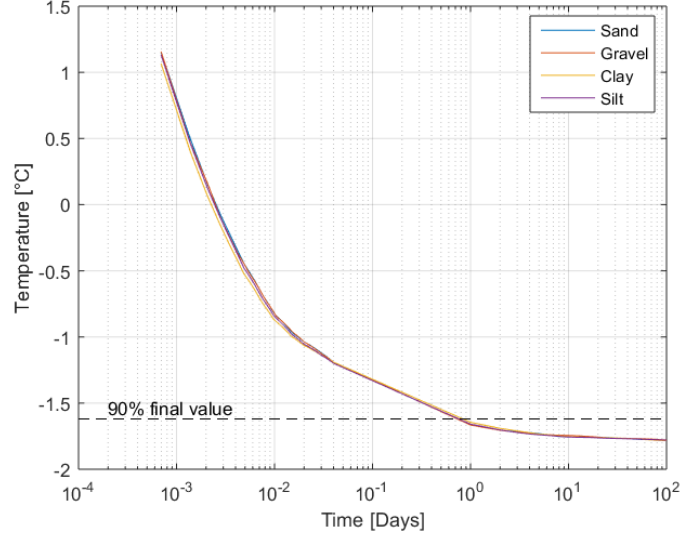


Figure 7.5: Different soil return temperatures over time

7.1.3 Heat flux

The direct effect of the fast decrease of the temperature inside the cylinder is a fast decrease in the heat flux through the wall, which can be seen in Figure 7.6. In Section 7.1 is elaborated that the heat transferred to the wall is defined as:

$$Q = UA\Delta T_{ln} \quad (7.3)$$

With:

$$R = \frac{1}{UA} = \frac{\ln(r_{wall}/r_0)}{2\pi k_{wall}l} + \frac{\ln(r_{soil}/r_{wall})}{2\pi k_{soil}l} \quad (7.4)$$

When rewriting this in the same approach as the first analysis, the ratio of thermal resistance becomes:

$$\begin{aligned} \frac{R}{R_0} &= 1 - \frac{k_{wall}}{k_{soil}} \frac{\ln(r_{wall})}{\ln(r_{wall}/r_0)} + \frac{k_{wall}}{k_{soil}} \frac{1}{\ln(r_{wall}/r_0)} \ln(r_{soil}) \\ &= 1 - \frac{k_{wall}}{(\varphi k_{ice}) + ((1 - \varphi)k_{ground})} \frac{\ln(r_{wall})}{\ln(r_{wall}/r_0)} \\ &\quad + \frac{k_{wall}}{(\varphi k_{ice}) + ((1 - \varphi)k_{ground})} \frac{1}{\ln(r_{wall}/r_0)} \ln(r_{soil}) \end{aligned} \quad (7.5)$$

And when applying the data of Table 2.1 the ratios are:

- $\frac{R_{sand}}{R_0} = 75 + 55\ln(r_{soil})$
- $\frac{R_{gravel}}{R_0} = 76 + 55\ln(r_{soil})$
- $\frac{R_{clay}}{R_0} = 83 + 61\ln(r_{soil})$
- $\frac{R_{silt}}{R_0} = 87 + 64\ln(r_{soil})$

For one meter of frozen ground, the thermal resistance is between the 88 and 101 times higher than the original thermal resistance. Because the thermal conductivity of the soils is lower compared to the thermal conductivity of ice, the values of the thermal resistance are higher compared to the first analysis, in Chapter 6. In this analysis, the thermal resistance was 83 times higher than its original value. In Figure 7.7 it is shown that the heat flux through the wall is, due to these high thermal resistance, halved within seven minutes for all soils (for sand 6.94 min, gravel 6.95 min, clay 6.50 min, and silt 6.66 min). Therefore, the heat flux of the different types of soils does not variate over a longer period of time.

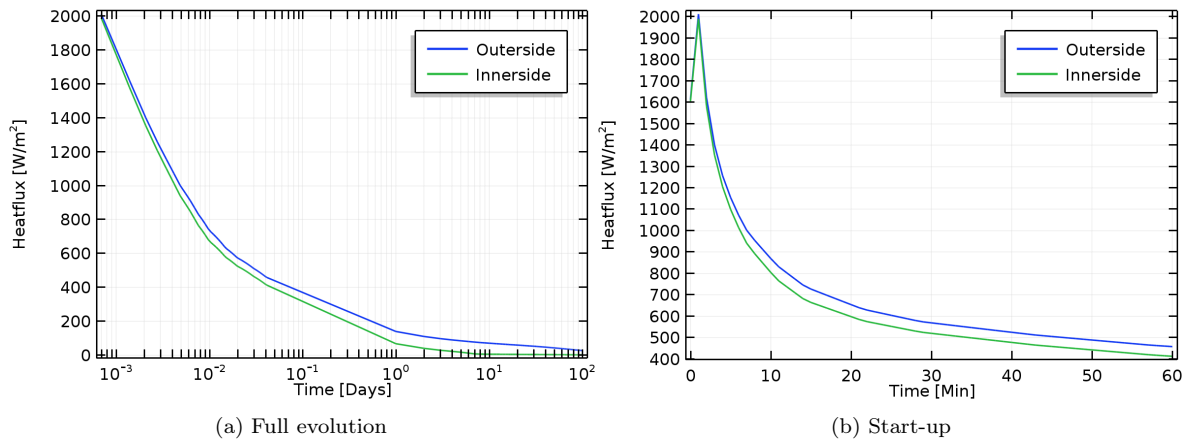


Figure 7.6: Heat flux (sand) through the wall over time

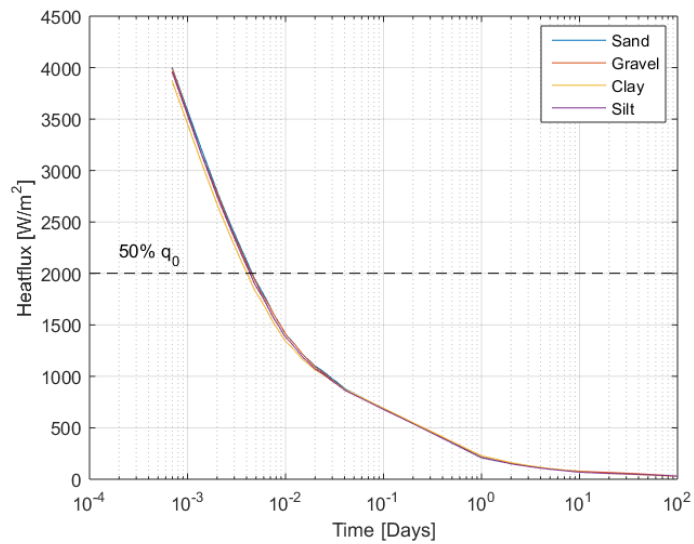


Figure 7.7: Heat flux through the wall over time of different frozen soils

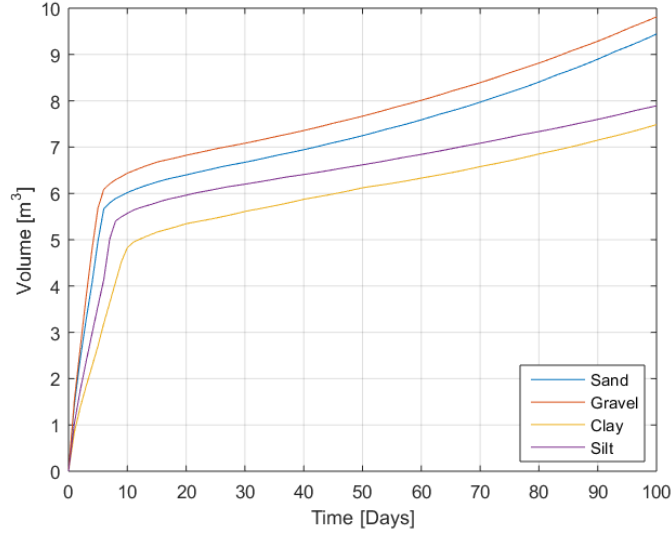


Figure 7.8: Different frozen grounds over time

Table 7.1: Trend lines frozen ground

	Turn point	First part	Second part	r^2
Sand	6 days	$V(t) = 0.843t + 0.691$	$V(t) = 0.036t + 5.565$	0.9859
Gravel	6 days	$V(t) = 0.936t + 0.817$	$V(t) = 0.036t + 5.992$	0.9825
Clay	10 days	$V(t) = 0.447t + 0.475$	$V(t) = 0.026t + 4.779$	0.9906
Silt	8 days	$V(t) = 0.628t + 0.456$	$V(t) = 0.024t + 5.431$	0.9925

7.1.4 Frozen ground volume

When plotting the different volumes of frozen ground against the time in Figure 7.8, the data can be approached by two linear trend lines. This is done in the same way as described in Chapter 6. The equations are represented in Table 7.1 and graphically shown in Figure 7.9. Here, the coefficients of determination show all a very strong correlation.

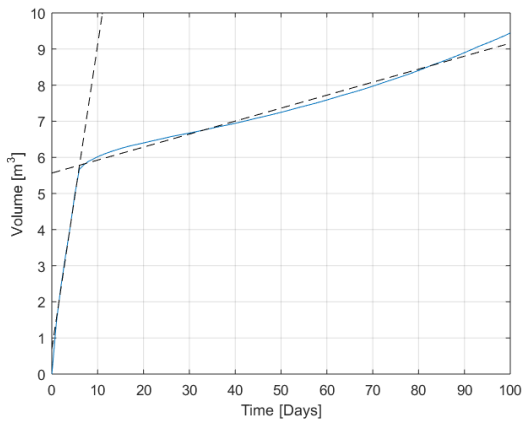
When looking at the trend lines of clay and silt, one can notice that for the first part of the trend line, the frozen volume of the silt ground is increasing faster. In the second part, the frozen volume of clay increases faster. Due to the physical properties of the soils, which do not change, this is not impossible. The reason for this change is, although the trend lines seem linear due to its high coefficient of determination, they are logarithmic over a longer period of time. Because silt is at its turn point closer by its steady-state solution, it will run slower compared to clay. The same is valid for sand and gravel, although this is a much smaller effect. The reason why in the first part clay increases fastest, followed by sand, silt, and clay, can be found at the thermal diffusivity:

$$\alpha_{soil} = (1 - \varphi)\alpha_{ground} + \varphi\alpha_{water} \quad (7.6)$$

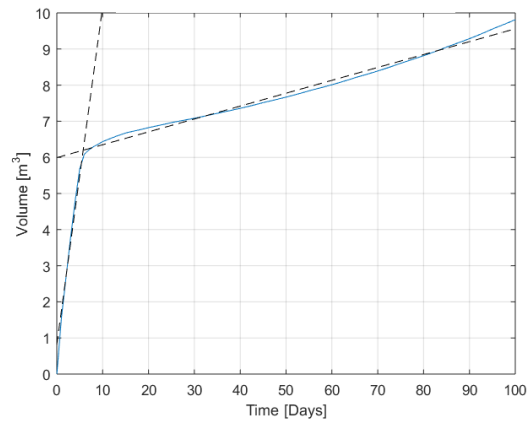
When applying this equation the thermal diffusivity of sand soil is $6.63 \cdot 10^{-7} m^2/s$, of gravel soil $7.05 \cdot 10^{-7} m^2/s$, clay soil $2.88 \cdot 10^{-7} m^2/s$, and silt soil $3.31 \cdot 10^{-7} m^2/s$. This implies that gravel gives its energy the fastest to the glycol and therefore freezes first. After gravel follows sand, silt and finally clay, which is the same order as can be seen in Figure 7.8.

7.1.5 Frozen ground layer thickness

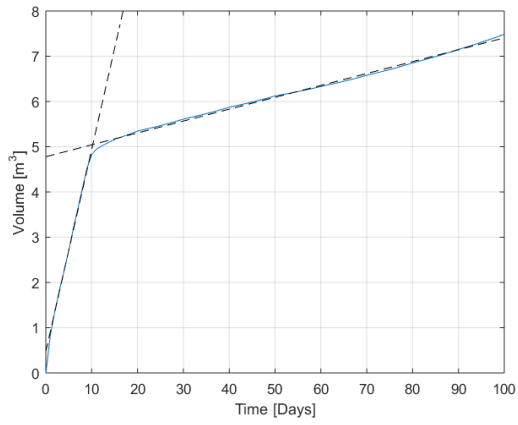
Finally, the frozen ground layer thickness is plotted against the time in Figure 7.10. Again it can be concluded that the frozen layer grows similar to an oval, with the largest thickness in the middle of the cylinder.



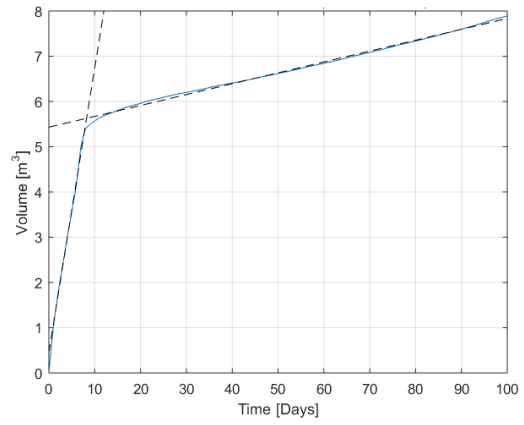
(a) Sand



(b) Gravel



(c) Clay



(d) Silt

Figure 7.9: Different frozen grounds with trend line

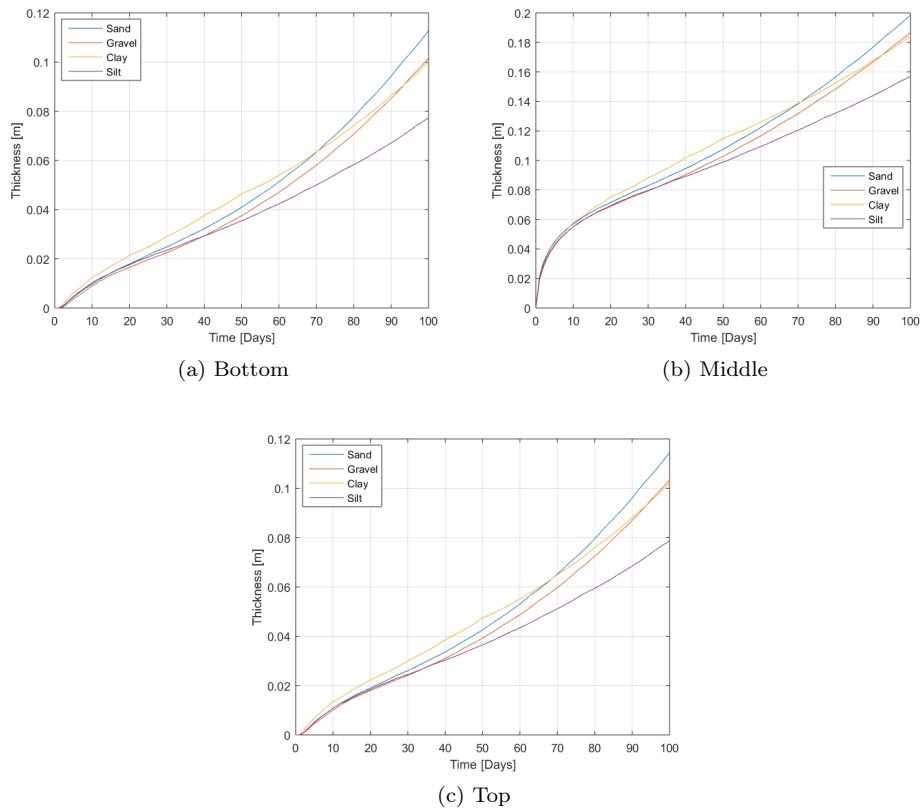


Figure 7.10: Frozen ground thickness (measured from outside cool element) over time

To give an answer on the two research questions, stated in Chapter 3. The return temperature after a hundred days is $-1.7793^{\circ}C$ for sand, $-1.7790^{\circ}C$ for gravel, $-1.7834^{\circ}C$ for clay and $-1.7800^{\circ}C$ for silt (see Figure 7.4). This is in the same range as the return temperature found in the first CFD-analysis. The frozen ground thickness in the middle of the cylinder is, according to Figure 7.10, after a hundred days 0.20 meter for sand, 0.19 meter for gravel, 0.18 meter for clay and 0.16 meter for silt. Due to the higher R/R_0 value, the frozen ground thickness is less, compared to the first calculation. Here the thickness was 0.24 meter. The most optimal ground to apply the natural heat column in practice is sand or gravel. These grounds have the lowest thermal resistance and they show the fastest decrease in temperature. Still, the problem remains that the heat transfer through the wall is almost directly equal to zero. In the next analysis, this problem will be solved.

7.2 Optimization

In the previous section, the result for the natural heat column is discussed. In the analysis was concluded that the glycol was not able to transfer its energy to the surroundings. A schematic representation of this problem is shown in Figure 7.11, here the glycol will heat up from the inlet temperature to a specific temperature. This will be done by freezing the ground which gives it energy through the wall to the glycol. This heat transfer can be calculated by:

$$Q = UA\Delta T_{ln} \quad (7.7)$$

With:

$$\Delta T_{ln} = \frac{(T_{ice} - T_{in}) - (T_{ice} - T_{out})}{\ln\left(\frac{T_{ice} - T_{in}}{T_{ice} - T_{out}}\right)} \quad (7.8)$$

After substituting $T_{out} - T_{in} = \frac{Q}{mc_p}$, this equation becomes:

$$T_{out} = T_{ice} - (T_{ice} - T_{in})e^{-\frac{UA}{mc_p}} \quad (7.9)$$

With $\frac{UA}{mc_p}$ as dimensionless heat resistance, which represents the resistance between the transferred heat and the incoming heat. Out of this energy equation follows: the larger the temperature difference between T_{out} and T_{in} , the more energy is transferred by the wall. This temperature difference can be accomplished by:

- Increasing the heat exchange surface by placing more natural heat columns on top of each other.
- Increasing the temperature difference by changing the glycol inlet temperature.
- Increasing the melting temperature of ice by changing the soil composition with the help of chemicals.
- Increasing the thermal conductivity of the soil by changing the soil composition.
- Decreasing the frozen soil layer by regenerating.
- Decreasing the glycol inlet velocity, to reduce the mass flow.
- Decreasing the average temperature, to decrease the average specific heat.

To investigate what the effect will be of each of these measurements, a parametric study will be performed for both the mass flow and the temperature of glycol. Furthermore, the minimum required space of the natural heat column will be calculated, to see if more columns can be placed on top of each other. Finally, the effects of regenerating will be elaborated.

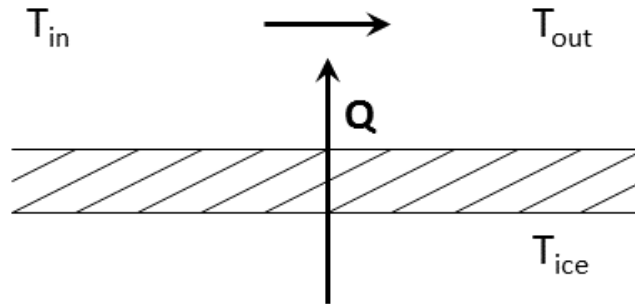


Figure 7.11: Schematic representation of the heat transfer over the wall

7.2.1 Parametric study inlet temperature

In Figure 7.12 the result of the parametric study are represented. This study is analyzed with Comsol, and has the purpose to declare the results which were obtained in Section 7.1. In Figure 7.12, the inlet glycol temperature is varied between 50% and 150% of its original value, with a step size of 10%. This means the glycol inlet temperature is varied with a temperature between $-2.7^{\circ}C$ and $-0.9^{\circ}C$ with a step size of $-0.18^{\circ}C$. When investigating the results there it can be concluded that the frozen ground volume increases when the inlet temperature decreases. These results show a linear correlation, because:

$$T_{out} = T_{ice} - (T_{ice} - T_{in})e^{-\frac{UA}{mc_p}} \quad (7.10)$$

And:

$$Q = \varphi_m c_p (T_{out} - T_{in}) \quad (7.11)$$

So:

$$Q = \varphi_m c_p (1 - e^{-\frac{UA}{mc_p}})(T_{ice} - T_{in}) \quad (7.12)$$

The volume of frozen ground is calculated by:

$$\frac{dV}{dt} = \frac{m_{ice}}{\rho} = \frac{Q}{\rho h_f} \quad (7.13)$$

When substituting both equations, the final equation for the frozen ground rate becomes:

$$\frac{dV}{dt} = \frac{\varphi_m c_p (1 - e^{-\frac{UA}{mc_p}})}{\rho h_f} (T_{ice} - T_{in}) \quad (7.14)$$

Or shortly:

$$\frac{dV}{dt} = -\alpha (T_{ice} - T_{in}) \quad (7.15)$$

Where α is a constant.

In Figure 7.13 a it is shown that the volume rate of frozen ground is almost constant. In the begin the volume rate fluctuate heavily, the reason for this can be found in in the thermal resistance of the wall:

$$R = \frac{1}{UA} = \frac{\ln(r_{wall}/r_0)}{2\pi k_{wall}l} + \frac{\ln(r_{soil}/r_{wall})}{2\pi k_{soil}l} \quad (7.16)$$

In the first part of the CFD-analysis, r_{soil} increase rapidly, which cause a fluctuation in the overall equation. When plotting the volume frozen ground over the in the glycol inlet temperature, in Figure 7.13 b, there it can be concluded that the frozen ground volume is directly negative proportional with the glycol inlet temperature.

7.2.2 Parametric study glycol mass flow

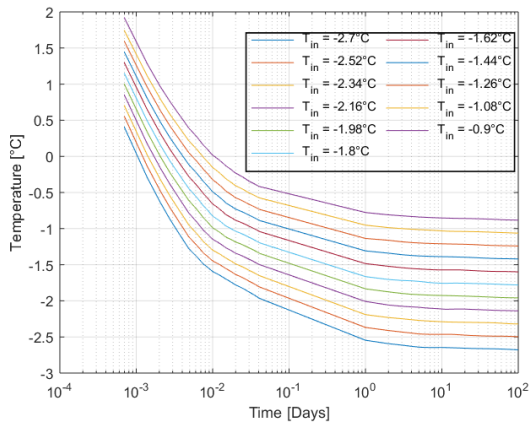
In the same way as the inlet temperature, a parametric study is done of the glycol mass flow. The results are represented in Figure 7.14. In this case, the glycol mass flow is varied between 70% and 150% of its original value, with a step size of 10%. When investigating the results, it can be concluded that the results do not change significantly. This can be explained by:

$$Q = mc_p (1 - e^{-\frac{UA}{mc_p}})(T_{ice} - T_{in}) \quad (7.17)$$

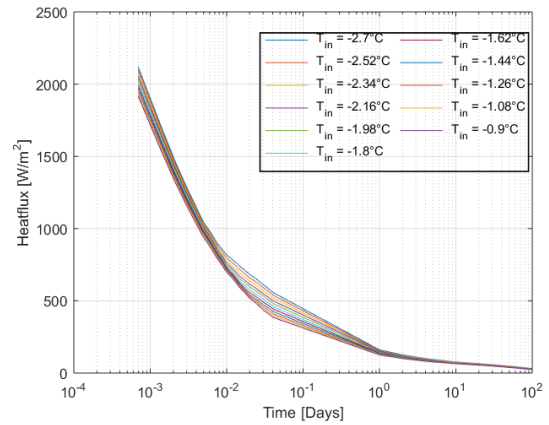
When the mass flow is going to infinity, it can be concluded that the heat flux reaches an asymptote (for full derivation, see Appendix H):

$$\lim_{m \rightarrow \infty} Q(m) = UA(T_{ice} - T_{in}) \quad (7.18)$$

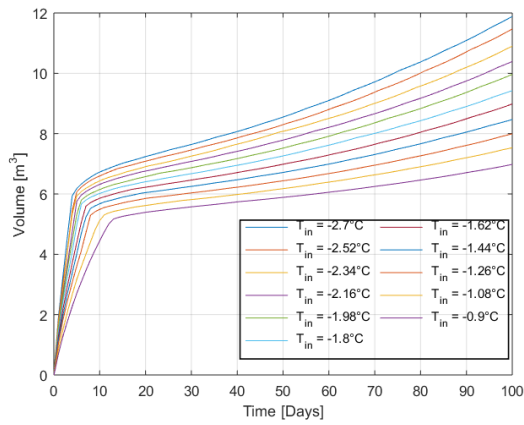
And therefore, the limit of Q has almost been reached. This explains why the results do not vary. When decreasing the mass flow significantly, the transferred heat will decrease as well. When increasing the mass flow, the transferred heat will remain the same, because the limit has already been reached. This is graphically represented in Figure 7.15.



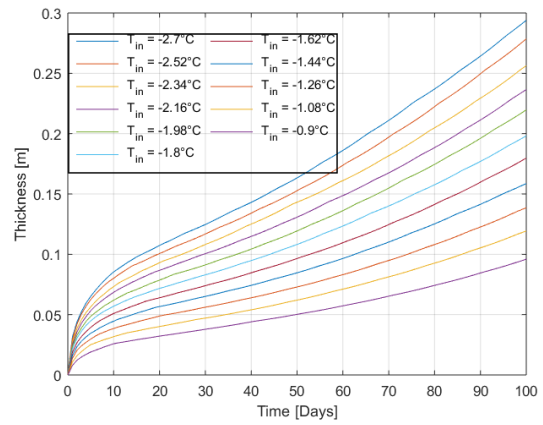
(a) Parametric study of the return temperature



(b) Parametric study of heatflux through the outer side wall

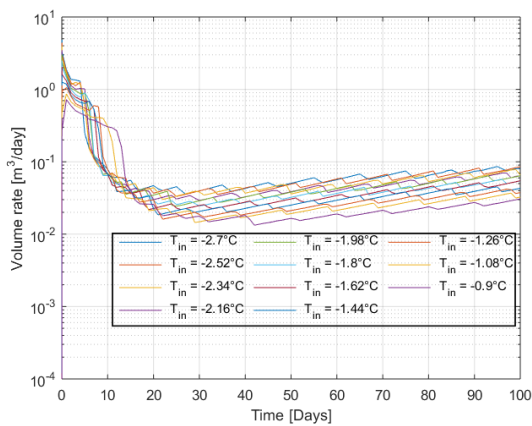


(c) Parametric study of frozen soil ground

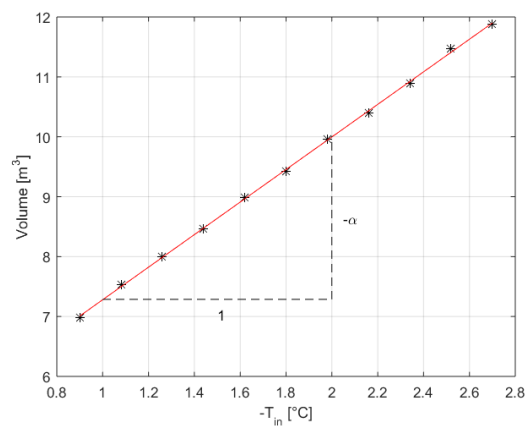


(d) Parametric study of frozen ground thickness at middle

Figure 7.12: Parametric study by changing inlet temperature (sand)

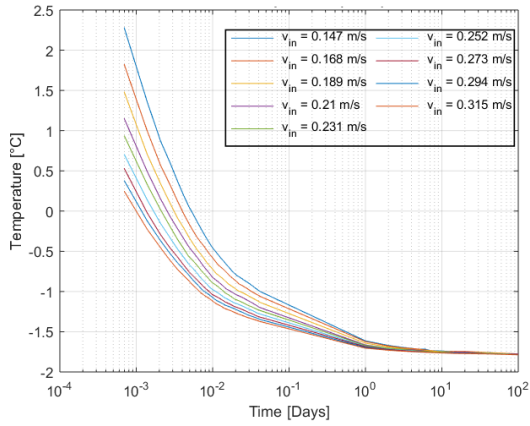


(a) Volume rate

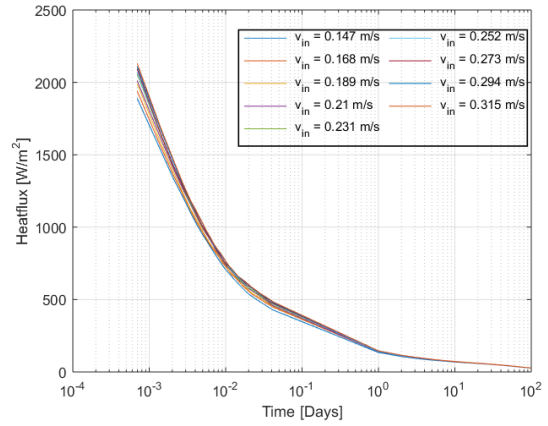


(b) Growth rate at 100 days

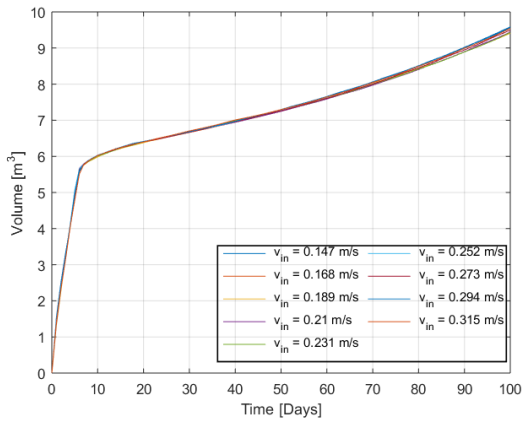
Figure 7.13: Parametric study of volume frozen ground by changing inlet temperature (Sand)



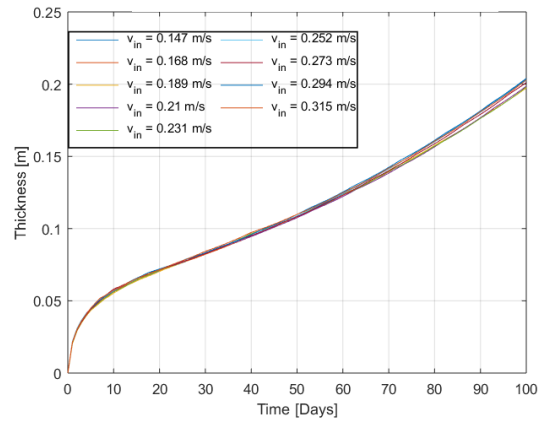
(a) Parametric study of the return temperature



(b) Parametric study of heatflux through the outer side wall



(c) Parametric study of frozen soil ground



(d) Parametric study of frozen ground thickness at middle

Figure 7.14: Parametric study by changing mass flow (sand)

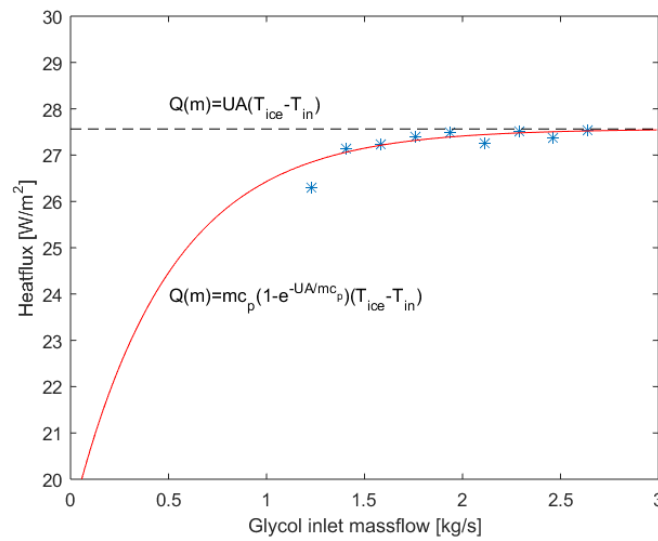
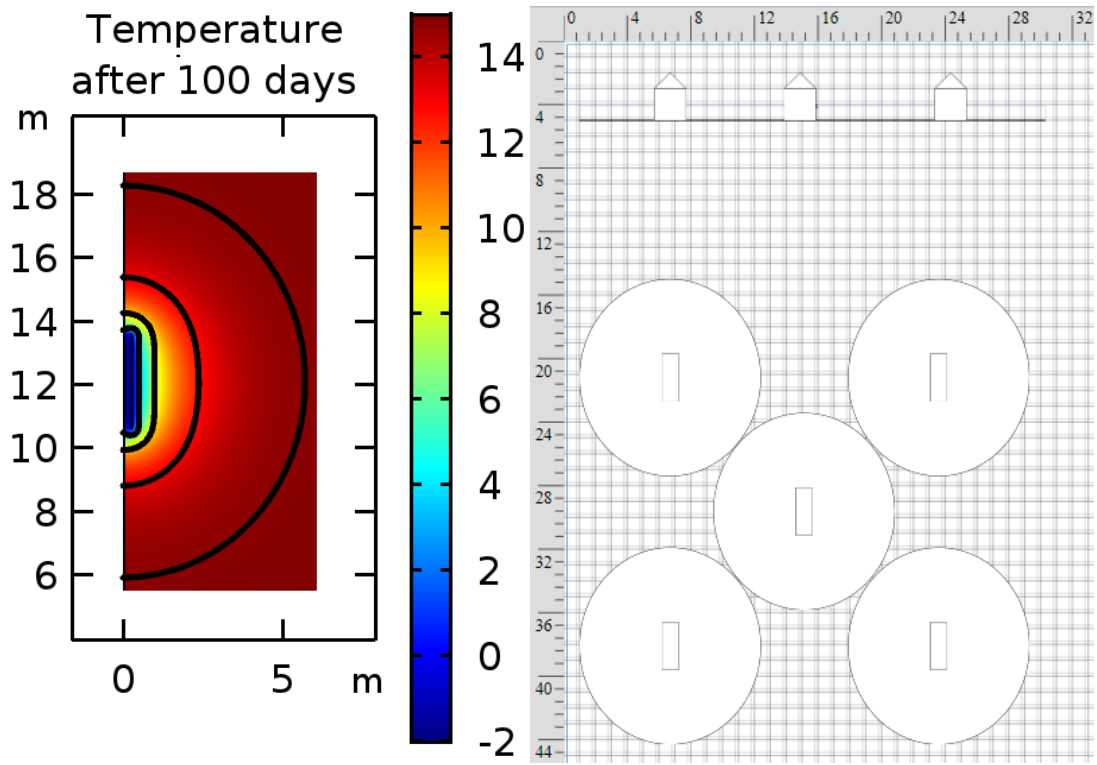


Figure 7.15: Visual graph of heat transfer by changing glycol mass flow



(a) Isothermal lines of natural heat column for $T = 14.832^\circ\text{C}$ at 0.1, 1, 10 and 100 days (b) Graphical representation of the location of multiple natural heat columns

Figure 7.16: Thermal range of the natural heat column

7.2.3 Minimum required area

The most pragmatic way of extracting more energy out of the natural heat column is to put multiple columns on top of each other. When this is done, the heat exchange surface, and therefore the transferred heat, is doubled. To do this, there is a need to investigate what the minimum required space is for the natural heat column, in a way that they do not interfere with each other. In Figure 7.16 a the natural heat column is simulated in a large volume of sand soil. The four black lines represent the isothermal lines for 14.832°C at 0.1 days, 1 day, 10 days and 100 days. The reason why is chosen for 14.832°C and not the initial ground temperature of 15°C , is because there is always a small temperature drop in the soil. So when the temperature would be 15°C , the isothermal lines became infinitely large. 14.832°C is the temperature which represents 99% of the dimensionless temperature $T^* = \frac{T_{soil} - T_\infty}{T_0 - T_\infty} \rightarrow T_{soil} = T_\infty + T^*(T_0 - T_\infty) = -1.8 + 0.99(15 + 1.8) = 14.832^\circ\text{C}$.

Figure 7.16 a shows the isotherm of a hundred days is 4.7 meters away from the top and bottom of the cylinder. So when two cylinders are placed on top of each other, the minimum distance will be 9.4 meters.

Furthermore, it can be concluded from Figure 7.16 a that the isotherm is maximal 5.7 meters away from the middle of the cylinder. So when there are two cylinders placed next to each other, the minimum distance will be 11.4 meters. The ground area of one cylinder is, therefore, 102m^2 . In Section 2.1 is stated that an average Dutch house has a usable ground area between fifty and a hundred square meters. Therefore, the natural heat column is not suitable in this setup. When the natural heat columns are placed 45° of each other, the minimum distance will be 8.06 meter and the ground area of one cylinder is, therefore, 51m^2 . This is more suitable for a Dutch household. However, the natural heat column will be 8.06 meter lower than its neighbor. A graphical representation of this is illustrated in Figure 7.16 b.

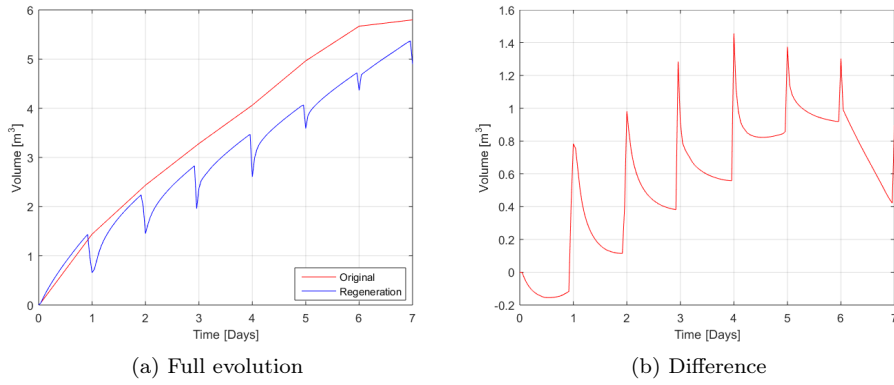


Figure 7.17: Regeneration of frozen sand soil ground

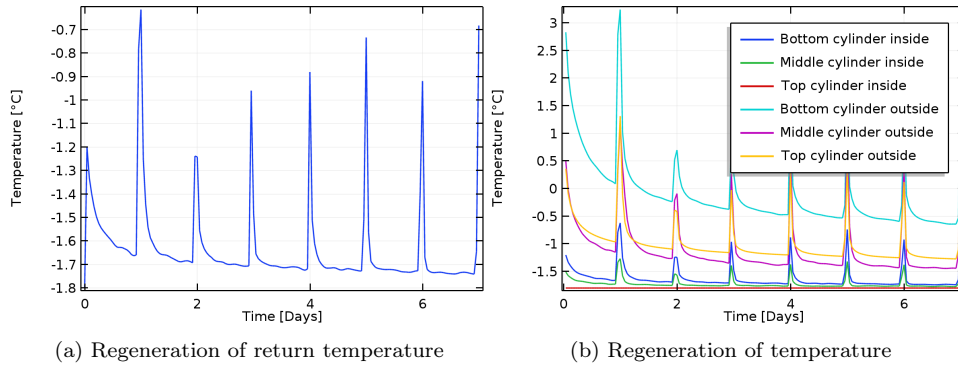


Figure 7.18: Regeneration temperature

7.2.4 Trace heating

Another solution for the poor heat conduction through the frozen soil is to regenerate the system. By regenerating, a heat source adds power to the natural heat column. Here the frozen soil near the walls will melt and the natural heat column can again deliver its power. In the simulation, the decision was made to regenerate with the help of trace heating. Trace heating cables are electrical heating elements which maintain an equipment (e.g. a pipe) on a certain temperature. It is wrapped around the cylinder and is easier to control. The heat comes from a standard 230 voltage system. With a certain electrical resistance, this voltage is transferred into heat [37]. The reason why is chosen for this setup is strictly for convenience reasons. This setup is easy to understand and the results are easy to implement. In reality, it is highly unsustainable and inefficient to use electricity (which has a high exergy density) for regenerating the ground (which has a low exergy density).

In this simulation the decision was made to add every day $1000W/m^2$ of electrical energy for the period one hour, this can be done during night time when the cost of electricity is lower. In Figure 7.17 a is the regeneration in sand soil compared to the original case for the time period for one week. Figure 7.17 b shows what the difference is between the two cases is after four days almost $1.5m^3$. However these results are significant, there will be investigated what the losses are of this mechanism. In Figure 7.18 a, not only the surrounding soil is heated but also the glycol. After the first regeneration, the glycol is almost $1^\circ C$ higher than before the regeneration. This can be a loss because the electrical energy is directly used to heat the glycol and not for melting the ground (which was supposed to happen). When comparing the temperatures close to inside and outside of the cylinder wall (see Figure 7.18 b), the frozen soil temperatures give a higher temperature difference by regeneration, compared to the glycol inside the cylinder. This indicates that there is no significant loss of the electrical trace heat.

Chapter 8

CFD-analysis 3: Natural heat column with active regeneration (daily storage)

In the previous analysis, as described in Chapter 7, is concluded that the natural heat column is not suitable for seasonal storage. This is due to the low thermal conductivity of ice. To investigate the natural heat column further, the aim of the research will be shifted from seasonal storage to daily storage. In Figure 8.1 is the typical energy demand of a Dutch household represented. This figure shows a morning and an evening peak demand. When the amount of thermal solar power is at its maximum, there is a low demand for energy. Therefore, the purpose of the natural heat column is to store this energy for the evening demand. This will result in a significantly smaller layer of frozen ground around the natural heat column and therefore, the insulating effect of ice will be interfering less.

To calculate the net heat demand of the natural heat column. The energy at the evaporator side of the heat pump is calculated by:

$$Q_{demand} = f_{load} \cdot V \cdot LHV \cdot \left(1 - \frac{1}{COP}\right) \quad (8.1)$$

Where f_{load} the intermittency load fraction is, which is represented in Figure 8.2 a [38]. Furthermore, the load is $1500m^3/year$ and the heating value of gas $31.67MJ/m^3$. As stated in Chapter 5, the coefficient of performance of the heat pump is 4.33. In this analysis is assumed that the average load fraction is equal to the average of all the working days (Monday till Friday) in December. This, because December is the month with the least amount of solar hours and therefore the most critical. Furthermore, there is investigated that there are no deviating days in this time period.

The net heat supply is defined as:

$$Q_{supply} = E_e \cdot A \cdot \eta \quad (8.2)$$

Where E_e the average solar radiation is, measured in December 2017 [39]. The thermal efficiency of the solar collector is 40% [4]. Finally, as a first assumption, there is an area of forty square meters with solar collectors. In this assumption, the supply meets the demand.

Finally, to calculate the final demand for the natural heat column, three scenarios are possible. Firstly, when the heat demand is smaller than five megajoules, there is assumed that a modern house can remain its heat and the final demand will be equal to zero. Secondly, when the heat demand is larger than the supply, the final demand is equal to this heat demand. Lastly, when the supply is larger than the demand, the supply is subtracted. This is shown in Figure 8.2 b. The black dashed line is an approximation line which will be used in this third analysis. In this line can four regimes be defined:

- Morning regime – from 6:00 to 10:00
During the morning regime the heat demand is high, furthermore, the solar energy supply is low. This will result in ice forming around the natural heat column.
- Afternoon regime – from 10:00 to 16:00
During the afternoon regime, the solar energy supply exceeds the energy demand. The remaining heat, originating from the thermal solar collectors, will be used to regenerate the system actively. This will be done by melting the frozen ice, which was formed during the morning regime.

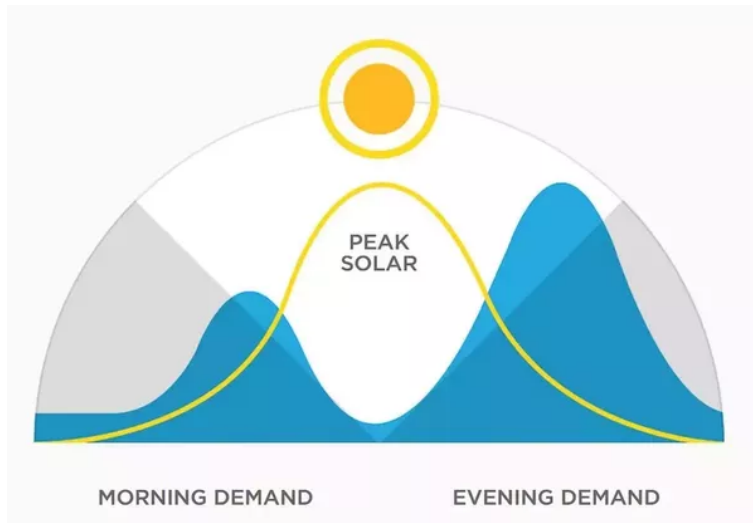
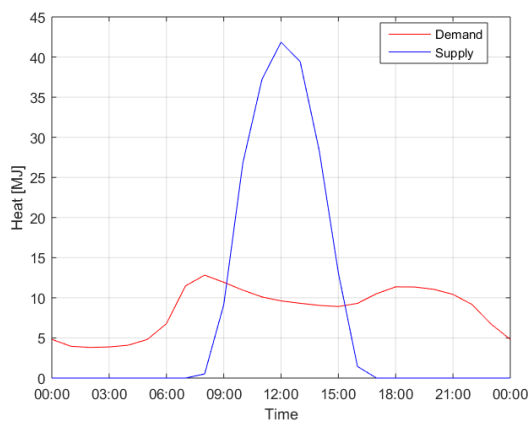
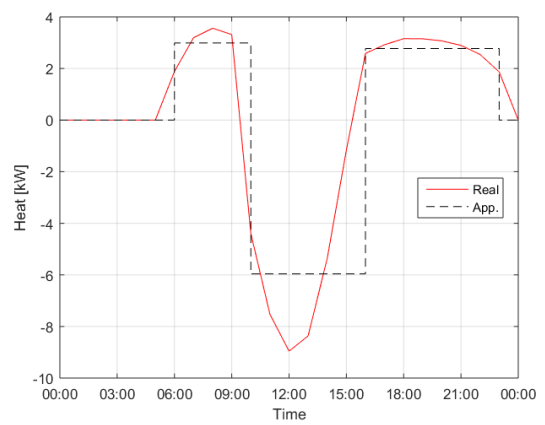


Figure 8.1: Intermittency in households energy demand and supply



(a) Demand and supply



(b) Net demand curve

Figure 8.2: Heat demand and supply for a typical December day

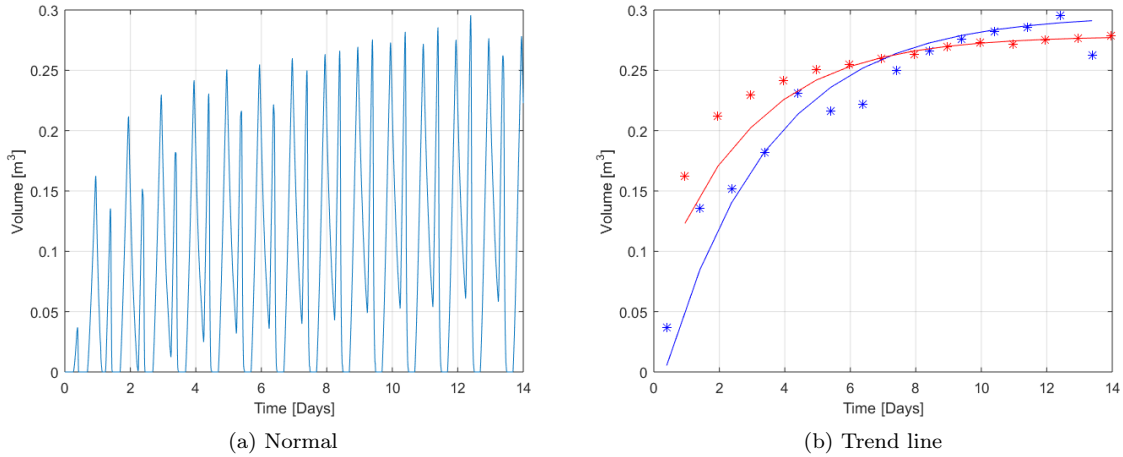


Figure 8.3: Start-up frozen ground (sand) over time

- Evening regime – from 16:00 to 23:00
During the evening regime the heat demand is high again, therefore the natural heat column will extract heat from the ground and the groundwater will freeze again.
- Night regime – from 23:00 to 6:00
During the night regime, both the demand and supply are low. During this time the ground heat will melt the ice. Although this is a slow process, the night regime is significantly large.

Again, in this third analysis, the answer will be found for the research questions which were proposed at the beginning of Chapter 3:

- What will be the refrigerant return temperature as a function over time?
- What will be the ice layer thickness as a function over time?

Furthermore, to promote the energy transfer by adding more heating area, the creator of the natural heat column has demanded to shift the length of the cylinder from one column of three meters to two columns seven meters. With a gap between the columns of one meter. This configuration is applied in this new CFD-analysis. The mesh of this analysis contains minimal ten elements over the width of the cylinder and minimal ten elements over the width of the surroundings. The only difference with the mesh described in Chapter 4, is that due to the increased length the ratio of the height elements inside of the cylinder is ten times larger than elements over the width of the cylinder. Detailed information and the results of this mesh convergence study can be found in Appendix I. In this chapter the results of the third CFD-analysis will be discussed, furthermore, the performances of the different types of soil will be investigated.

8.1 Simulation results

Before discussing the results of CFD-analysis 3, the start-up effects have to be defined. Initially, the ground temperature is 10.5°C . When storing and regenerating energy into the ground, this temperature will change. In Figure 8.3 a the volume of ice is represented over time. After two weeks there is assumed that the initial condition is reached, and the volume of frozen ground over a single day is constant. In Figure 8.4 the temperature plot after two weeks is represented, this temperature plot is used as initial condition for this third analysis.

When plotting the peaks of the morning and evening demand over time, it can be concluded that there is an exponential correlation in the form of:

$$V(t) = c(1 - e^{b-at}) \quad (8.3)$$

When modifying this to:

$$\ln\left(1 - \frac{V(t)}{c}\right) = b - at \quad (8.4)$$

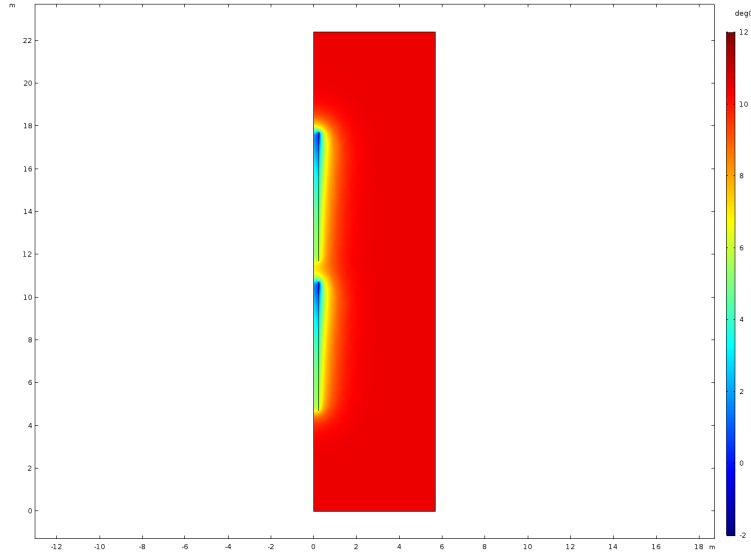


Figure 8.4: Temperature plot after fourteen days (initial condition)

The equation is suitable for least square regression (see Chapter 6). As shown in Figure 8.3 b the morning peak has an approximation of:

$$V(t) = 0.296(1 - e^{0.105}e^{-0.315t}) \quad (8.5)$$

Which is with a coefficient of determination of $r^2 = 0.9064$ very strong. The evening peak has an approximation of:

$$V(t) = 0.279(1 - e^{-0.442}e^{-0.360t}) \quad (8.6)$$

Which is with a coefficient of determination of $r^2 = 0.676$ still strong.

The simulation has run for one day with the initial conditions of the end of day fourteen and a time step of five minutes. It took Comsol 1 hour, 13 minutes and 56 seconds to solve the calculations. Again the solver PARDISO is used.

8.1.1 Boundary heat flux

Before evaluating the different results, there is mentioned that the boundary condition of the open boundary is changed to a fixed temperature boundary of $10.5^\circ C$. This modification is applied to make the analysis suitable for regeneration during nighttime, and it is only allowed when there is no heat flux added to the system. The temperature near the outer wall stays constant. In Figure 8.5 can be seen that the heat flux to the system is negligibly small and therefore this can be applied.

8.1.2 Soil temperature

When investigating the ground temperature, measured one millimeter from the cylinder. The results of Figure 8.6 a are obtained. There is immediately shown that the day is cyclic and therefore the steady state, as described earlier, is reached. Moreover, from Figure 8.7 it can be noticed that the latent heat transfer only takes place at the top of the cylinder. Here the temperature of the glycol inside the cylinder is at its colds. At the other measures points, the heat transfer takes only place as sensible heat. The ratio of latent heat over the total heat is during the morning peak 51% and during the evening peak 29%. This efficiency is defined as:

$$\eta_{lat} = \frac{Q_{lat}}{Q_{tot}} = \frac{Q_{lat}}{Q_{lat} + Q_{sens}} \quad (8.7)$$

An explanation of why the morning peak has a higher rate of latent heat is because the soil temperature at the beginning of the morning peak is lower in comparison with the beginning of the evening peak. Therefore, the temperature is closer to the freezing temperature and less sensible heat is needed to reach this point. (as seen in Figure 8.6).

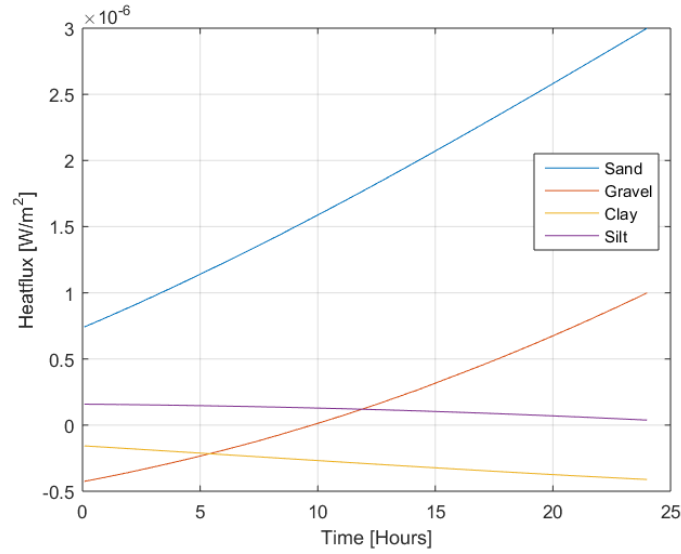


Figure 8.5: Different soil heat flux added to the system over time

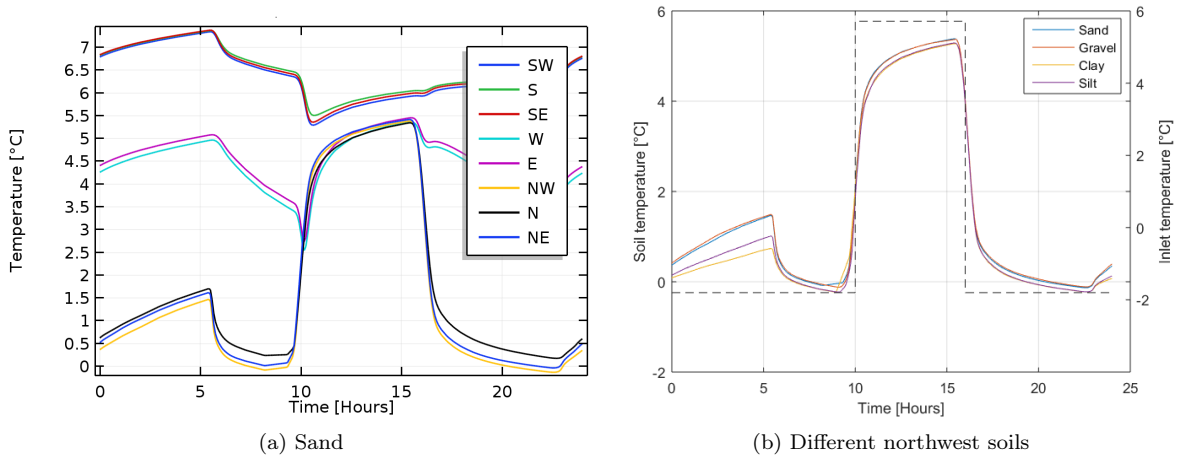


Figure 8.6: Soil temperature over time

Figure 8.6 b shows for the top of the cylinder that all the soils respond in the same way, according to the glycol inlet temperature. Through the higher thermal diffusivity of sand and gravel (see Chapter 7), they respond slightly faster, however, this is almost negligible. More temperature plots for different times can be found in Appendix J and Appendix K.

8.1.3 Glycol return temperature

The glycol return temperature, which is represented in Figure 8.8, is constant between the temperatures of 3.5°C and 7.5°C and is strongly dependent on the glycol inlet temperature. Although the different soils have the same temperature range, sand and gravel have, due to their higher thermal diffusivity, a higher average temperature. Therefore, sand and gravel show a better heat transfer during the start-up period of the natural heat column. This effect is shown in Figure 8.9.

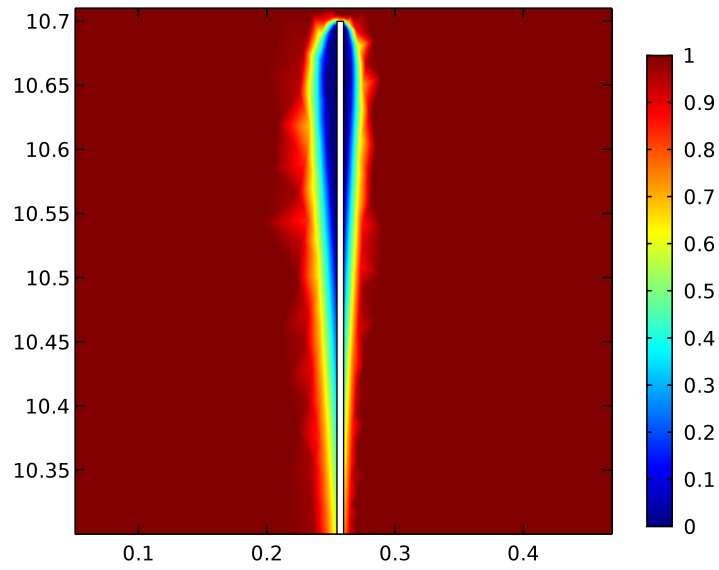


Figure 8.7: 2D plot of phase change (0 = ice)

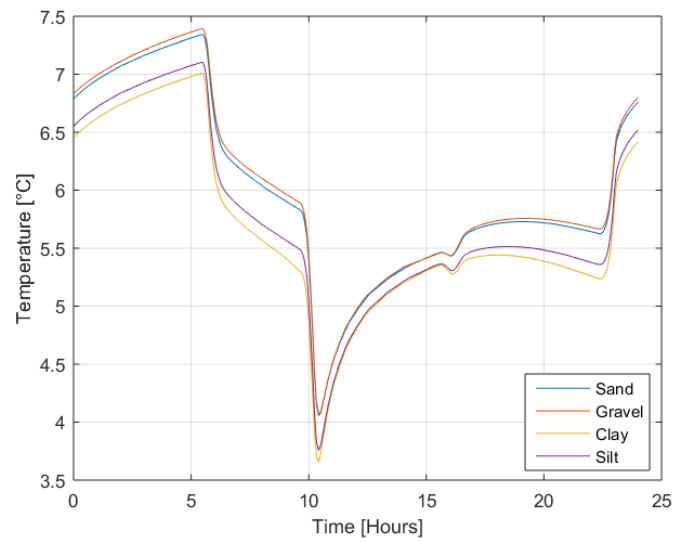


Figure 8.8: Different soil return temperatures over time

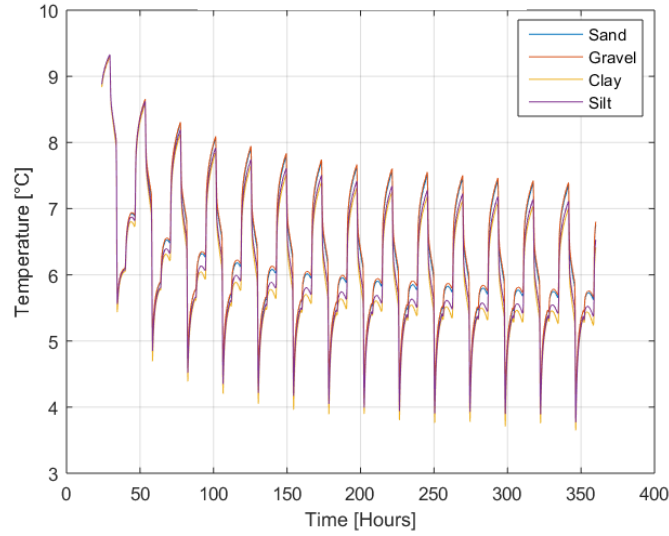


Figure 8.9: Different soil return temperatures over their start-up time

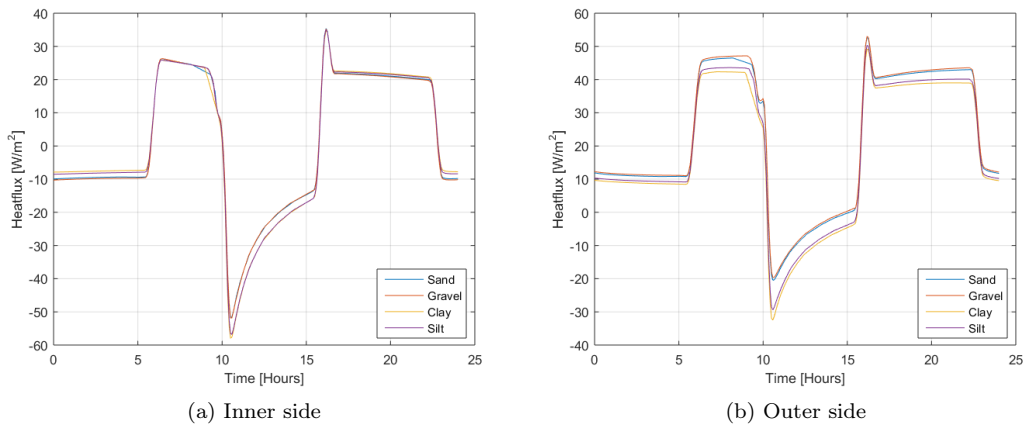


Figure 8.10: Different soil heat flux through the wall over time

8.1.4 Heat flux

In Figure 8.10 can be seen that due to the lower average return temperature of clay and silt, the heat they transfer is smaller. This follows out the equation:

$$Q = UA\Delta T_{ln} \quad (8.8)$$

Furthermore, in Figure 8.10 can be seen that the heat transfer at the inner side of the cylinder is lower, compared with the outer side. This is due to the geometry where in the middle of the cylinder the temperature is lower because the heat is added from two sides. This is physically represented in Figure 8.7. By shifting from seasonal storage to daily storage the heat transfer ratio is improved. This, due to the small frozen ground layer, where $\frac{R}{R_0}$ becomes close to one.

8.1.5 Frozen ground volume

In Figure 8.11, the volume of ice is plotted over time. Here it can be concluded that during the regeneration with the solar collector all the frozen ground is molten. Therefore, an amount of forty square meters solar collector is sufficient. During the morning peak, there will freeze an amount between $0.22m^3$ for clay and $0.35m^3$ for gravel of ice. During the evening peak, this is between $0.19m^3$ for clay and $0.33m^3$ for gravel. Unfortunately, during nighttime, the ground will not regenerate all of the frozen soil.

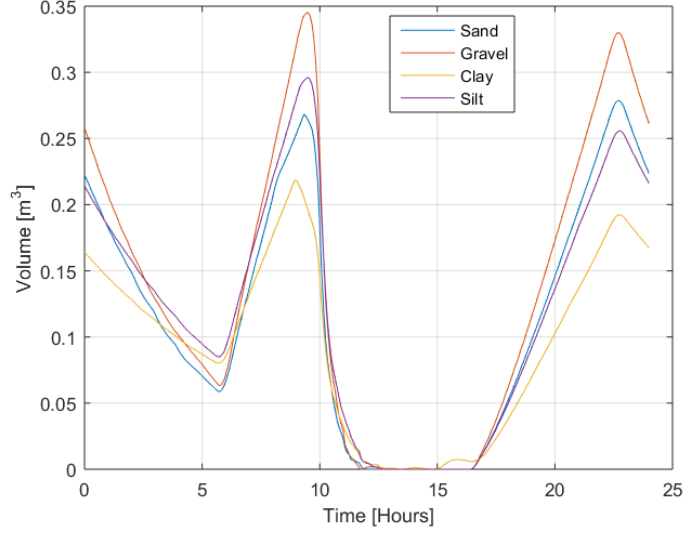


Figure 8.11: Different frozen grounds over time

Table 8.1: Trend lines frozen ground

	Morning peak Trend line	r^2	Evening peak Trend line	r^2
Sand	$V(t) = 0.0594t - 0.2741$	0.9884	$V(t) = 0.0476t - 0.8043$	0.9981
Gravel	$V(t) = 0.0812t - 0.4114$	0.9999	$V(t) = 0.0564t - 0.9526$	0.9980
Clay	$V(t) = 0.0444t - 0.1783$	0.9996	$V(t) = 0.0325t - 0.5475$	0.9990
Silt	$V(t) = 0.0611t - 0.2702$	0.9998	$V(t) = 0.0436t - 0.7350$	0.9988

For the evening peak it can be concluded that gravel has the most volume of frozen ground, followed by sand, silt, and clay. This is due to the physical properties of the soil which was concluded in Chapter 7.

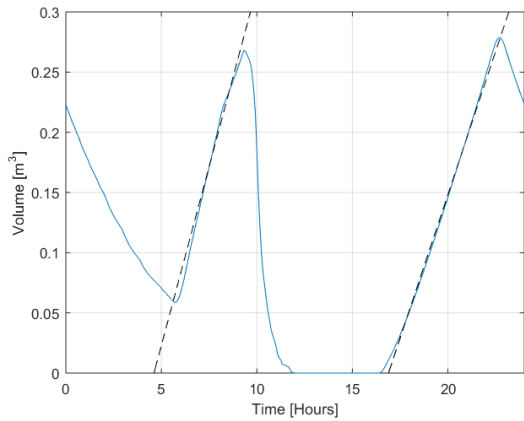
In the same way as the previous analysis, the volume of frozen soil can be analyzed with the least square regression method. The equations are represented in Table 8.1 and are graphically shown in Figure 8.12. Out of this data can be seen that the coefficient of determination, r^2 , is high and that the correlation is very strong until almost perfect [36]. On average the trend lines show an ice forming velocity of $0.9L/min$, which is a factor ten less than an average household shower [40]. Furthermore, there is reminded that in Chapter 7 is elaborated that the lines, in reality, are not linear, but logarithmic. Therefore, the trend lines of the morning peak are slightly steeper than the trend lines of the evening peak. This because the lines in the morning peak are closer to its steady state condition.

8.1.6 Frozen ground layer thickness and height

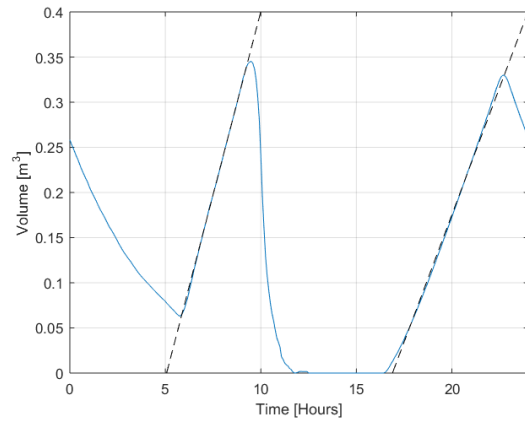
Finally the frozen ground layer thickness is plotted against the time in Figure 8.13. Different from the previous CFD-analysis is that there is only a small frozen ground layer at the top. At the middle and bottom of the cool element, there is no forming of frozen ground. This is due to the shifting from seasonal storage to daily storage. Furthermore, it can be noticed that the frozen ground is significantly larger at the inner side of the cool element. This is due to the fact the inner side has also the effect of the other side of the cylinder.

When assuming that the frozen ground layer at the top is the maximum ice thickness layer and the ice decreases linearly. The volume of the frozen ground layer can be expressed as a function of the height and the radius by the following equation (the derivation can be found in Appendix L):

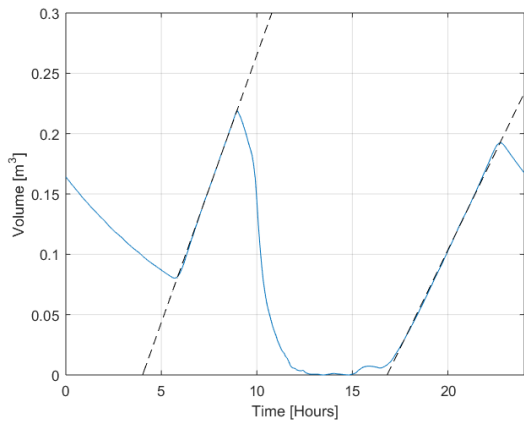
$$h = \frac{3V}{\pi((R - r_{out})(R + 2r_{out}) + (r_{in} - R')(2r_{in} + R'))} \quad (8.9)$$



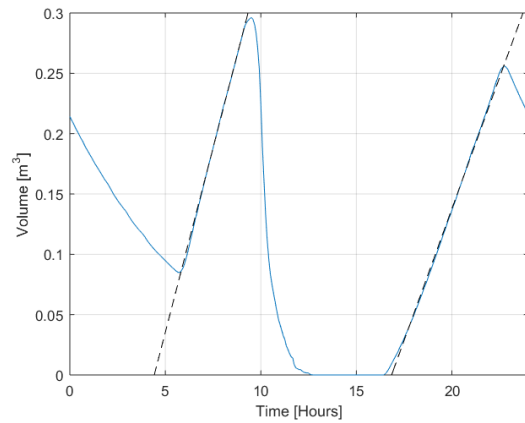
(a) Sand



(b) Gravel

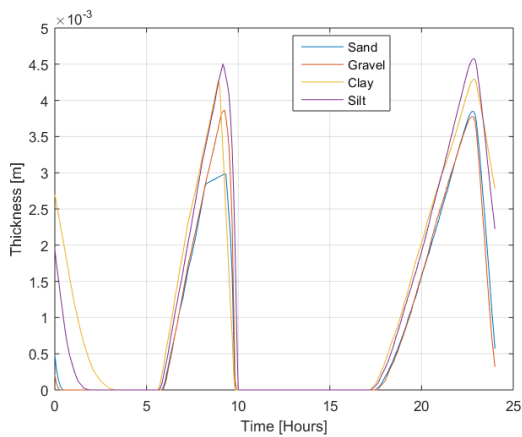


(c) Clay

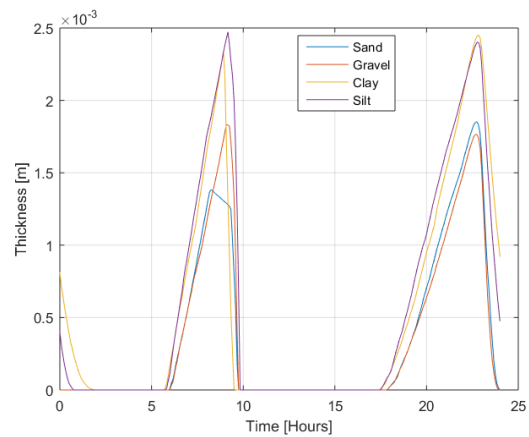


(d) Silt

Figure 8.12: Different frozen grounds with trend line



(a) Inner side



(b) Outer side

Figure 8.13: Frozen ground thickness at top cool element over time

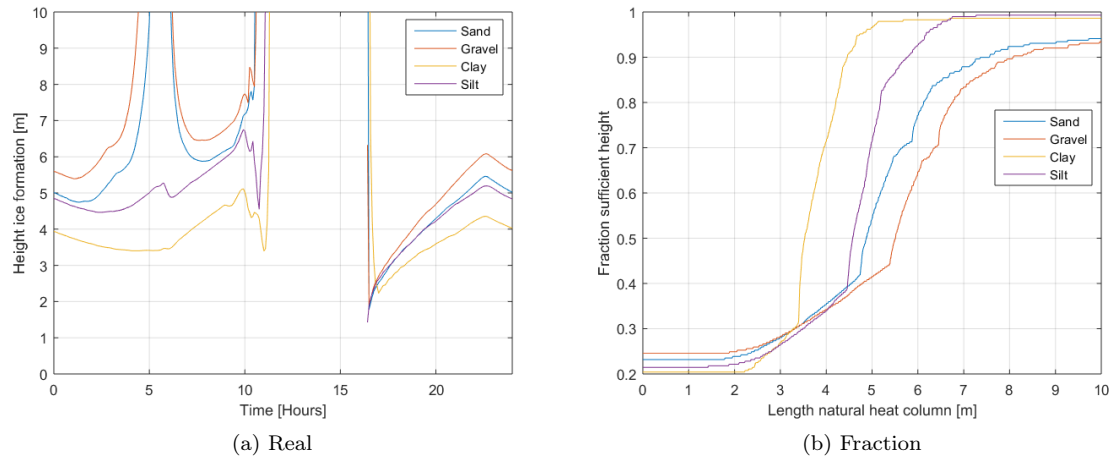


Figure 8.14: Height frozen ground over time

The height as a function over time is represented in Figure 8.14 a. Around six hours and around sixteen hours, it seems the value goes to infinity, this is due to rounding errors. In Figure 8.14 b is shown that a column with a length of six meter is sufficient for 77% of the time for sand (i.e. there is a mismatch for $(1 - 0.77) \cdot 24 = 5.5h$ per day). For gravel this is 65%, for clay 98% of the time and silt 93% of the time.

In this third CFD-analysis, the goal of the investigation is shifted from seasonal storage to daily storage. At the beginning of this chapter, there was asked what the refrigerant return temperature as a function over time would be. In Figure 8.8 can be seen that the return temperature is between $3.5^{\circ}C$ and $7.5^{\circ}C$. However, the return temperature is strongly dependent on the inlet temperature. Furthermore, there was asked what the volume of the ice layer would be as a function over time. In morning peak there will be an amount between $0.22m^3$ and $0.35m^3$ be formed, in the evening peak this is between $0.19m^3$ and $0.35m^3$ (see Figure 8.11). Out of this numbers is calculated that a cool element height of six meters is sufficient. In general, it can be concluded that daily storage shows significantly better results in comparison with seasonal storage. In the next section, individual parameters will be investigated to see if this setup can be improved.

8.2 Optimization

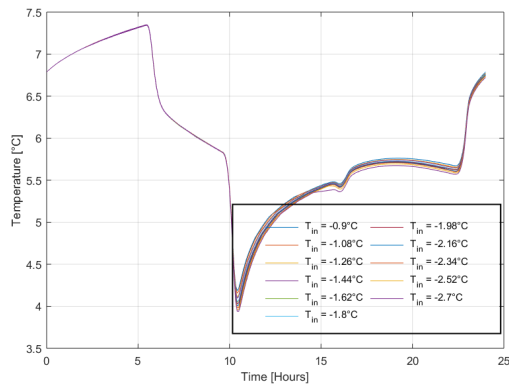
In Section 8.1, the CFD-analysis is shifted from seasonal storage to daily storage. In this section, the results will be discussed and there will be investigated how these results can be optimized. To do so, a parametric study of the mass flow and the glycol temperature will be executed. Furthermore, a parametric study will be made of the number of solar collectors, to see if this can be reduced. Finally, the minimum required space will be calculated. In all subsections, the results are compared with the results obtained in Section 7.2.

8.2.1 Parametric study inlet temperature

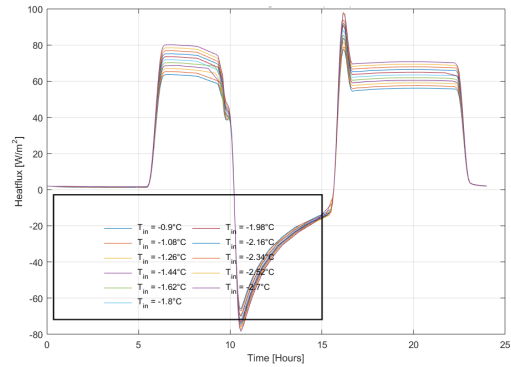
In Figure 8.15 are the results of the parametric study represented. In this study, the inlet temperature of glycol is varied between 50% and 150% of its original value, with a step size of 10%. This means the glycol inlet temperature is varied with a temperature between $-2.7^{\circ}C$ and $-0.9^{\circ}C$ with a step size of $-0.18^{\circ}C$. In Section 7.2 is stated that:

$$\frac{dV}{dt} = \frac{\varphi_m c_p (1 - e^{-\frac{UA}{m c_p}})}{\rho h_f} (T_{ice} - T_{in}) \quad (8.10)$$

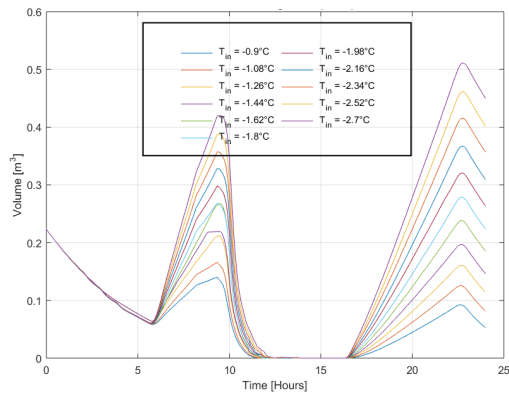
From Figure 8.16 it can be concluded that this is valid for this analysis, as well. Therefore, the statement in Section 7.2 holds that the frozen ground volume is directly negative proportional with the glycol inlet temperature.



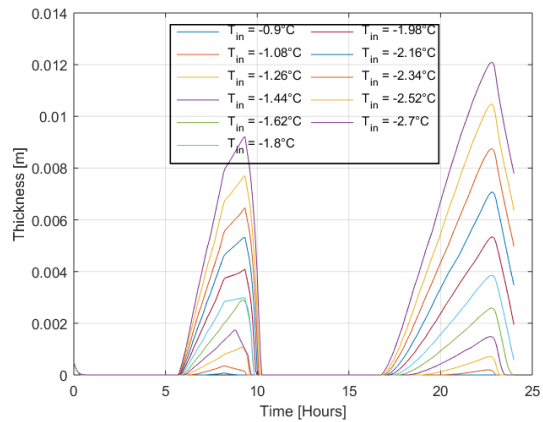
(a) Parametric study of the return temperature



(b) Parametric study of heatflux through the wall



(c) Parametric study of frozen soil ground



(d) Parametric study of frozen ground inner side thickness at top

Figure 8.15: Parametric study by changing inlet temperature (sand)

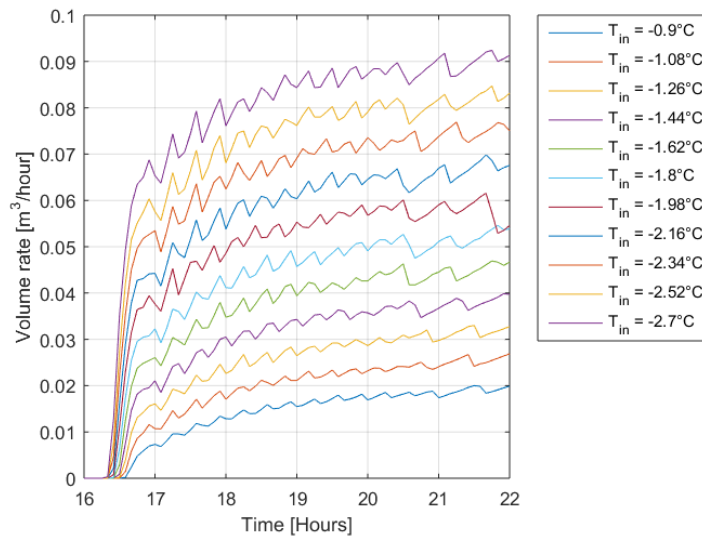
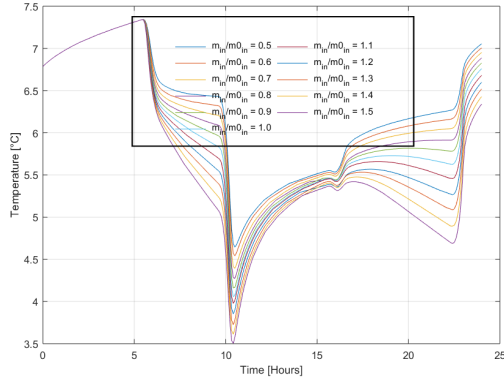
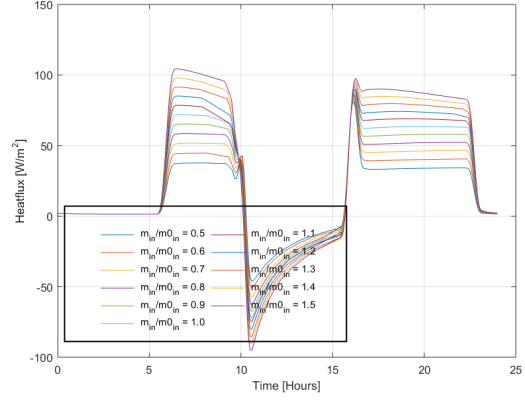


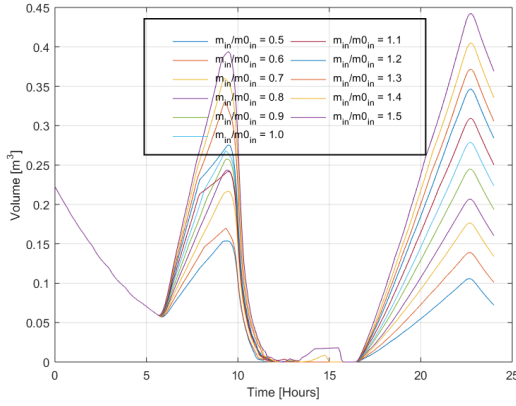
Figure 8.16: Parametric study of frozen ground rate by changing inlet temperature



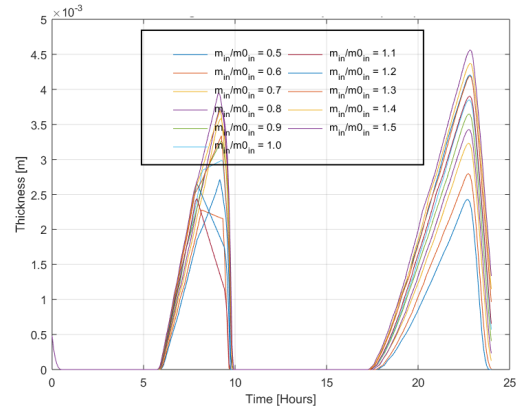
(a) Parametric study of the return temperature



(b) Parametric study of heatflux through the wall



(c) Parametric study of frozen soil ground



(d) Parametric study of frozen ground inner side thickness at top

Figure 8.17: Parametric study by changing glycol mass flow

8.2.2 Parametric study mass flow

In the same way as the inlet temperature, a parametric study is done for the glycol mass flow. The results are represented in Figure 8.17. In this case, the glycol mass flow is varied between 50% and 150% of its original value, with a step size of 10%. For the morning peak, this means a variation between 0.0230kg/s and 0.0690kg/s with a time step of 0.0046kg/s . For the evening peak this is between 0.0213kg/s and 0.0639kg/s , with a time step of 0.0043kg/s . The mass flow during regeneration remains the same, this will be discussed in the next section.

From the results can immediately be seen that the conclusions, drawn in Section 7.2, do not hold stand. The transferred heat does not reach a limit when the mass flow is becoming large. This is because in the previous analysis is assumed that, due to a large amount of frozen ground around the cool element, the temperature directly outside the cool element is constant. However, when switching from seasonal to daily storage, not all the ground is frozen. Furthermore, in Figure 8.6 b it is shown that the glycol return temperature is strongly dependent on the inlet temperature and therefore, the transferred heat is only dependent on the glycol mass flow. This lead to the equation:

$$Q(m) = \varphi_m c_p (T_{out} - T_{in}) \quad (8.11)$$

In Figure 8.18 is the total energy flux consumption during the morning and evening period plotted against the glycol mass flow. Here, it is concluded that the relation in both cases is directly proportional ($r_{morning}^2 = 0.9984, r_{evening}^2 = 0.9972$) and therefore the statement, $Q(m) = \varphi_m c_p (T_{out} - T_{in})$, is true.

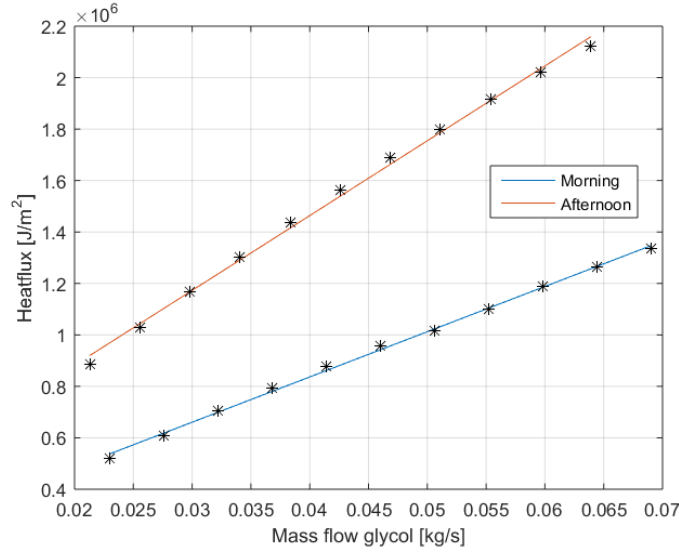
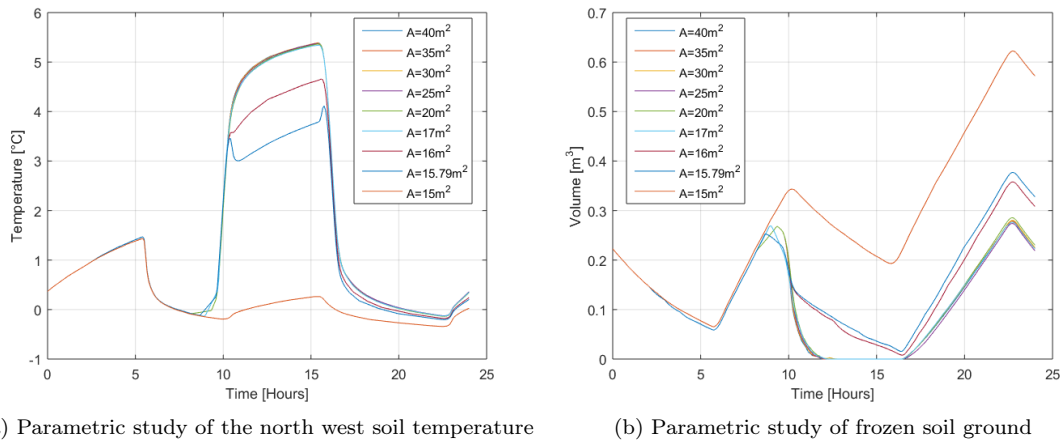


Figure 8.18: Parametric study of energy flux rate through the wall by changing glycol mass flow



(a) Parametric study of the north west soil temperature (b) Parametric study of frozen soil ground

Figure 8.19: Parametric study by changing number of solar panels

8.2.3 Parametric study regeneration

At the beginning of this chapter is there roughly assumed that is an area of forty square meters of the thermal solar collector was sufficient to regenerate the system. Here, no effects of ground regeneration were taken into account. In this last parametric study, the number of the area for the thermal solar collector is decreased with five square meters per step. This is done until the results are close to the minimum required of the solar collector area. To see which effects occur, when the size of the thermal solar collector will be reduced, the results are shown in Figure 8.19. In Figure 8.2 at the beginning of Chapter 8, it is stated that the net demand during the regeneration period for a single household is $57.96 MJ$. Furthermore, in Figure 8.2 it can be seen that the solar radiation for this period is $9.177 MJ/m^2$. When is reminded that the efficiency of the thermal solar collector is 40%, the minimum area of the thermal solar collector is:

$$A = \frac{E_{demand}}{\eta P_{supply}} = \frac{57.96[MJ]}{0.40 \cdot 9.177[MJ/m^2]} = 15.79m^2 \quad (8.12)$$

This amount of energy will be used to warm the house when the natural heat column is regenerating. In Figure 8.19 b it can be seen that when the area of thermal solar collector is increased, the volume frozen soil will not change significantly. Therefore, it can be concluded that an area of $17m^2$ thermal solar collector is sufficient to heat the house and regenerate the system.

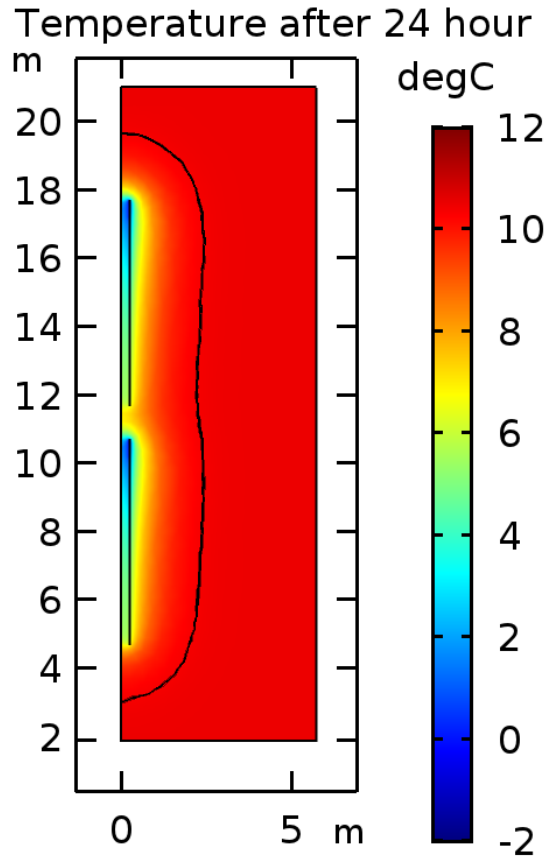


Figure 8.20: Isothermal lines of natural heat column for $T = 10.377^{\circ}C$ at 6, 10, 16 and 23 hours

8.2.4 Minimum required area

When designing the natural heat column, again there is to be investigated what the minimum required area of the natural heat column is. In this way, there can be decided if multiple columns can be placed on top of each other, without interfering. Furthermore, the ground area of the natural heat column can be determined. In Figure 8.20 a two-dimensional plot of the natural heat column is represented. The black lines represent the isotherm temperature of $T = 10.377^{\circ}C$ at six, ten, sixteen and twenty-three hours. As discussed in Section 7.2, this temperature is 99% of the dimensionless temperature.

Figure 8.20 shows that it can be concluded that the isotherms do not change over the day. The isotherm is over the day two meter away from the top and the bottom. So when placing multiple cylinders on top of each other, the distance will be four meters, if they not interfering with each other. However, in this case, there are already two columns with a distance of one meter. So the columns interfere with each other, however, this is a problem.

Finally, it can be seen in Figure 8.20 that the horizontal distance of the isotherms is 2.5 meter. So the natural heat column needs a minimum ground diameter of 5 meters. Therefore, the ground area which is needed for this natural heat column is $18.10m^2$. In Section 2.1 it is stated that an average Dutch household has a usable ground area between fifty and a hundred square meters. Therefore, the natural heat column for daily storage is suitable for domestic housing.

Out of the results which are presented in this chapter it can be concluded that the natural heat column is suitable for daily storage when active regeneration is used. In the next chapter, this result will be economically evaluated with a business case.

Chapter 9

Business Case

The final step of analyzing the natural heat column is to execute a financial cost-benefit analysis to see if it is financially attractive to execute this project. In this business case will be investigated what possible alternatives are and the advantages of the natural heat column will be discussed. Furthermore, a risk assessment and a project schedule will be discussed. Finally, the costs and revenues of the project will be elaborated to see what the investment will be.

9.1 Alternatives

As mentioned in Chapter 1, there are a number of alternatives to achieve the goals as stated in the energy agenda. Electricity can be generated by solar photovoltaic cells, however, they have a maximum efficiency of 31% and it is not possible to cool the building during the summer months. Another alternative is an underground thermal energy system, however, this can give significant damage to the ground. Finally, an alternative close to the natural heat column is the ice storage system, however, this has high investment costs due to ground digging and it takes a significant amount of space.

9.2 Advantages

In Chapter 1 is elaborated that the natural heat column has multiple advantages. Due to the use of the groundwater, the installation costs are significantly lower than the ice storage system. And due to the use of the latent heat of the groundwater, the required space is significantly lower, compared to other systems. Finally, houses with this system can both be cooled during summer and heated during winter.

9.3 Risks

The following risks could occur:[41]

- No financial support:
Although the natural heat column is a sustainable solution, the investment costs are high. When these costs are too high, the owner must decide if it is financially attractive to install the natural heat column. Furthermore, the government is responsible for regulating and subsidizing the project when needed to meet the demands stated in the energy agenda.
- Insufficient quality control:
Due to continuing freezing and melting of the groundwater, chances are that the cylinder breaks, due to erosion, and glycol leaks into the soil. Although the biodegradation of glycol in both oxic and anoxic environments, the owner of the natural heat column be sure, there is no glycol leaking into the soil [42]. This can be done, by installing a leakage detection. When there is a leakage, the owner will inform the RIVM, who will take further measures [43].
- Increasing competition in the underground:
The underground contains not only ground and groundwater, a network of, electrical wires, gas and water tubes and a sewage system is also present underground. When the natural heat column is becoming more popular, there is a significant chance the columns will interfere with those networks

and with each other. Because the owner does not have the knowledge of this information. The city government will control if the ground is suitable for a natural heating column when giving the building permit.

- Insufficient consensus on ground energy near drinking water extraction sites:
When the natural heat column is located near a groundwater drinking location, it could occur that this water will freeze and no drinking water can be won. The chance that this will happen is relatively small, groundwater for drinking purposes is located fifty and a hundred meters below the surface [44]. This is far deeper than the natural heat column. However, the owner is responsible for this problem and must contact the water board before installing the natural heat column.
- Lack of information available:
Although the above risks are partly the responsibility of the owner, the owner does not always have the right knowledge to take the right action. To prevent this risk a building permit will be asked when installing a natural heating column. In this way, the city government can control the number of natural heating columns and intervene when there is a potential risk.

9.4 Cashflow

In a business case is made a distinction between two types of costs. The first one is the capital expenditure (CAPEX), which is the money spend to buy, maintain or improve its fixed assets. The second costs are operating expenditure (OPEX), which is an ongoing cost for running a system. In this project, the CAPEX costs, are the costs for installing the natural heating column, which is estimated in Chapter 1 of a cost of €30 000. The OPEX costs are the electric costs of the heat pump, which is needed for running the compressor. The revenues of the project are the savings which are earned to not spend money on burning natural gas. This heat can be calculated as:

$$Q_{cond} = V_{gas} \cdot LHV \quad (9.1)$$

As mentioned in Section 2.1, the annual gas consumption for an average Dutch household is 1500 cubic meter of gas, with €0.80 per cubic meter and the lower heating value of natural gas ($31.67 MJ/m^3$), the revenues are €1200 per year.

In Chapter 5 is elaborated that the power of the compressor can be calculated with:

$$W_{pump} = \frac{Q_{cond}}{COP} \quad (9.2)$$

In Section 2.1 is elaborated that the electric costs for an average Dutch household are €0.19 per kWh and that the COP of the heat pump is 4.33. When using this numbers, the annual OPEX of the project are €590.

The total cashflow is defined as:

$$cashflow = revenues + subsidies - OPEX \quad (9.3)$$

There are numerous subsidy schemes available for urban energy projects. However, these subsidies are highly dependent on the phase of the project and the time when the subsidy is applied for. Because of these uncertainties, there is assumed there are no subsidies available for this project, however, a list of subsidies can be found on the website of TKI [45]. In the next section will be elaborated what the investment will be with this cashflow.

9.5 Project plan

A building project has in general six phases:

- Initiative phase:
The customer contact different contractors for building the natural heat column.
- Definition phase:
The contractors make a contract or a program of demands where they include a risk assessment.

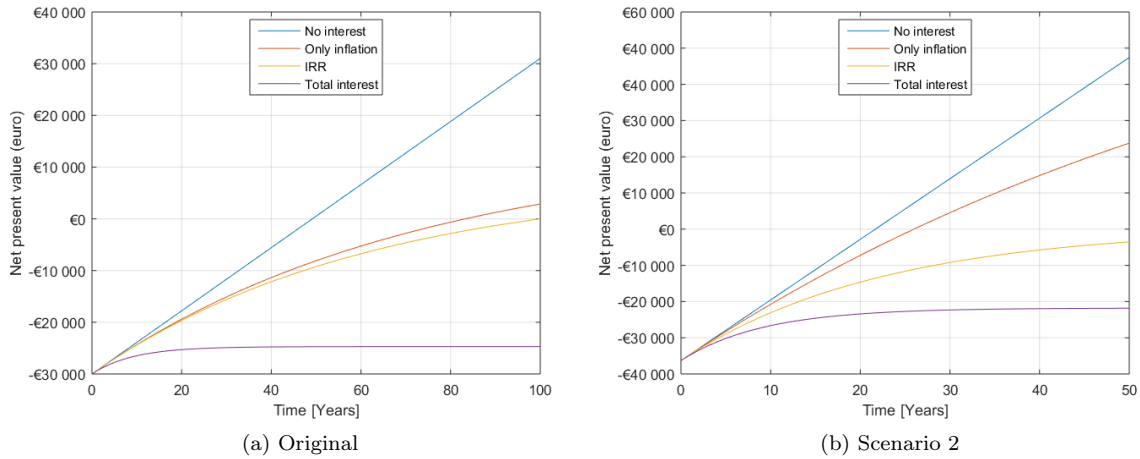


Figure 9.1: Net present value

- Design phase:
When the customer has chosen a contractor, this contractor will make a design for the natural heat column.
- Preparation phase:
In this phase is applied for to the building permits and possible subsidies.
- Realization phase:
When the above phases are going on, the natural heat column is being built.
- Aftercare phase:
When the project is finished the project has to be evaluated and the contractor has to give a guarantee.

9.6 Investment

Finally, the return on investment can be calculated. Due to inflation and the profit the owner wants to make, the money is decreasing in value when the time is going by. For this, the return on investment has to be recalculated to the value what is money worth today. This is done with the net present value:

$$NPV = -CAPEX + \sum_{t=1}^{t=t} \frac{cash\ flow}{(1+i)^t} \quad (9.4)$$

Here, i is the market interest rate, which is defined as:

$$i + 1 = (1 + r)(1 + p) \quad (9.5)$$

Where p is the inflation, which was on average 1.39% in 2017 [46]. And r the profit rate the owner of the natural heat column want to make, this is assumed at 10%. When knowing this, it can be calculated that the interest rate is 11.53%.

When applying these equations, the net present value after a hundred years is -€24 707. Based on the NPV, the internal rate of return (the time when the NPV is zero, by changing the investment) is 1.63%. When the inflation is subtracted from this, there can be calculated a profit of 0.24%. When there is assumed that there is no profit or inflation, the return on investment can be calculated by dividing the CAPEX by the cashflow per year, which are calculated in the previous section. When knowing the cashflow is €610.30 per year, the return on investment is 49 years. This is graphically represented in Figure 9.1 a.

9.7 Scenario 2

In case the thermal solar collectors are replaced by PV-T panels, the system can generate both heat and electricity. In this case, the natural heat column has no costs for generating the heat pump compressor, and the surplus of electricity can be sold. According to the owner of the natural heat column, the PV-T panels generate yearly $5500kWh$ of electricity, from previous sections can be seen that the heat pump consumes $3048kWh$. Therefore, the extra revenue source of selling $2452kWh$ is added. In this scenario, the OPEX is equal to zero. For this modification, the CAPEX is increased to €36 300.

When applying the financial analysis to these numbers, the net present value after a hundred years is -€21 775. Based on the NPV, the internal rate of return is 4.56%. When the inflation is subtracted from this, there can be calculated a profit of 3.13%. When there is assumed that there is no profit or inflation, the cashflow is €1675 per year. This result in a return on investment of 22 years (see Figure 9.1 b).

Based on this business case, with its high investment costs and relatively high interest rates, there is advised to reconsider this project. Although the technical results are acceptable, the only way to succeed this project is by heavy subsidize this project. Furthermore, it should be executed by a non-governmental organization, which does not want to make a profit, but only compensates for inflation.

Chapter 10

Conclusion and recommendations

In the previous chapters, the natural heat column was introduced. Furthermore, the methodology and the physics of this thesis were elaborated. Finally, the performances of the natural heat column were investigated and discussed, in three CFD-analyses. In this chapter, an answer will be given to the main research question and several recommendations will be made for both the natural heat column as for further research.

10.1 Conclusion

At the end of Chapter 1, the following main research question is stated: What is the optimal configuration of a natural heat column and how can this be analyzed with CFD?

To find an answer to this question, in Chapter 5, a first thermodynamic analysis is made. Here, the advantage is that the natural heat column requires 87% less ground volume in compare to a traditional sensible heat pump system. The disadvantage of the natural heat column is that it uses 0.61 kW more electrical power to drive the heat pump compressor compared to the sensible heat pump. The advantage of the smaller volume is significantly higher than the disadvantage of the electrical power. Finally, in Section 3.2.2 it is stated that the groundwater flow is equal to zero. By assuming this, there is no movement in the soil, and only the (reduced) conservation of energy equation has to be solved here. The conservation of mass and momentum are solved in the glycol interface, inside the natural heat column. Because the soil interface is the significant large, the number of calculations is reduced significantly. Which saves a significant amount of computational time.

By using the results which are found in the thermodynamic analysis, the first two CFD-analyses are further investigated with the help of Comsol Multiphysics (see Chapter 6 and 7). Here, the natural heat column is investigated in water and different types of soil surroundings (sand, gravel, silt, and clay) for a simulation time of one hundred days. This to investigate the seasonal performances of the natural heat column. Due to the good insulating effect of frozen ground, there is almost no heat being transferred to the soil. For all soil interfaces, the heat flux is halved within the first seven minutes of the simulation. The fraction of thermal resistance over the initial thermal resistance, R/R_0 , for one meter of frozen ground is in some cases more than a factor of one hundred. Due to this, the glycol return temperature is 90% of its initial temperature within one day. After this first day, there was almost no heat transferred. Based on these numbers, it can be concluded that the natural heat column is not suitable for seasonal storage and the focus has to shift to daily storage with active regeneration.

In the third CFD-analysis (see Chapter 8), the scope of the research is shifted from seasonal storage to daily storage with active regeneration. During the morning and evening heating peak, the natural heat column freezes the groundwater to deliver heat the house. The ratio latent heat over the total heat is 51% for the morning peak and 29% for the evening peak. Furthermore, the glycol return temperature varies between $3.5^{\circ}C$ and $7.5^{\circ}C$ and is strongly dependent on the inlet conditions. The morning peak generates between $0.22m^3$ and $0.35m^3$ of ice, in the evening this is between $0.19m^3$ and $0.35m^3$. When the ice, during the afternoon, is melted by the thermal solar collectors, the optimal area of the collectors is $17m^2$. Of this area $15.76m^2$ is needed to warm the house when the natural heat column is regenerating. Furthermore, it can be concluded that a natural heat column with a length of six meters is sufficient for daily storage.

Finally, the minimum distance for placing two columns on top of each other is four meters. In this way, the columns do not interfere with each other. However, it is stated that interference does not lead to big problems. The minimum distance for placing two columns next to each other is five meters. In this way, they do not interfere. For this, the required ground circumference is $18.0m^2$. This is far less compared to the living area of an average house in the Netherlands, which is between the fifty till a hundred square meters. In general, this third CFD-analysis meet the specified performances and is representative for other days. Therefore, the results are acceptable and this configuration is technically feasible.

The final step of analyzing the natural heat column is to write a business case. In Chapter 9 it is elaborated that, with an investment cost of €30 000 and a total interest rate of 11.53%, the return on investment is larger than a hundred years. When the return on investment is a hundred years, the internal rate of return would be 1.63% per year. When only inflation is taken into account, the return on investment is 83 years. Finally, when there is no interest rate taken into account the payback period is 49 years. When considering the risks over the years, these return on investments are relatively high.

Based on this data, it is concluded that the concept of the natural heat column has a high potential, however, due to the low conductivity of ice, seasonal storage is not feasible. The technical results for daily storage with active regeneration are acceptable. To succeed in this project, the natural heat column has to be subsidized and executed by a non-governmental organization, which does not want to make a profit, but only compensates for the inflation.

10.2 Recommendations

In this section, the recommendations for future action are given. A distinction is made between recommendations for further research and recommendations for the research itself.

Recommendations for further research:

1. In this thesis, it is concluded that the ground freezes significantly more towards the inside of the cylinder, instead of outside. Investigate what the effect is of the diameter of the cylinder annulus on this phenomenon and if there can be multiple columns placed inside each other.
2. Investigate what will occur when another refrigerant is used instead of glycol.
3. Investigate what will occur when another natural heat column material is used.
4. Investigate what the effect of the natural heat column is during the summer months, when the house needs to be cooled.
5. Investigate how multiple columns will interfere with each other when they are placed closer to each other.
6. Do a parametric study for regeneration time, versus the number of thermal solar collectors.
7. Investigate the transient effects (e.g. when an input parameter is suddenly changed).
8. Investigate which forces occur on the ground and on the natural heat column when freezing the soil.
9. Investigate the effect of heavy rainfall.
10. Investigate what the effect is when gravity is simulated.

Recommendations for installing the natural heat column:

1. Apply the natural heat column as daily storage with active regeneration, and not as seasonal storage.
2. Decrease the glycol inlet temperature. The inlet temperature is directly negatively proportional to the volume of the frozen ground.
3. Increase the glycol mass flow. The mass flow is directly proportional to the volume of the frozen ground (only for daily storage).
4. Apply the natural heat column in a sand or gravel soil. These soils have a higher thermal conductivity and produce more frozen ground.
5. Investigate for what kind of subsidy the natural heat column can apply.
6. Do a stakeholder analysis.
7. Decide who is the owner of the natural heat column.
8. Find investors and investigate which interest rate they charge.
9. Investigate if it is needed to apply for any building permits.
10. Investigate if the natural heat column can improve the energy label of a house.
11. Monitor the natural heat column and notice when the results are different from the results in this thesis.

Bibliography

- [1] European Commission. Paris agreement, 2018.
- [2] Ministry of Economic Affairs. Energy agenda, 2016.
- [3] M. Creatore. *Photovoltaic Conversion*. Eindhoven University of Technology, 2016.
- [4] J. Hermans. *Energie Survival Gids*. BetaText v.o.f., 2009.
- [5] Nationale Energie Atlas. Potentieel warmte koude opslag, 2018.
- [6] Ministry of Infrastructure and Water Management. Bodem als energiebron en -buffer, 2004.
- [7] Viessmann climate of innovation. Heat pump brochure, 2018.
- [8] G. Fang, X. Liu, and S. Wu. Experimental investigation on performance of ice storage air-conditioning system with separate heat pipe. *Experimental thermal and fluid science*, 2009.
- [9] C. Chaichana, W.S. Charters, and L. Aye. An ice thermal storage computer model. *Applied thermal engineering*, 2001.
- [10] H.J. Chen, W.P. Wang, and S. Chen. Optimization of an ice-storage air conditioning system using dynamic programming method. *Applied thermal engineering*, 2005.
- [11] Z. Kang, R. Wang, X. Zhou, and F. Feng. Research status of ice-storage air-conditioning system. *Procedia engineering*, 2017.
- [12] A.H. Abedin and M.A. Rosen. A critical review of thermochemical energy storage systems. *The open renewable energy journal*, 2011.
- [13] J. Herpt. *Heat column*. Solevo B.V., 2018.
- [14] P. Eslami and M. Bernier. Freezing of geothermal borehole surroundings: A numerical and experimental assessment with applications. *Applied energy*, 2012.
- [15] J.M. McKenzie, C.I. Voss, and D.I. Siegel. Groundwater flow with energy transport and water-ice phase change: numerical simulations, benchmarks, and application to freezing in peat bogs. *Advances in water resources*, 2007.
- [16] C.J. Lunardini. Freezing of soil with an unfrozen water content and variable thermal properties. *CRREL Report*, 1988.
- [17] USGS. Sutra and related programs (sutraste), 2018.
- [18] C. Zheng. *FEFLOW: A finite-element ground water flow and transport modeling tool*. National Ground Water Association, 2017.
- [19] Y. Wang, Q. GAO, X. Zhu, M. Yu, and X. Zhao. Experimental study on interaction between soil and ground heat exchange pipe at low temperature. *Applied thermal engineering*, 2013.
- [20] T. Yang, X. Zhang, B. Zhou, and M. Zheng. Simulation and experimental validation of soil cool storage with seasonal natural energy. *Energy and buildings*, 2013.
- [21] OpenGeoSys. Opengeosys, 2018.

- [22] T. Zheng, H. Shao, S. Schelens, P. Hein, T. Vienken, Z. Pang, O. Kolditz, and T. Nagel. Efficiency and economic analysis of utilizing latent heat from groundwater freezing in the context of borehole heat exchanger coupled ground source heat pump systems. *Applied thermal engineering*, 2016.
- [23] S.P. Kavanaugh. Field tests for ground thermal properties – methods and impact on ground-source heat pump design. *ASHRAE Transactions*, 2000.
- [24] C. Zhang, G. Huangjun, L. Yufeng, X. Cong, and D. Peng. A review on thermal response test of ground-coupled heat pump systems. *Renewable and sustainable energy reviews*, 2014.
- [25] Centraal Bureau voor de Statistiek. Woningen, hoofdbewoner/huishouden, 1998-2012, 2012.
- [26] Nibud. Energie en water, 2017.
- [27] VDI-Gesellschaft Verfahrenstechnik und Chemieingenieurwesen. *VDI Heat Atlas*. Springer, 2010.
- [28] A.R. Freeze and J.A. Cherry. *Groundwater*. Prentice-Hall, 1979.
- [29] J.R. Welty, G.L. Rorrer, and D.G. Foster. *Fundamentals of momentum heat and mass transfer*. Wiley, 2015.
- [30] M.A. Biot. Theory of propagation of elastic waves in a fluid-saturated porous solid. *The journal of the acoustical society of America*, 1956.
- [31] D. Smeulders. *Darcy and Beyond*. Eindhoven University of Technology, 2017.
- [32] J.A. Dean. *Lange’s Handbook of Chemistry*. McGRAW-HILL, INC, 1973.
- [33] D.A. Nield and A. Bejan. Convection in porous media. *Springer Science*, 2013.
- [34] B. Sjodin. What’s the difference between fem, fdm, and fvm?, 2016.
- [35] J. Gasia. *Informe de la pràctica de programació en C*. University of Lleida, 2014.
- [36] 18bits. Correlatie en regressie, 2018.
- [37] Heatmat. What is trace heating, 2014.
- [38] Vreg. Verbruiksprofielen aardgas, 2018.
- [39] KNMI. Uurgegevens van het weer in nederland, 2018.
- [40] waterbedrijfgroen. Hoeveel liter water gebruiken we per dag, 2010.
- [41] H.A. Zondag. *Thermal energy storage*. Eindhoven University of Technology, 2017.
- [42] T. Klotzbücher, A. Kappler, K. Straub, and S. Haderlein. Biodegradability and groundwater pollutant potential of organic anti-freeze liquids used in borehole heat exchangers. *Geothermics*, 2007.
- [43] P. Beelen. A method to rank the relative environmental hazard of coolants leaking directly into groundwater. *RIVM*, 2013.
- [44] Thinkquest. drinkwaterzuivering, 2018.
- [45] TKI. Urban energy subsidie, 2018.
- [46] Centraal Bureau voor de Statistiek. Jaarmutatatie consumentenprijsindex, 2018.

Appendix A

TU/e code of scientific conduct

Declaration concerning the TU/e Code of Scientific Conduct for the Master's thesis

I have read the TU/e Code of Scientific Conduct¹.

I hereby declare that my Master's thesis has been carried out in accordance with the rules of the TU/e Code of Scientific Conduct

Date

01-10-2018

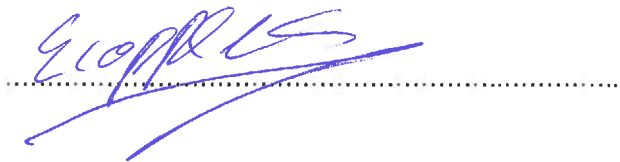
Name

E. Coppens

ID-number

0909263

Signature



Submit the signed declaration to the student administration of your department.

¹ See: <http://www.tue.nl/en/university/about-the-university/integrity/scientific-integrity/>
The Netherlands Code of Conduct for Academic Practice of the VSNU can be found here also.
More information about scientific integrity is published on the websites of TU/e and VSNU

TU/E CODE OF SCIENTIFIC CONDUCT

Preamble

In 2004, the Netherlands Code of Conduct for Academic Practice was established; revised versions were published in 2012 and 2014. TU/e fully supports this code. This TU/e Code fulfils the need for a more concise version. It also clarifies certain elements of the code in the light of recent developments and the specific characteristics of scientific activities at a technical university.

This TU/e Code is organized around five central values that jointly characterise good scientific conduct. From each of these values certain behavioural norms and principles follow, of which the most important are listed below. This Code is meant to be inclusive of the variety of research, design and educational activities at TU/e, and to leave room for differences in disciplinary context.

Adherence to this code of scientific integrity is the responsibility of *all* scientists, engineers and students at TU/e, whether they work individually or in groups. They may expect to work in an institutional environment that is supportive of fulfilling this responsibility, through various institutional policies and regulations on scientific integrity. Supervisors and group leaders have a special responsibility to teach junior staff members what is acceptable scientific conduct, and to function as examples of such conduct. Institutional responsibilities include: to create a climate that stimulates regular discussions about correct practices in research, design and education (especially when there seems to be a conflict between the principles of the code, or a conflict between principles and actual practices); and to facilitate accessible, unbiased and confidential procedures for reporting and investigating possible violations of the TU/e Code and for taking adequate measures in case they have occurred.

Code

TU/e expects its academic staff and students¹ to respect the following five central values of scientific integrity and to conform to the norms and principles that follow from them for their research, design and educational activities:

1. Trustworthiness

Academic staff and students ground their views as academics on scientific evidence. This entails that:

- They do not fabricate, falsify or suppress evidence. The selective omission of research results is reported and justified.
- In presenting results of their activities, they do so with the corresponding uncertainties.
- In scientific communication, they strive for precision and nuance.
- They do not present as established facts speculations, personal opinions and claims that go beyond available evidence.

2. Intellectual honesty

Academic staff and students respect standards of quality in their field and they respect the achievements of others. This entails that:

- They acknowledge and respect intellectual property and authorship. Plagiarism is unacceptable.
- They only claim authorship if they have made a genuine contribution.
- They carry out peer-review tasks seriously and make assessments solely on scientific grounds.
- They only accept tasks for which they have the necessary expertise.
- In educational activities, they accurately present available knowledge in the discipline.

¹ This includes guests of TU/e who have access to the university's facilities.

3. *Openness*

Open and unbiased communication is essential for science and engineering. For academic staff and students, this entails that:

- They contribute actively to an academic climate in which insights and criticisms are welcome from all, regardless of academic rank and personal characteristics.
- They give room to others to develop or take their own intellectual stance in research, design and education.
- Whenever they publish research results, they present their research such that its results may in principle be replicated.
- They make accessible, after publication, all information needed for intersubjective testing of design results and design processes.
- They make accessible, after publication, research data for re-use by colleagues.

4. *Independence*

Academic staff and students operate in a context where academic freedom and independence are of great importance. Where needed, they guard this independence against commercial, political and personal interests. This entails that:

- In research, they chose their methods and criteria primarily to realize scientifically valuable goals.
- With external sponsors of scientific research, they arrange that all relevant results of this research may be published within a specified, reasonable amount of time.
- They report interests that may potentially conflict with the independence of research activities.
- They avoid situations in which reasonable doubt concerning the objectivity of their scientific judgements may arise.

5. *Societal responsibility*

Science and engineering are vital for the health and well-being of people and for a sustainable economy. They may also be the cause of harm and risks. For academic staff and students this entails that:

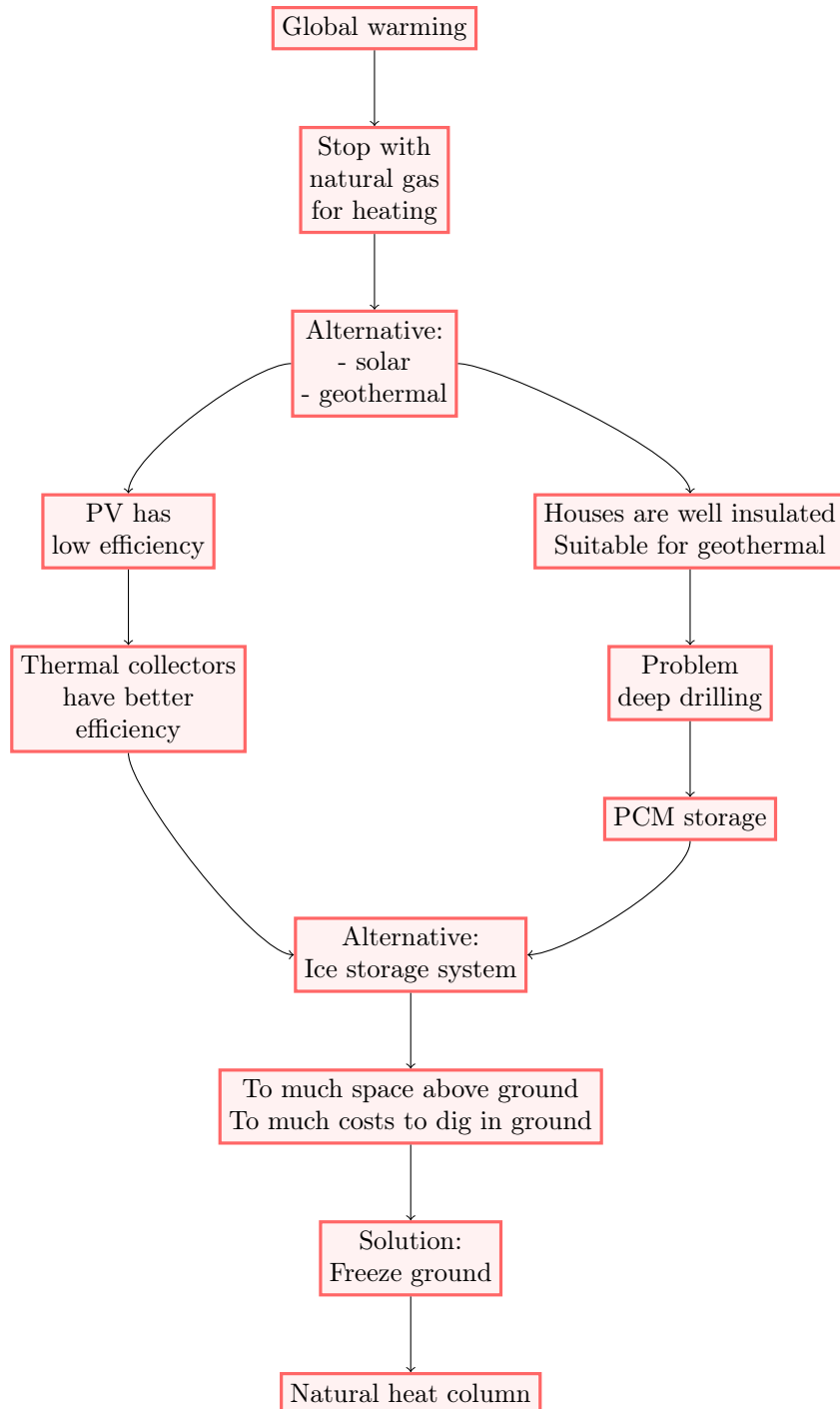
- They actively seek, within the limits and standards appropriate to their field, to contribute to society through research, design, knowledge dissemination and/or public debate.
- In their research and design, they adhere to the ethical codes for activities in which human subjects and animals are involved.
- They report possible harm and risks of scientific and technological developments to the relevant authorities; in case of doubt, they consult ethical advisory bodies or signal the need for such ethical advice.

Possible cases of violations of this code of conduct should be reported to relevant supervisors or to the confidential officer for scientific integrity at TU/e. See <http://www.tue.nl/en/research/scientific-integrity/>. The website also contains information about the complaints procedure.

Appendix B

Cause-consequence analysis of background

In this appendix is the cohesion shown of the background information which is elaborated in the introduction in Chapter 1. The figure starts at the top with the cause of the project (global warming) and ends at the bottom, by the solution (the natural heat column).



Appendix C

Derivation equation ice melting due to thermal losses

The derivation of Equation (5.17) on Page 30 is starting calculating the energy balance:

$$\frac{dQ}{dt} = -Q_{loss} \quad (C.1)$$

When is assumed that the losses only occur by conduction, and the heat transfer only take place by melting, the equation become:

$$\frac{d(m_{ice}H_f)}{dt} = -\frac{k_{ground}A(T_{ground} - T_{ice})}{dx} \quad (C.2)$$

And when is assumed that ice forms as a perfect sphere (which means $A = 4\pi(\frac{3m_{ice}}{4\pi\rho})^{2/3}$ and $dx = (\frac{3m_{ice}}{4\pi\rho})^{1/3}$), the equation becomes:

$$H_f \frac{dm_{ice}}{dt} = -\left(\frac{3m_{ice}}{4\pi\rho\varphi}\right)^{1/3} k_{ground} 4\pi (T_{ground} - T_{ice}) \quad (C.3)$$

$$\int m_{ice}^{-1/3} dm_{ice} = \int -\left(\frac{3}{4\pi\rho\varphi}\right)^{1/3} \frac{k_{ground} 4\pi}{H_f} (T_{ground} - T_{ice}) dt \quad (C.4)$$

$$\frac{2}{3} m_{ice}^{2/3} = -\left(\frac{3}{4\pi\rho\varphi}\right)^{1/3} \frac{k_{ground} 4\pi}{H_f} (T_{ground} - T_{ice}) t + C_1 \quad (C.5)$$

When is known that on time $t = 0$ the mass of the ice is equal to $m_{ice} = m_{ice0}$, C_1 is equal to $m_{ice0}^{2/3}$ the final equation is:

$$m_{ice}^{2/3} = -\left(\frac{3}{4\pi\rho\varphi}\right)^{1/3} \frac{k_{ground} 6\pi}{H_f} (T_{ground} - T_{ice}) t + m_{ice0}^{2/3} \quad (C.6)$$

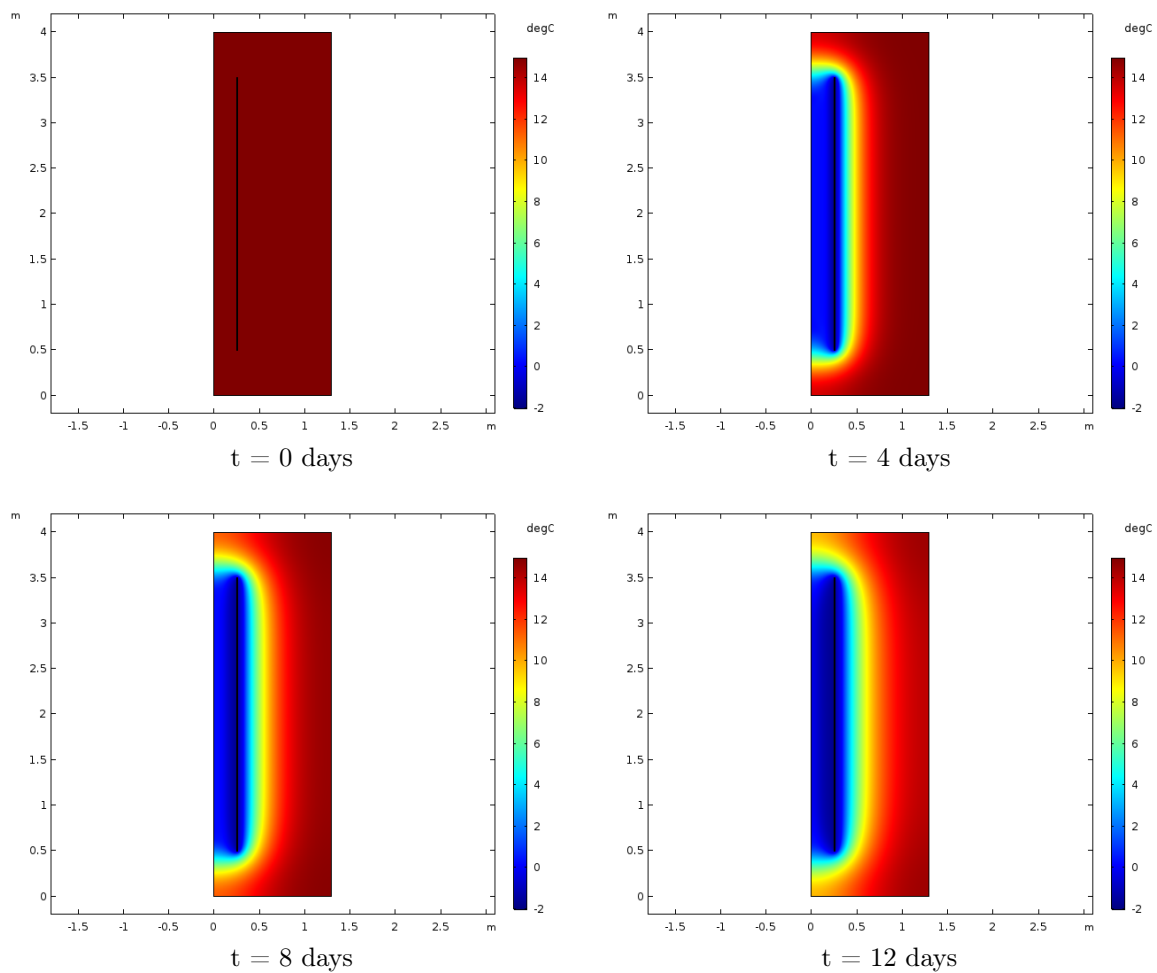
And the final equation to calculate how much the ice is molten is:

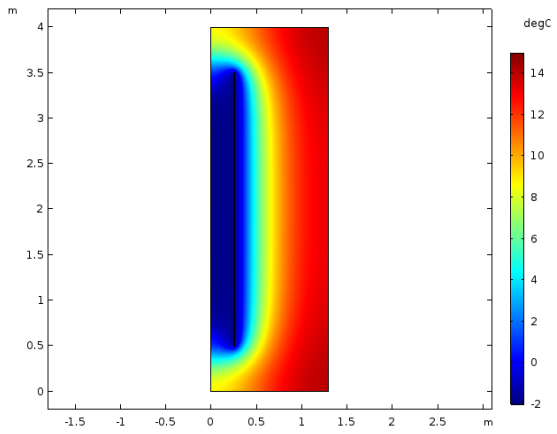
$$t(m_{ice}) = \frac{m_{ice0}^{2/3} - m_{ice}^{2/3}}{\left(\frac{3}{4\pi\rho\varphi}\right)^{1/3} \frac{k_{ground} 6\pi}{H_f} (T_{ground} - T_{ice})} \quad (C.7)$$

Appendix D

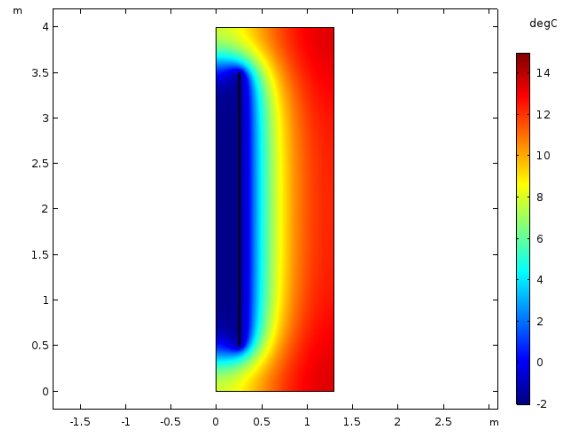
Temperature distribution CFD-analysis 1

In this appendix is the temperature evolution over time represented, for CFD-analysis 1 in Chapter 6.

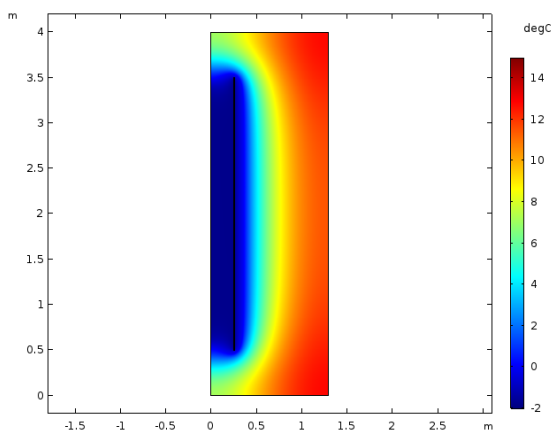




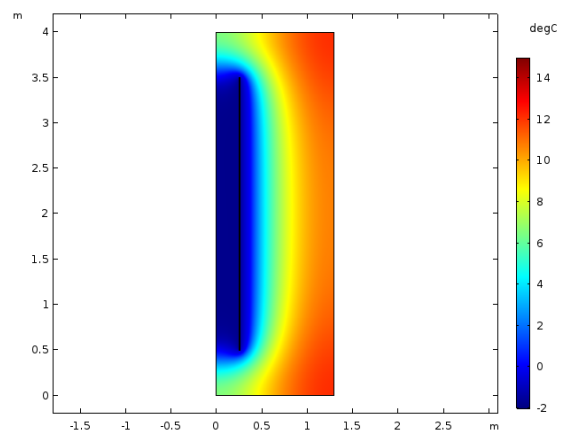
$t = 16$ days



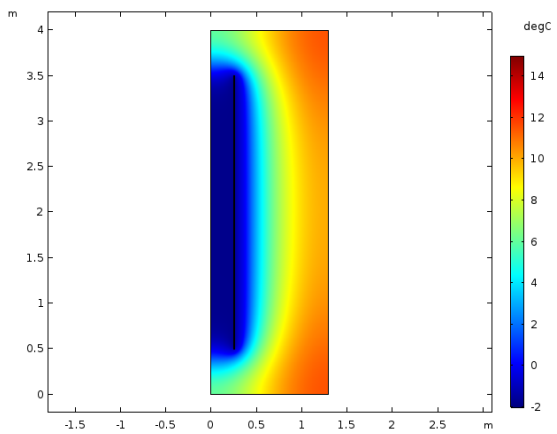
$t = 20$ days



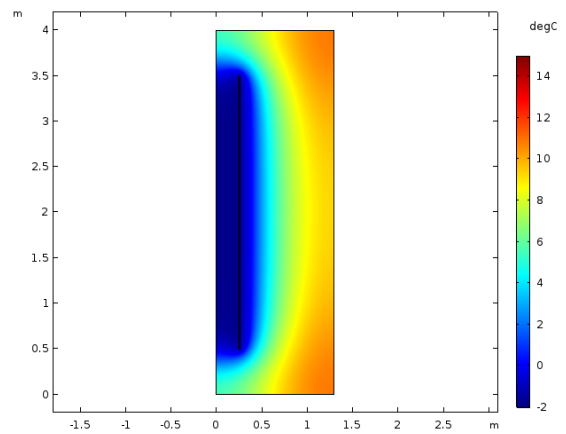
$t = 24$ days



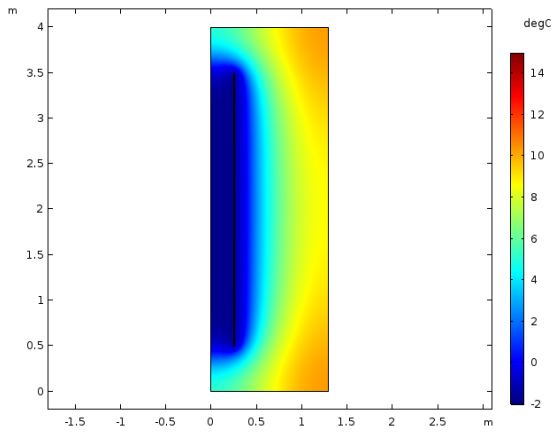
$t = 28$ days



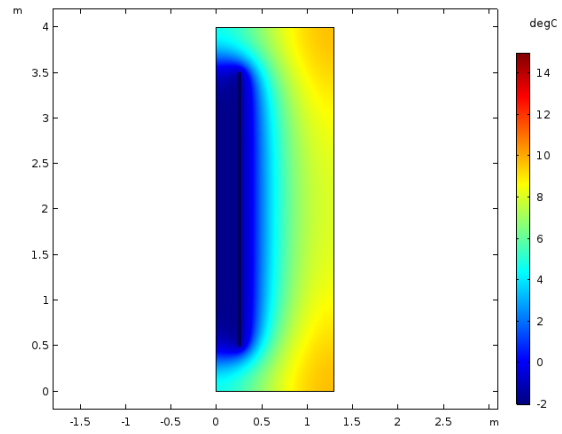
$t = 32$ days



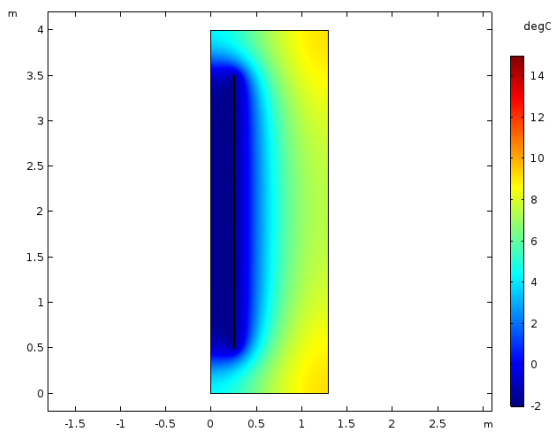
$t = 36$ days



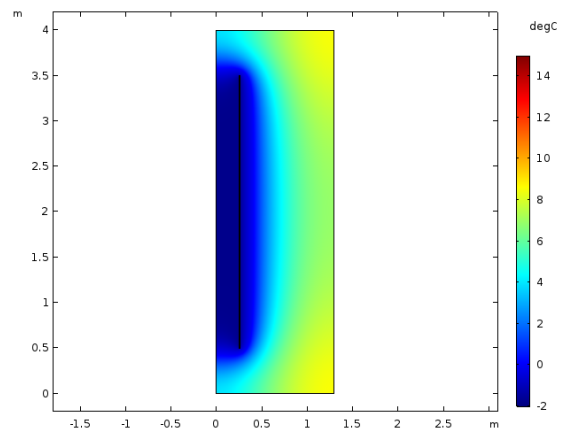
t = 40 days



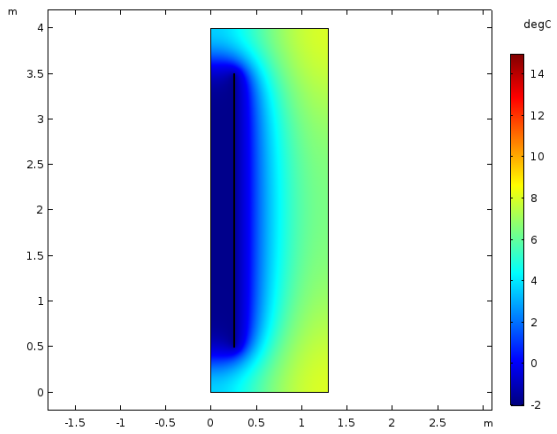
t = 44 days



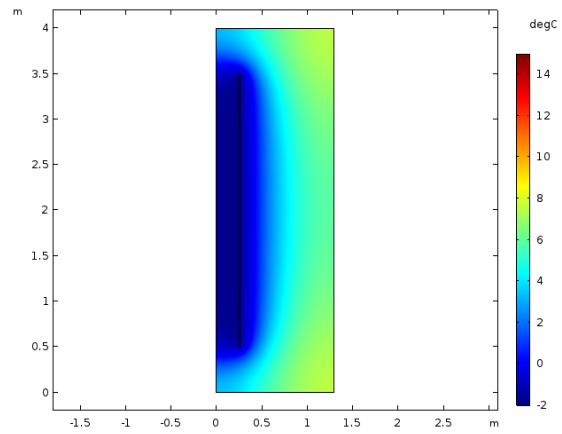
t = 48 days



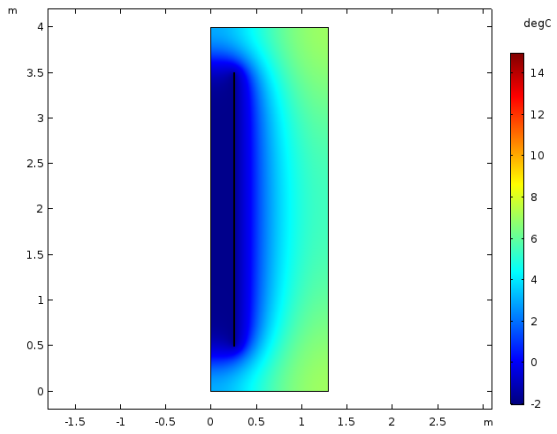
t = 52 days



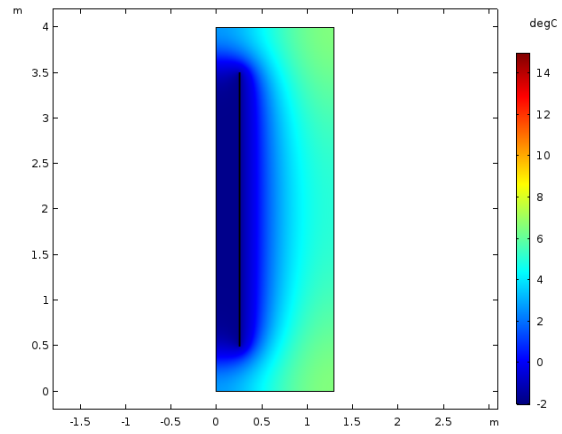
t = 56 days



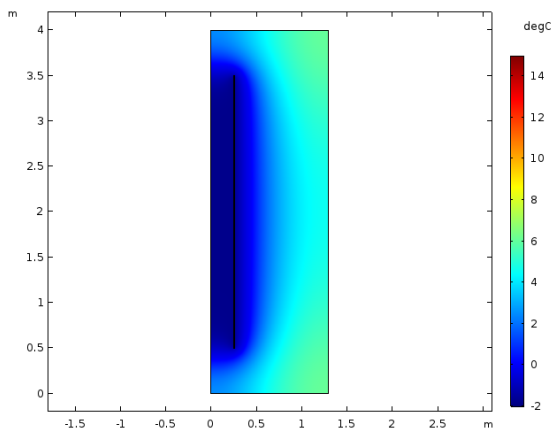
t = 60 days



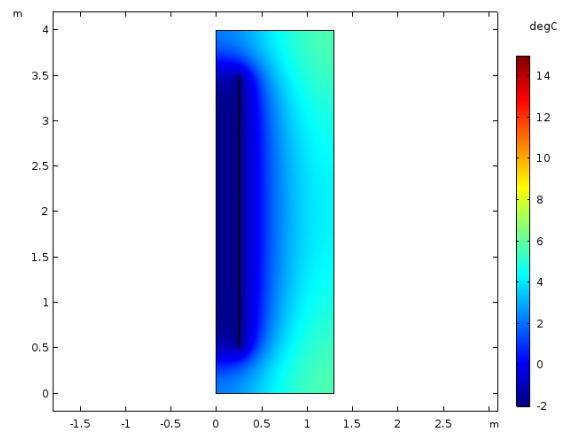
t = 64 days



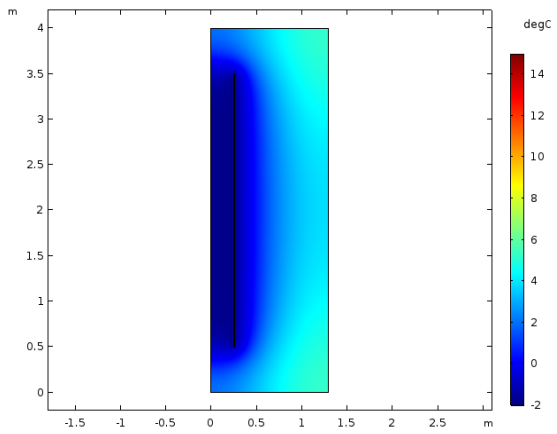
t = 68 days



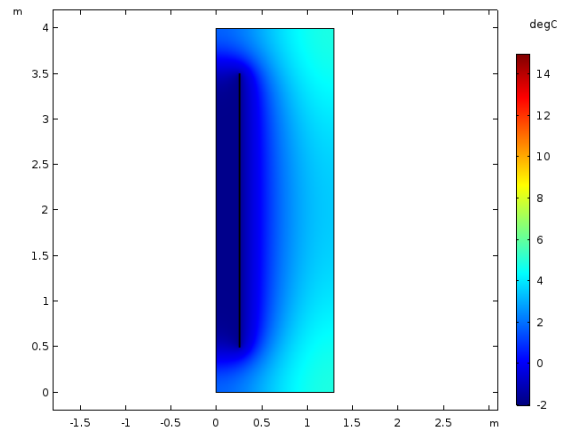
t = 72 days



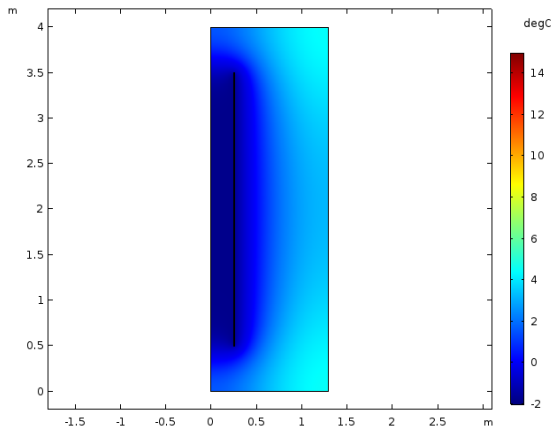
t = 76 days



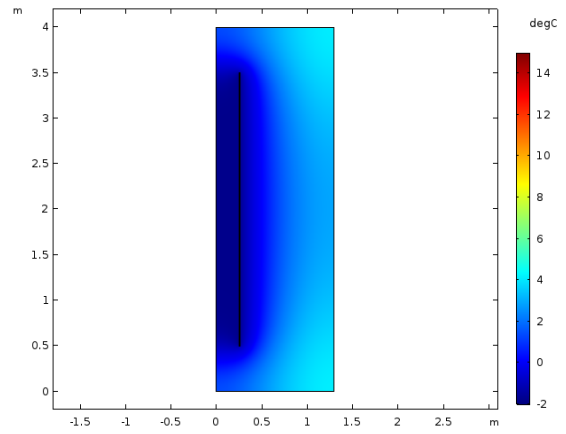
t = 80 days



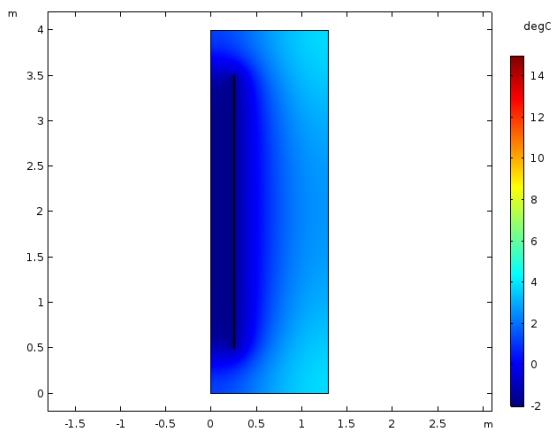
t = 84 days



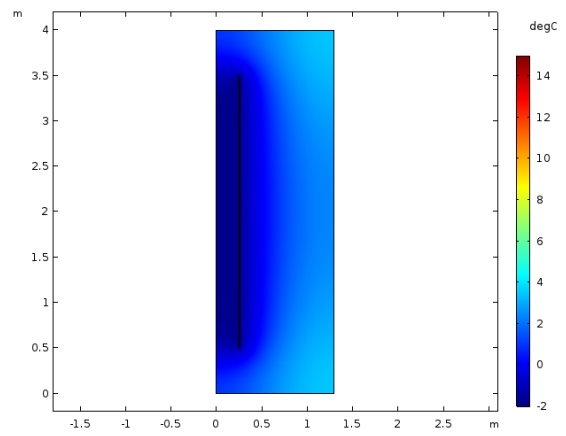
$t = 88$ days



$t = 92$ days



$t = 96$ days



$t = 100$ days

Appendix E

Derivation equation ice growing

In Chapter 6 is stated that the volume of ice in CFD-analysis can be approximated by two linear trend lines, which have an intersection at twelve days. In this appendix the intersection will be derived from the laws of thermodynamics (as shown in Equation (6.8) on Page 34). This will be done, according to Figure E.1. Starting with the one dimensional law for conduction in a cylinder:

$$Q(t) = 2\pi kL \frac{T(t) - T_\infty}{\ln(r_{out}/r_{in}(t))} \quad (\text{E.1})$$

And substituting $T^* = T(t) - T_\infty$ and $r_{in}(t) = \sqrt{\frac{vt}{\pi L}}$, the transient energy equation become:

$$\frac{dQ}{dt} = \frac{d}{dT} \left(2\pi kL \frac{T^*}{\ln(r_{out}) - \ln(\sqrt{\frac{v}{\pi L}}) - \ln(\sqrt{t})} \right) = q_{added} \quad (\text{E.2})$$

When rearranging and solving this equation:

$$dT^* = \frac{q_{added}}{2\pi kL} (\ln(r_{out}) - \ln(\sqrt{\frac{v}{\pi L}}) - \ln(\sqrt{t})) dt \quad (\text{E.3})$$

$$T(t) - T_\infty = \frac{q_{added}}{2\pi kL} \ln(r_{out} \sqrt{\frac{\pi L}{v}}) t - \frac{q_{added}}{2\pi kL} \frac{1}{2} t (\ln(t) - 1) + C \quad (\text{E.4})$$

At $t = 0$ the boundary condition $T(t) = 0$ is valid. Therefore $C = T_0 - T_\infty$.

$$\frac{T(t) - T_\infty}{T_0 - T_\infty} = \frac{q_{added}}{2\pi kL} (\ln(r_{out} \sqrt{\frac{\pi L}{v}}) t - \frac{1}{2} t (\ln(t) - 1)) \quad (\text{E.5})$$

When all the groundwater is frozen, $T(t)$ is equal to T_∞ , so:

$$0 = t (\ln(r_{out} \sqrt{\frac{\pi L}{v}}) - \frac{1}{2} (\ln(t) - 1)) \quad (\text{E.6})$$

After rewrite, the equation when all the ice is frozen become:

$$t = e^{\frac{\pi r_{out}^2 L}{v}} \quad (\text{E.7})$$

$$t = e^{\frac{\pi \cdot 0.255^2 \cdot 3}{0.2706/2}} = 12.3 \text{ day} \quad (\text{E.8})$$

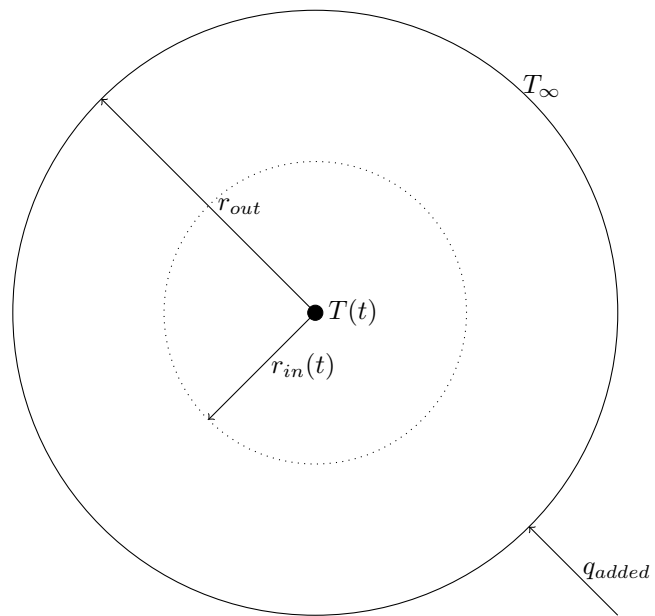


Figure E.1: Schematic representation of ice growing

Appendix F

Mesh convergence study CFD-analysis 2

The results of the mesh convergence study which is elaborated in Chapter 7, can be found in Table F.1. This mesh convergence study is performed in the same way as the mesh convergence study for analysis 1, which is elaborated in Chapter 4. This implies that mesh 1 has a minimum number of eight elements inside the cylinder, mesh 2 has a minimum number of ten elements inside the cylinder and mesh 3 has a minimum number of twelve elements inside the cylinder. From the results in Figure F.1, it can be concluded that the temperature almost immediately converges. For the velocity this is more difficult. Because mesh 2 and mesh 3 seems the same, there is chosen to use mesh 2 for simulating the results of analysis 2.

Table F.1: Mesh convergence study for analysis 2 – statistics

	Mesh 1	Mesh 2	Mesh 3
Min. size cylinder [m]	6.25e-4	5.00e-4	4.17e-4
Min. size ground [m]	0.2654	0.2123	0.1769
Min. element quality	0.05926	0.07638	0.06928
Avg. element quality	0.8885	0.8922	0.8933
Triangular element	896 189	1 158 736	1 417 383
Quadrilateral elements	38 698	48 300	57 898
Edge elements	10 059	12 470	14 877
Vertex elements	8	8	8

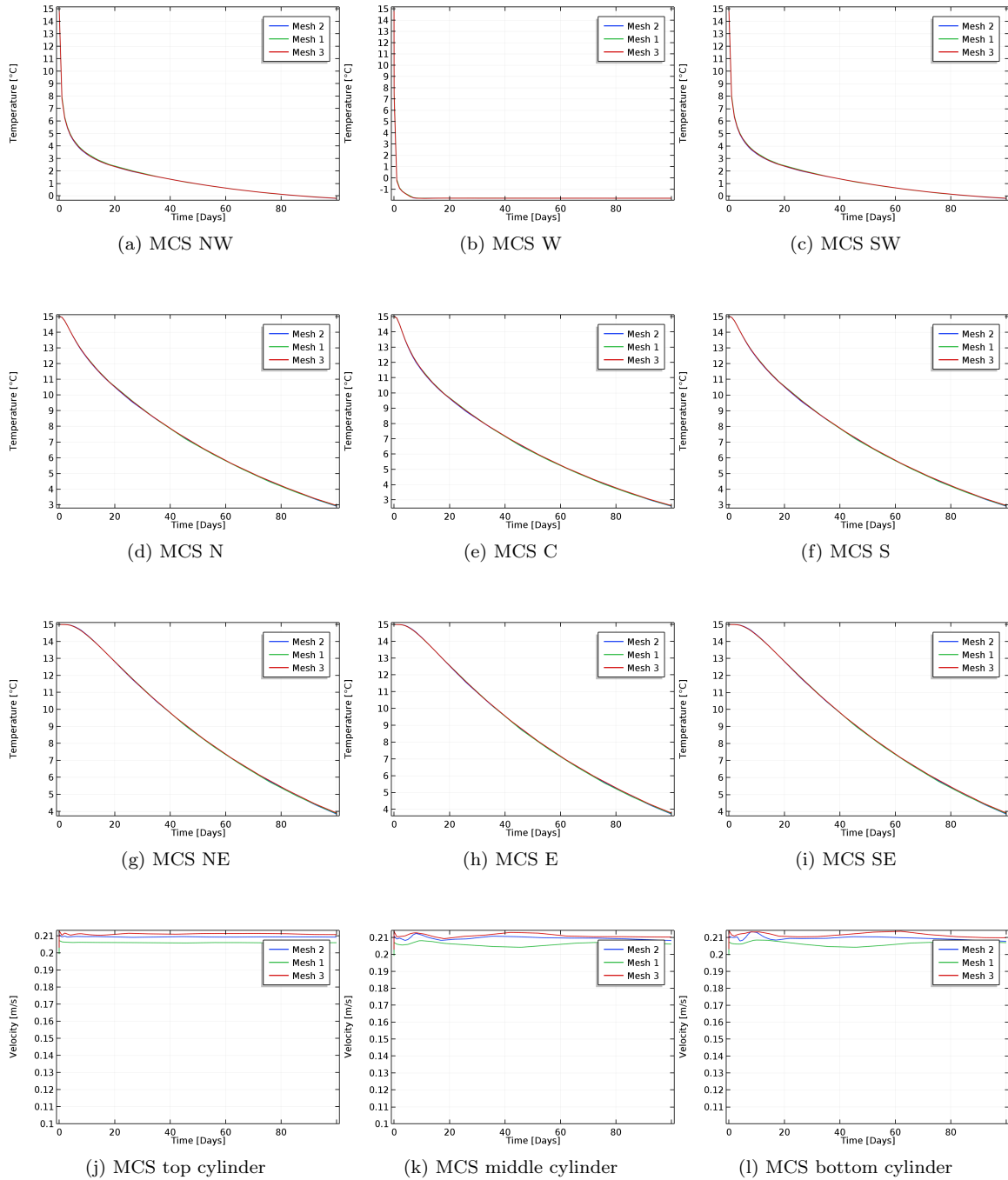
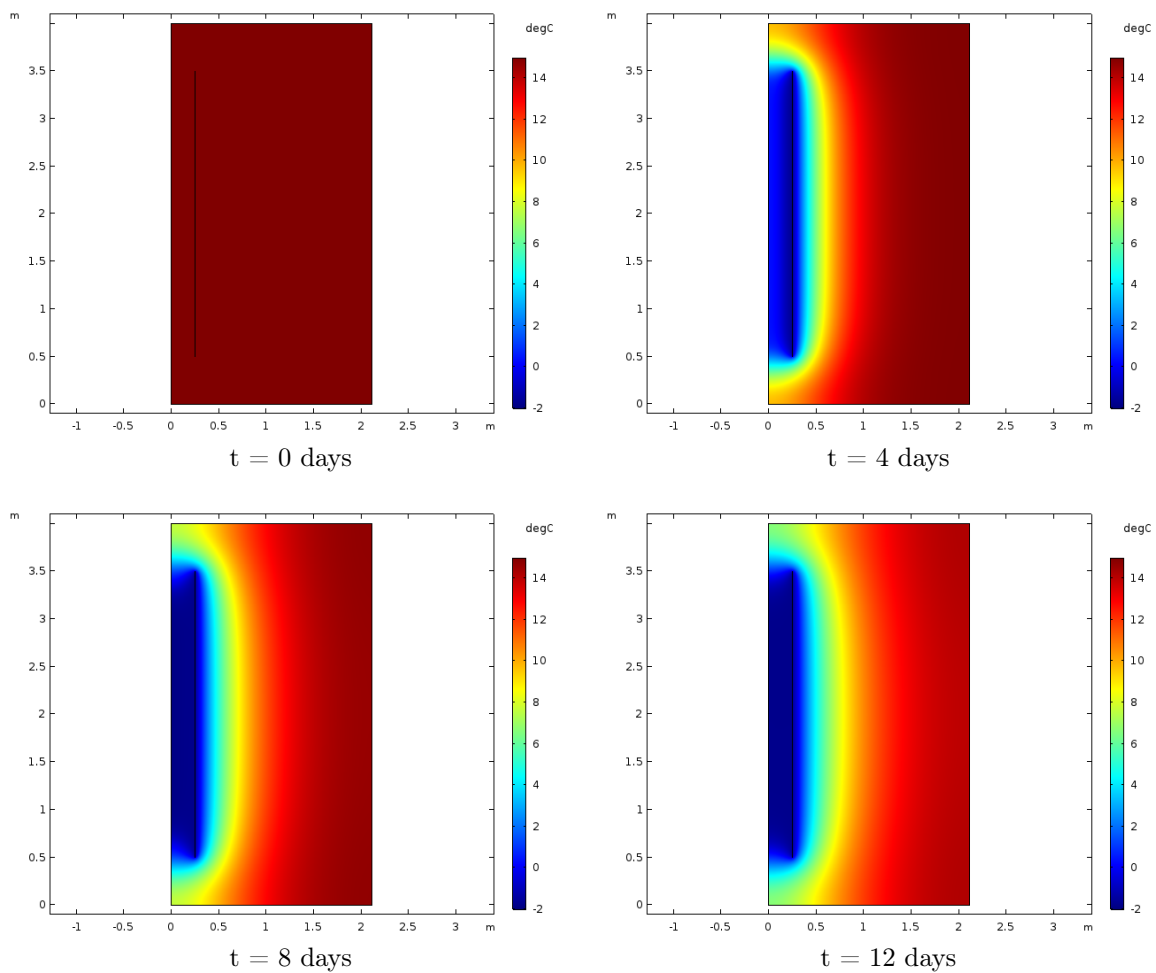


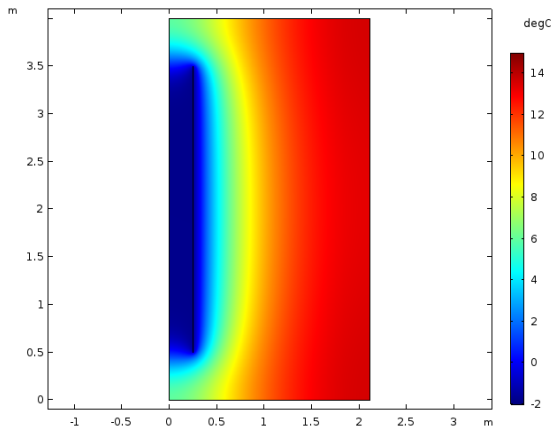
Figure F.1

Appendix G

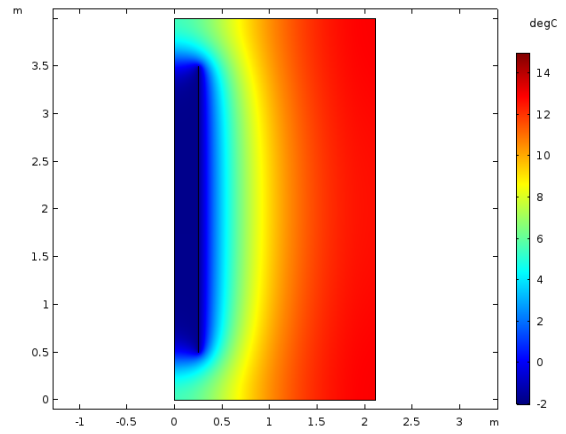
Temperature distribution CFD-analysis 2

In this appendix is the temperature evolution over time represented, for CFD-analysis 2 in Chapter 7.

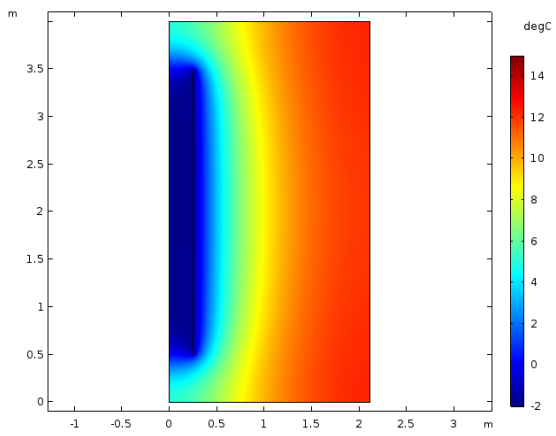




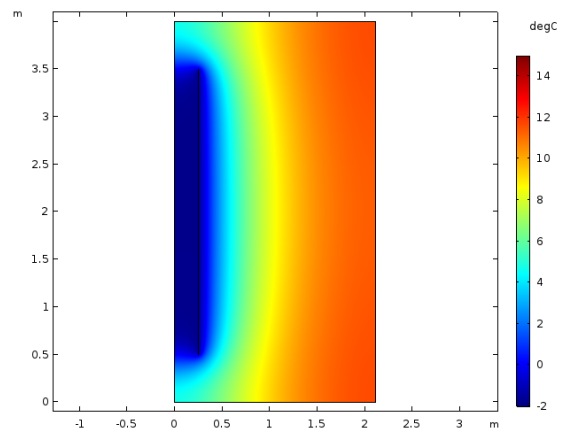
$t = 16$ days



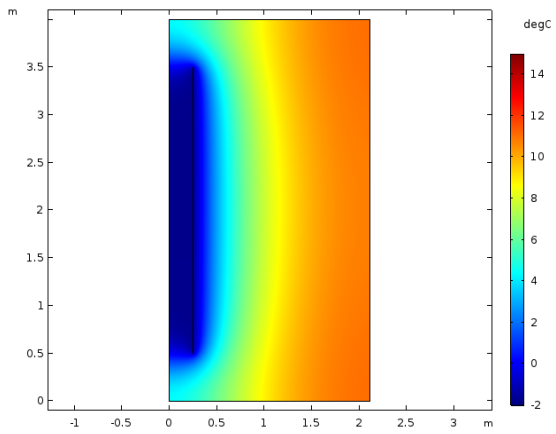
$t = 20$ days



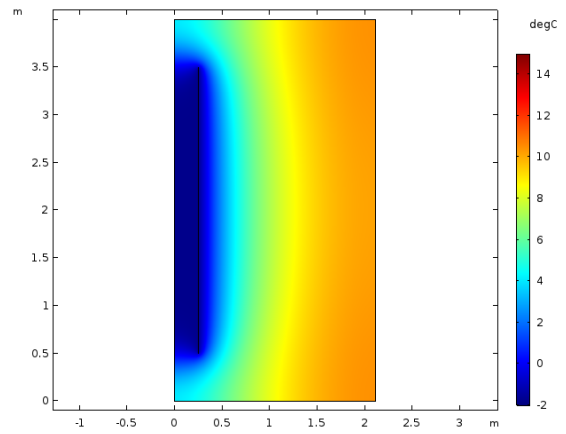
$t = 24$ days



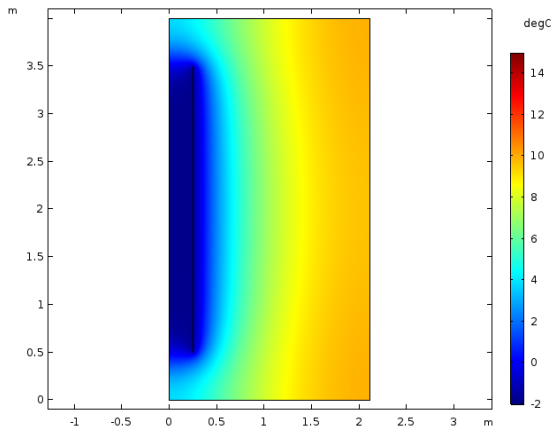
$t = 28$ days



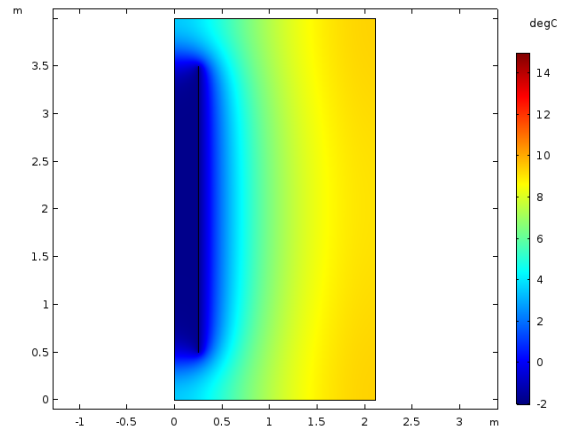
$t = 32$ days



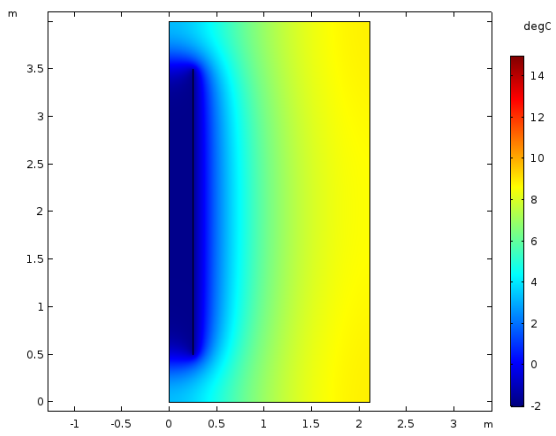
$t = 36$ days



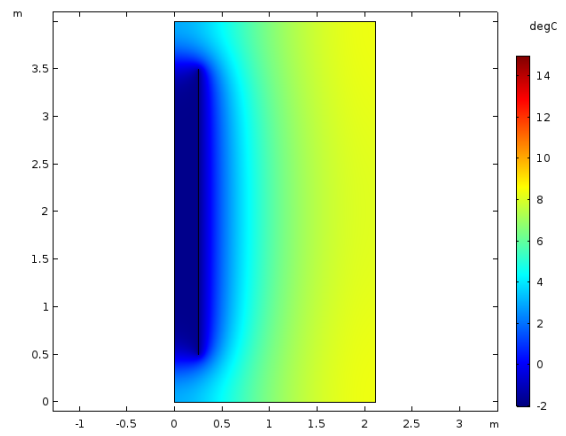
$t = 40$ days



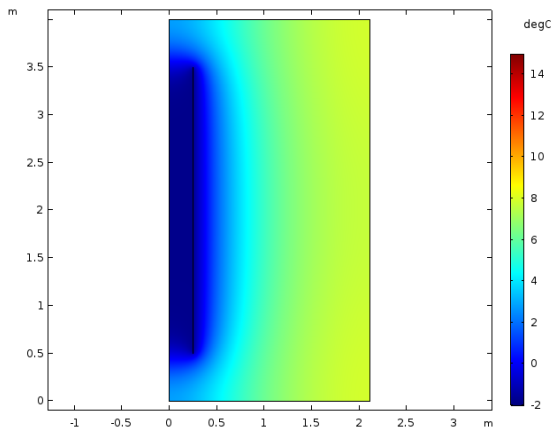
$t = 44$ days



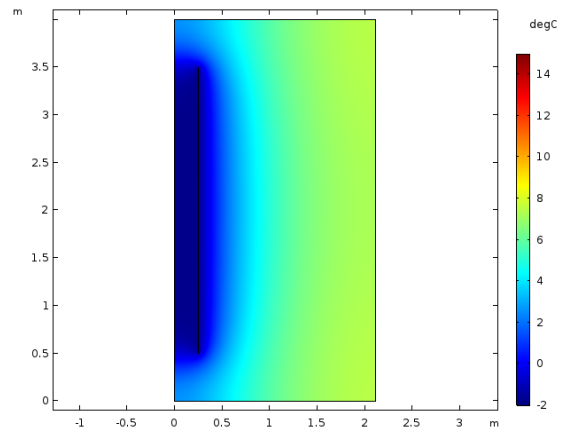
$t = 48$ days



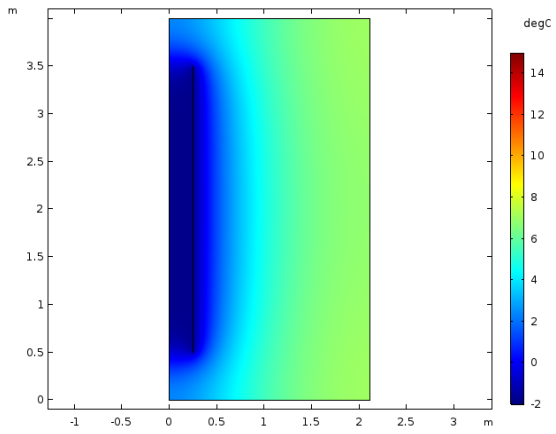
$t = 52$ days



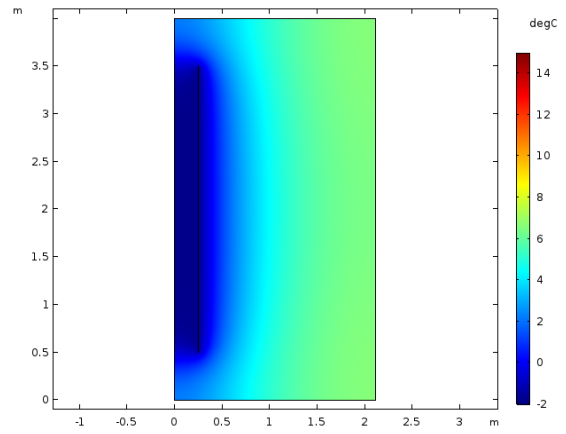
$t = 56$ days



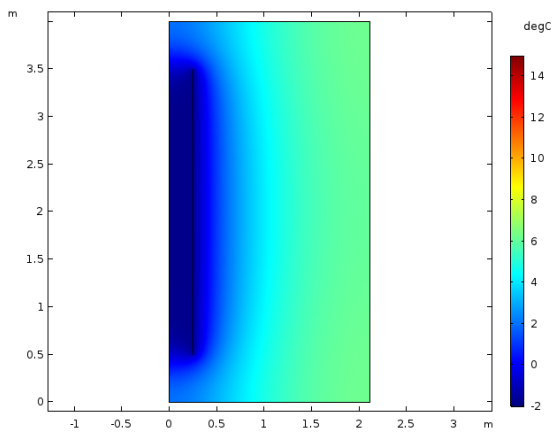
$t = 60$ days



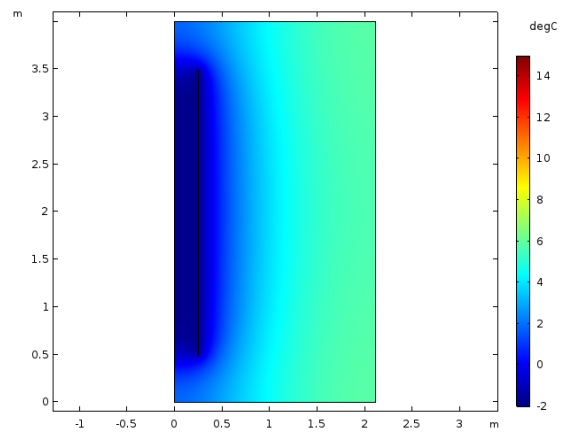
$t = 64$ days



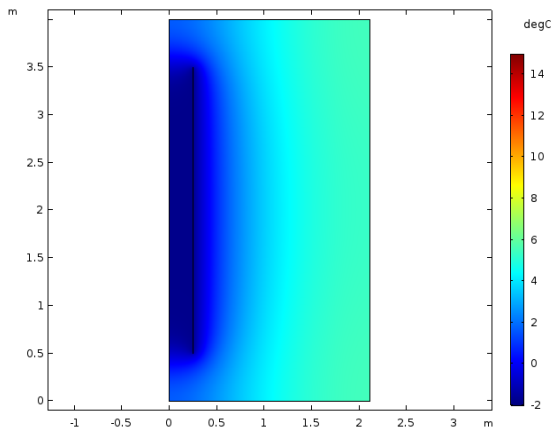
$t = 68$ days



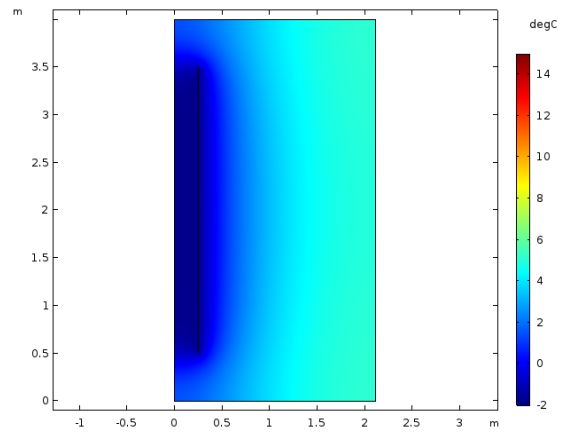
$t = 72$ days



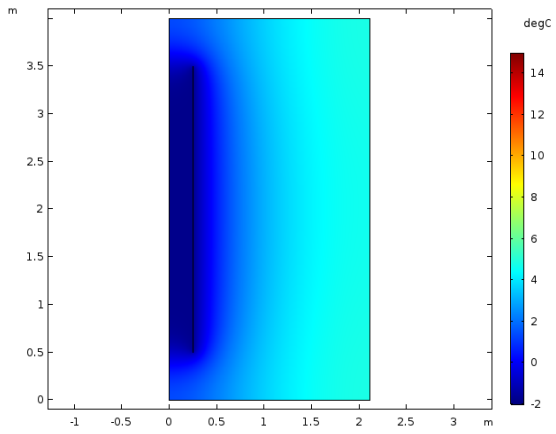
$t = 76$ days



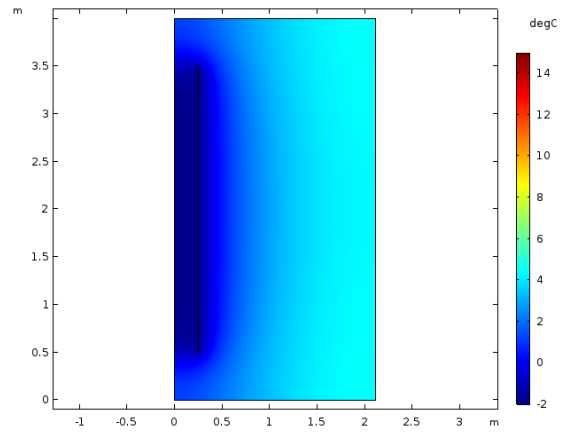
$t = 80$ days



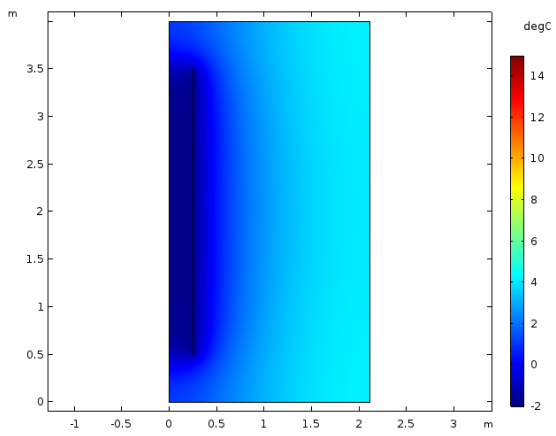
$t = 84$ days



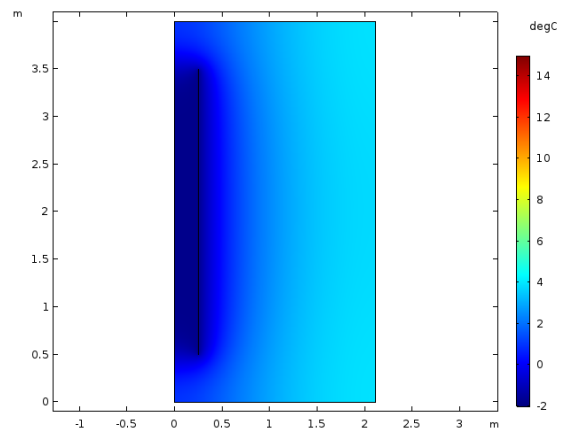
$t = 88$ days



$t = 92$ days



$t = 96$ days



$t = 100$ days

Appendix H

Derivation parametric study glycol mass flow

The derivation of the limit for the parametric study of the glycol mass flow in Equation (7.18) on Page 47 is starting with:

$$Q = mc_p(1 - e^{-\frac{UA}{mc_p}})(T_{ice} - T_{in}) \quad (\text{H.1})$$

When m is equal to x and Q equal to y (a and b are constants), this equation can be written to:

$$y(x) = c_p(T_{ice} - T_{in})x(1 - e^{-\frac{UA}{c_p}/x}) = ax(1 - e^{-b/x}) \quad (\text{H.2})$$

And when approaching $e^{-b/x}$ as a Taylor series at $x = \infty$:

$$e^{-b/x} = 1 - \frac{b}{x} + \frac{b^2}{2x^2} - \frac{b^3}{6x^3} + \mathcal{O}\left(\left(\frac{1}{x}\right)^4\right) \quad (\text{H.3})$$

The equation can be rewritten to:

$$y(x) = ab - \frac{ab^2}{2x} + \frac{ab^3}{6x^2} \quad (\text{H.4})$$

The result of letting the limit of x to infinity is:

$$y(x) = \lim_{x \rightarrow \infty} ab - \frac{ab^2}{2x} + \frac{ab^3}{6x^2} = ab \quad (\text{H.5})$$

When filling in the numbers of a, b and x , it can be concluded that:

$$Q(m) \approx c_p(T_{ice} - T_{in})\frac{UA}{c_p} \approx UA(T_{ice} - T_{in}) \quad (\text{H.6})$$

Appendix I

Mesh convergence study CFD-analysis 3

The results of the mesh convergence study which is elaborated in Chapter 8, can be found in Table I.1. This mesh convergence study is performed in the same way as the mesh convergence study for analysis 1 and 2, which are elaborated in Chapter 4. This implies that mesh 1 has a minimum number of six elements inside the cylinder, mesh 2 eight elements, mesh 3 ten elements and mesh 4 has a minimum number of twelve elements inside the cylinder. However there is an exception for this. In this way of building a mesh there is chosen to make the elements, inside the cylinder, ten times larger in the y-direction compare to the x-direction. This assumption is made, due to the fact the height of the cylinder is, in this model, significant larger compared to its radius (1400 times). When investigating the results in Figure I.1, it can be concluded that both the temperature and velocity converges very accurate. Because mesh 3 and mesh 4 are almost the same, there is chosen to use mesh 3 for simulating the results of analysis 3.

Table I.1: Mesh convergence study for analysis 3 – statistics

	Mesh 1	Mesh 2	Mesh 3	Mesh 4
Min. size cylinder [m]	8.33e-4	6.25e-4	5.00e-4	4.17e-4
Min. size ground [m]	0.95	0.7125	0.57	0.475
Min. element quality	0.01764	0.02618	0.02713	0.02650
Avg. element quality	0.5106	0.4334	0.3872	0.3711
Triangular element	42 158	56 531	85 171	114 214
Quadrilateral elements	11 560	15 424	19 288	23 150
Edge elements	3008	3993	4977	5958
Vertex elements	12	12	12	12

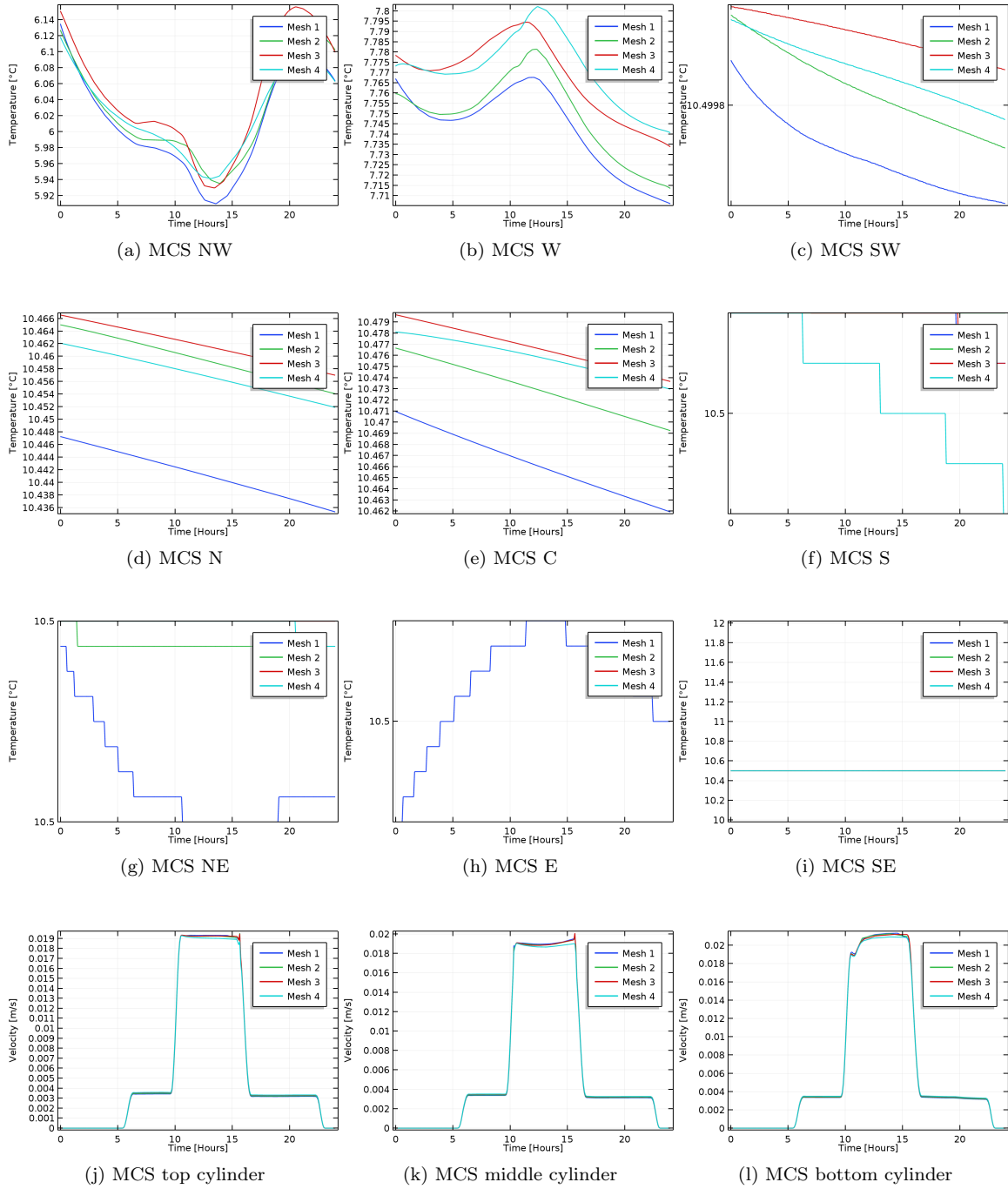
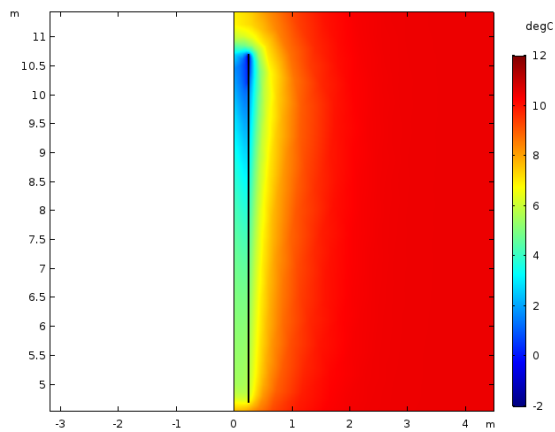


Figure I.1

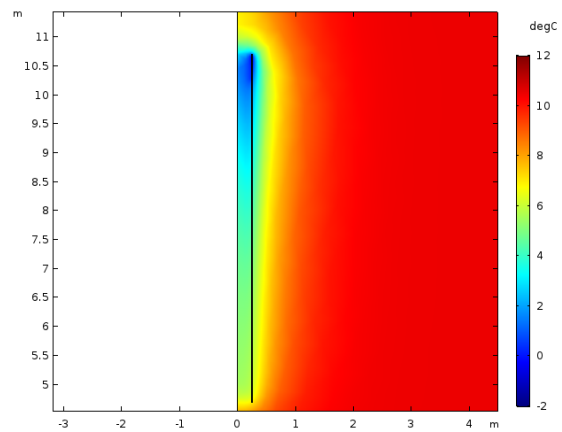
Appendix J

Temperature distribution CFD-analysis 3

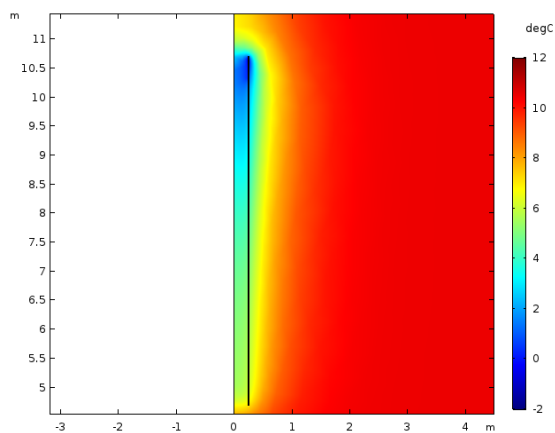
In this appendix is the temperature evolution over time represented, for CFD-analysis 3 in Chapter 8.



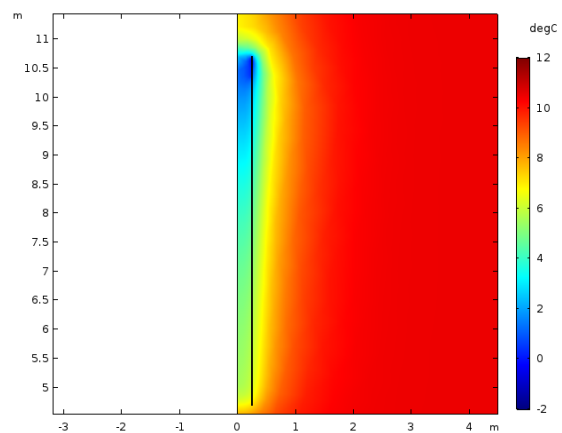
$t = 0$ hours



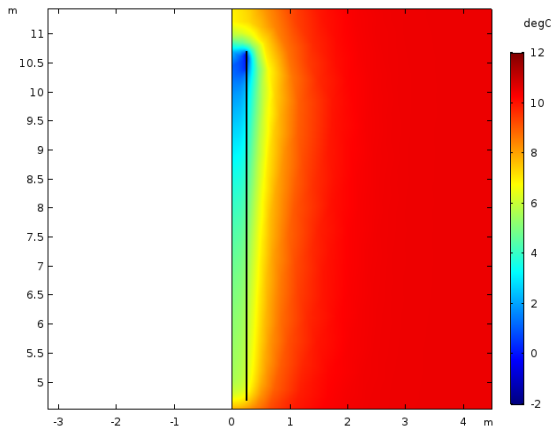
$t = 1$ hours



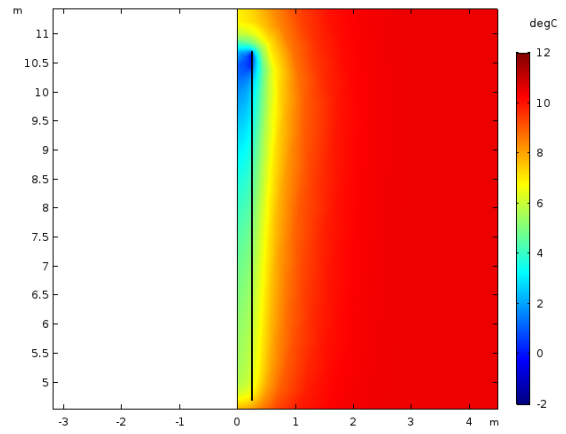
$t = 2$ hours



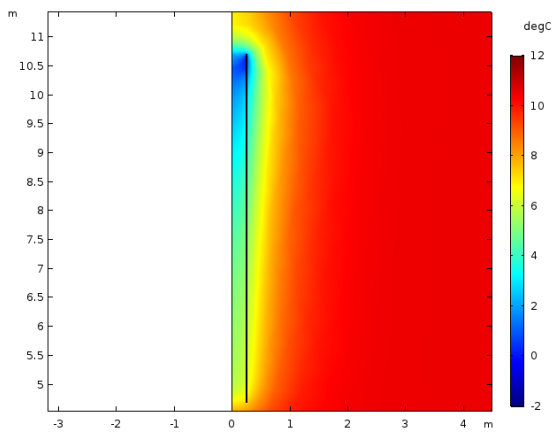
$t = 3$ hours



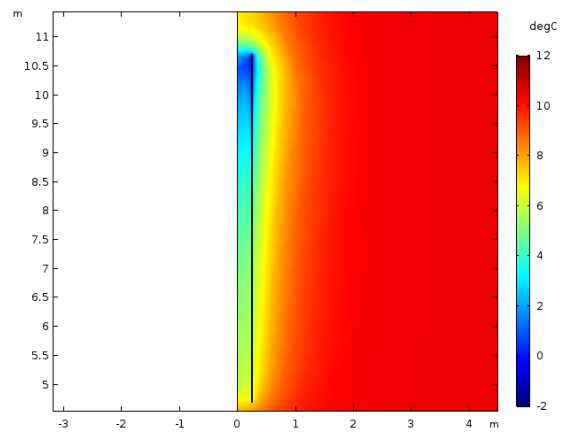
t = 4 hours



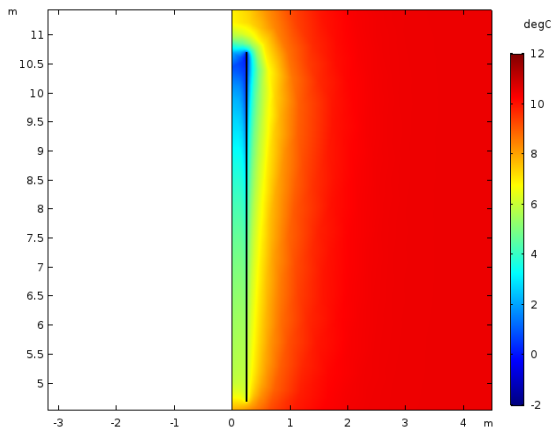
t = 5 hours



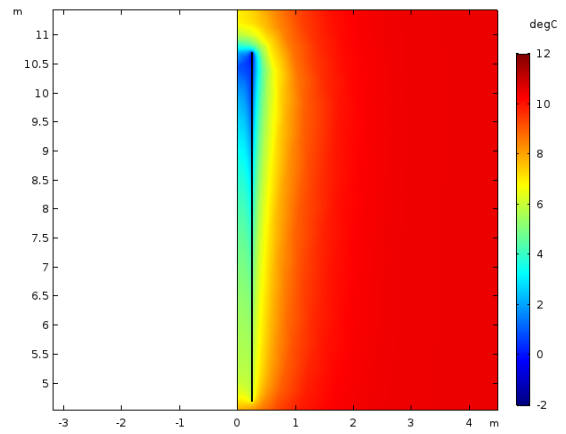
t = 6 hours



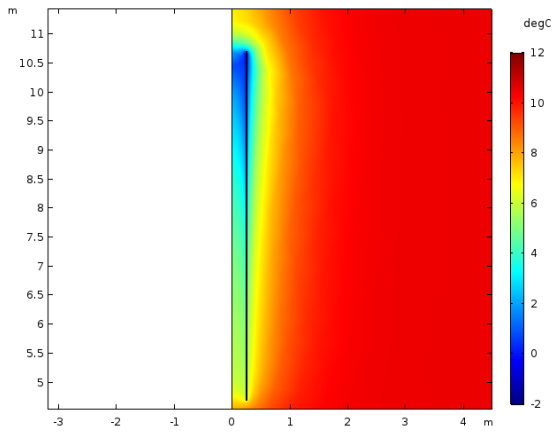
t = 7 hours



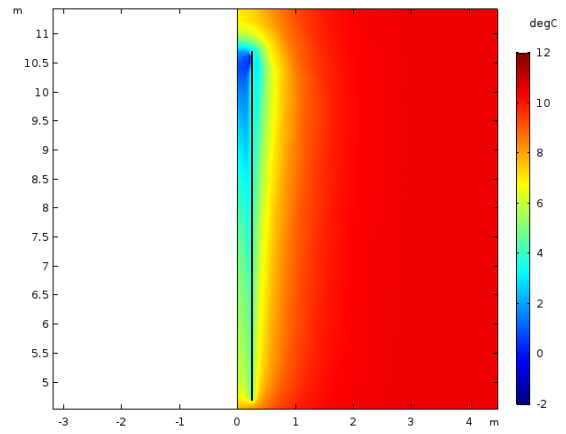
t = 8 hours



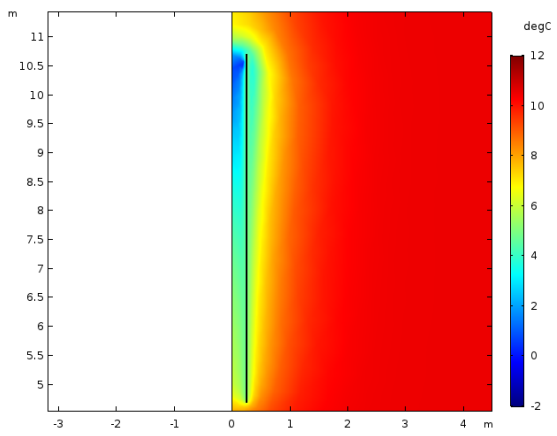
t = 9 hours



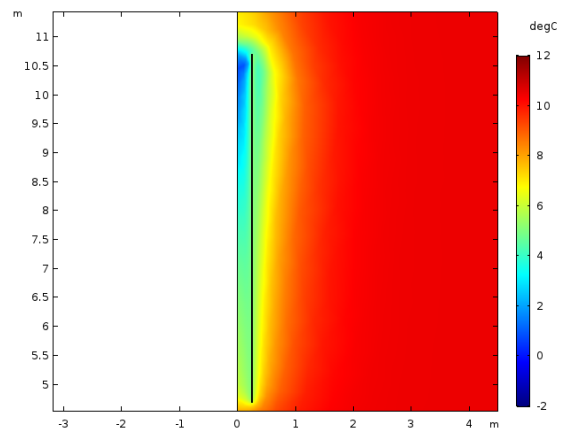
t = 10 hours



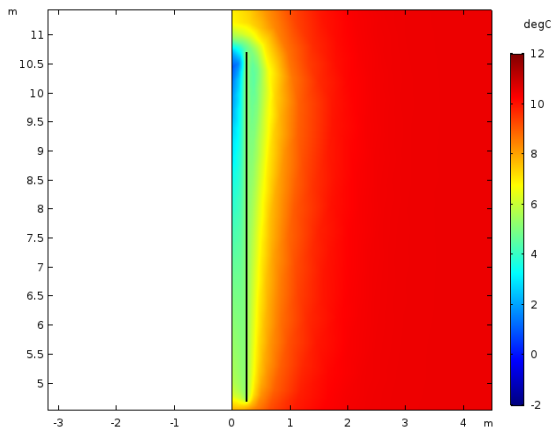
t = 11 hours



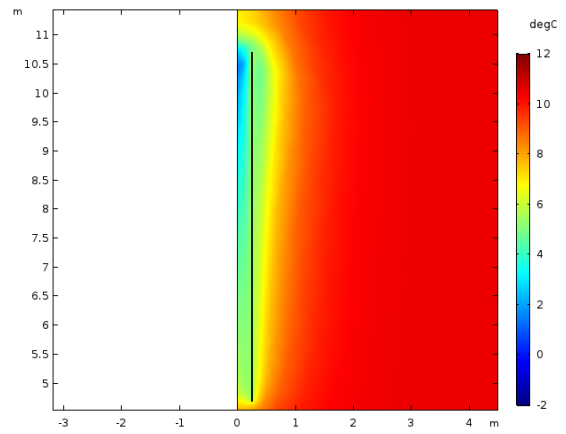
t = 12 hours



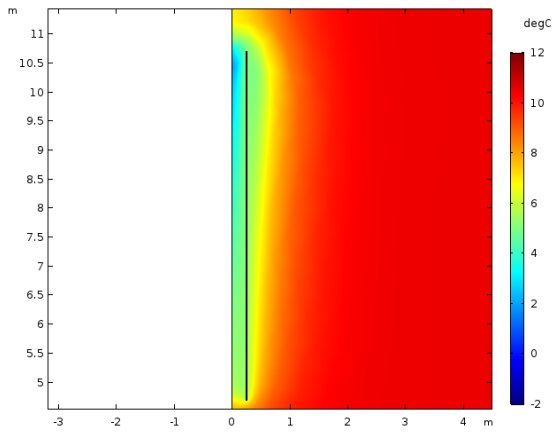
t = 13 hours



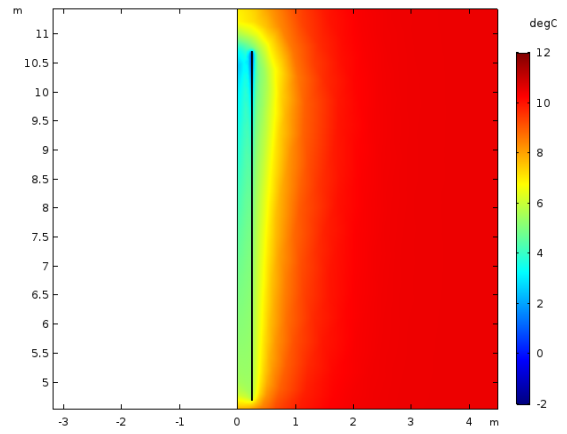
t = 14 hours



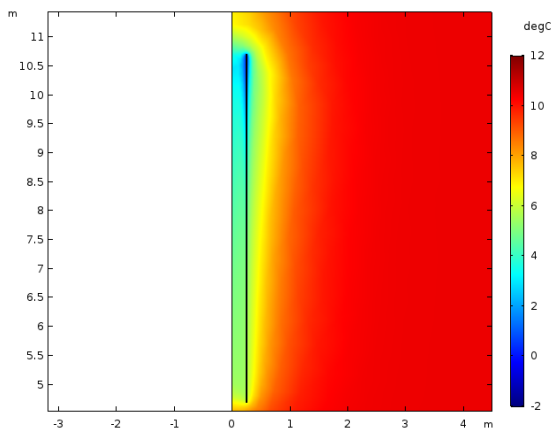
t = 15 hours



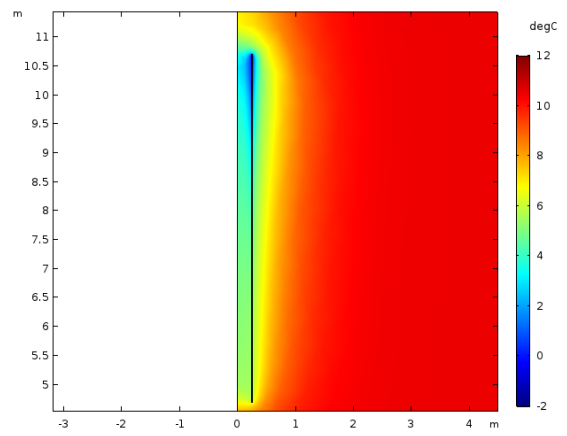
t = 16 hours



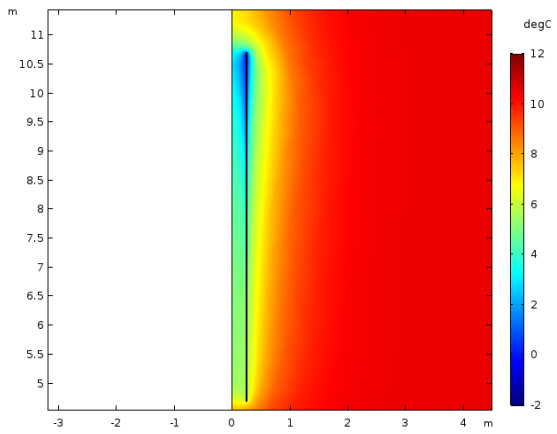
t = 17 hours



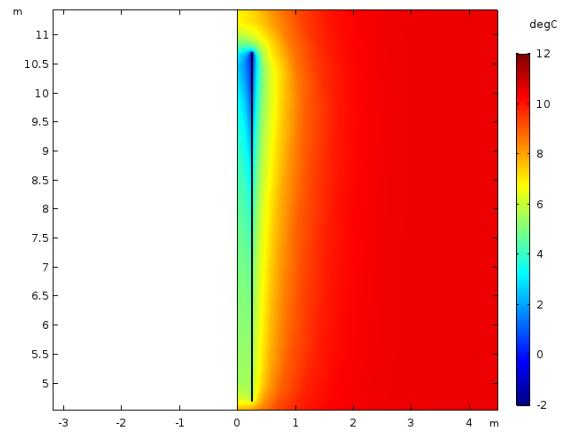
t = 18 hours



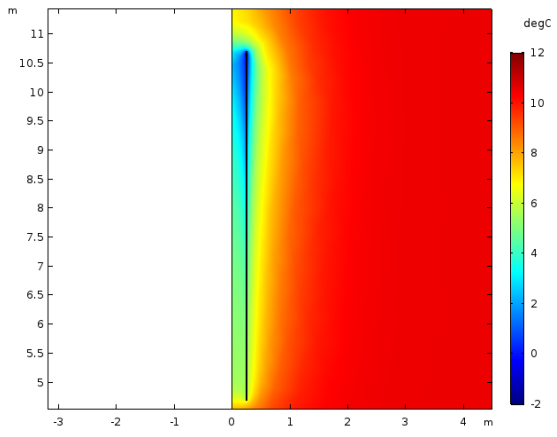
t = 19 hours



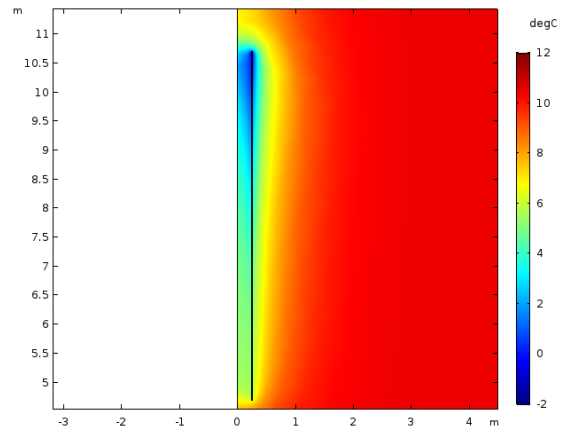
t = 20 hours



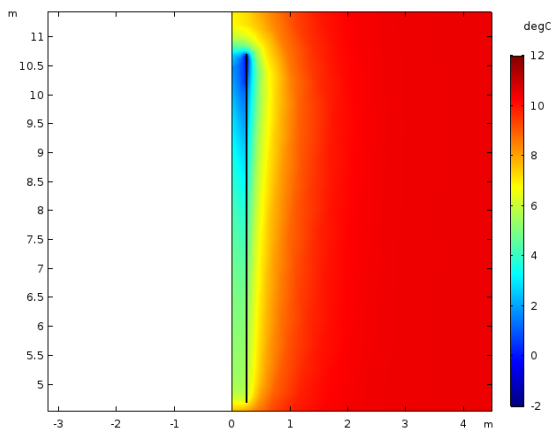
t = 21 hours



t = 22 hours



t = 23 hours

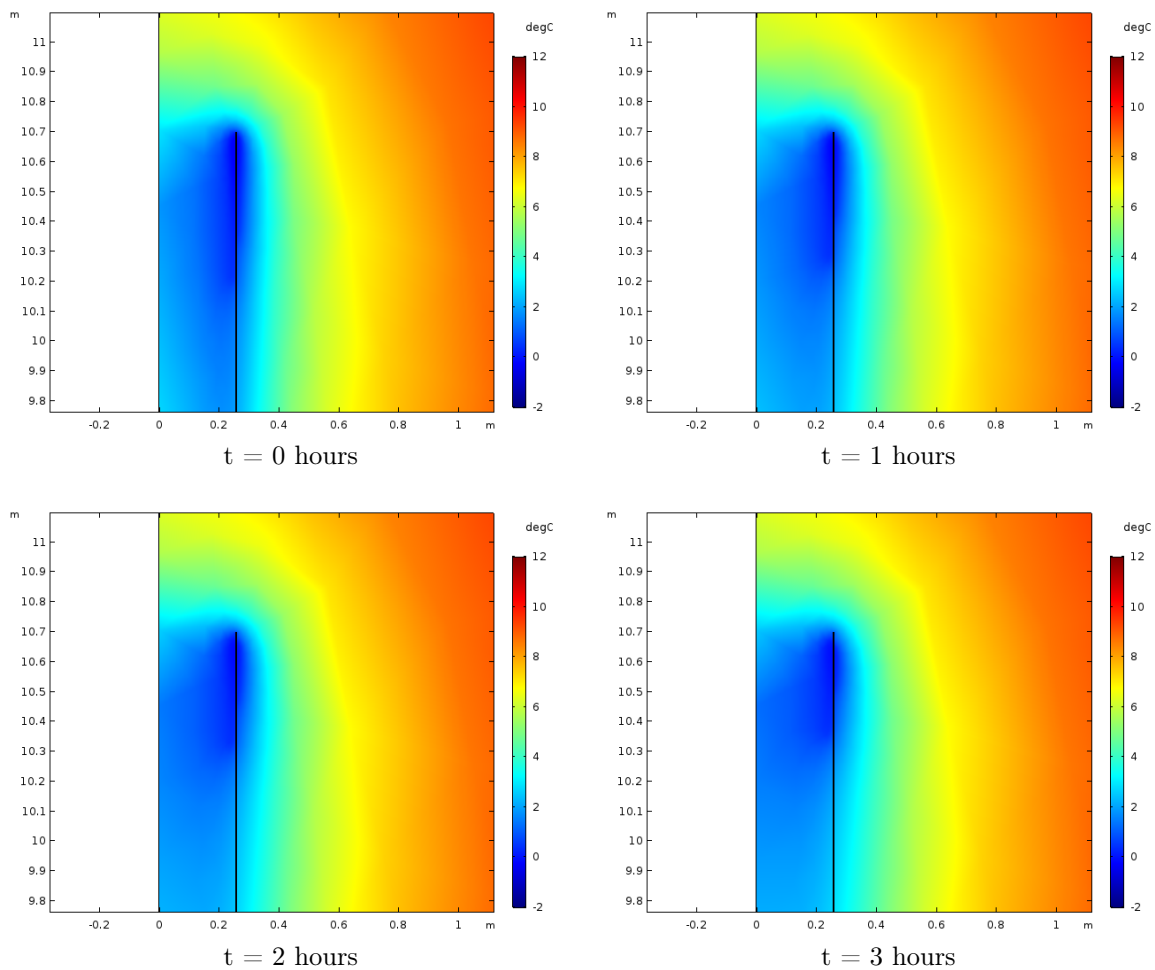


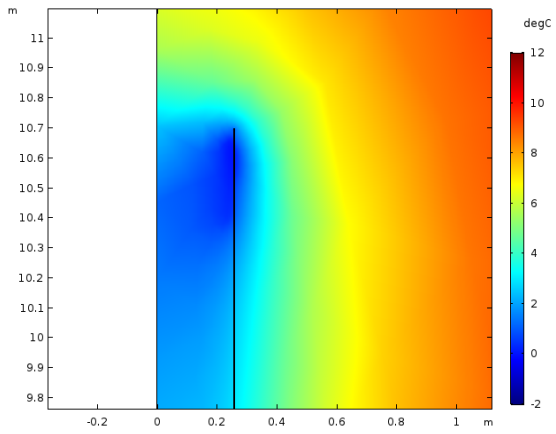
t = 24 hours

Appendix K

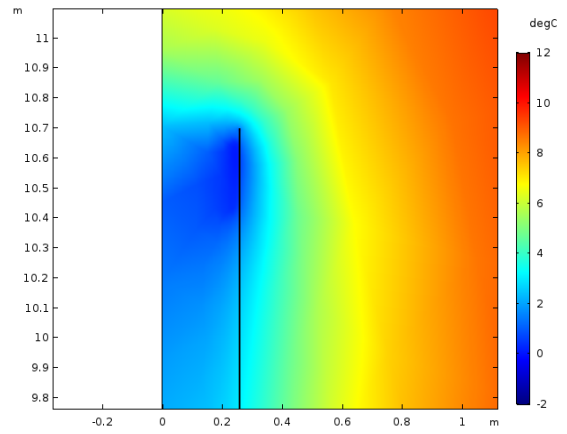
Temperature distribution CFD-analysis 3 (detailed)

In this appendix is the temperature evolution over time represented, for CFD-analysis 3 in Chapter 8.

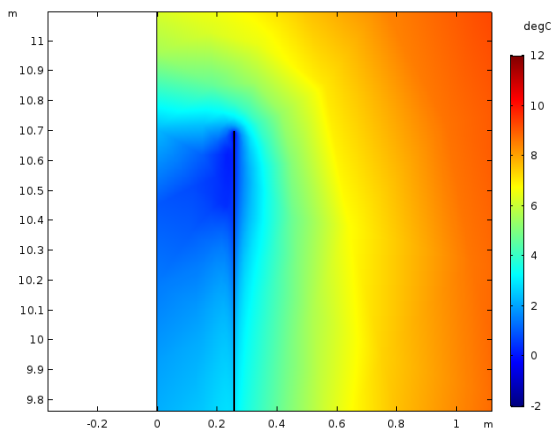




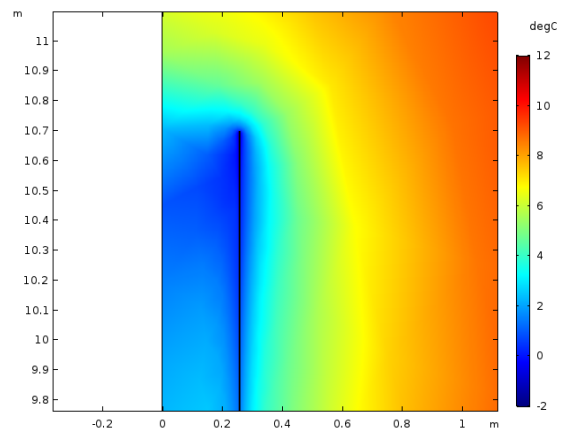
$t = 4$ hours



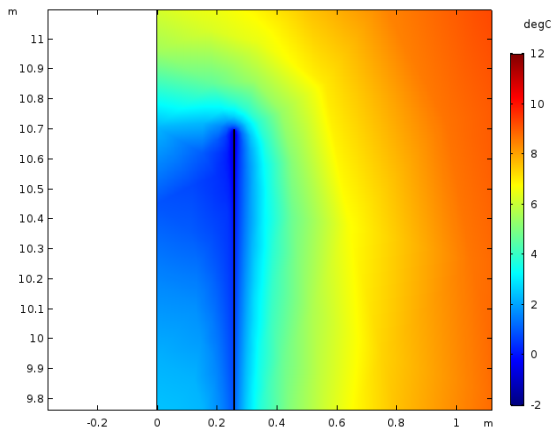
$t = 5$ hours



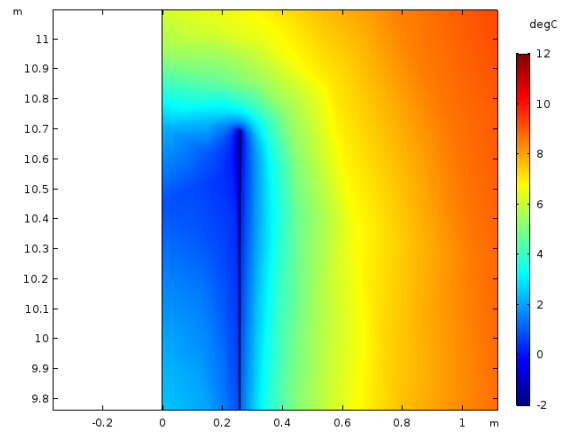
$t = 6$ hours



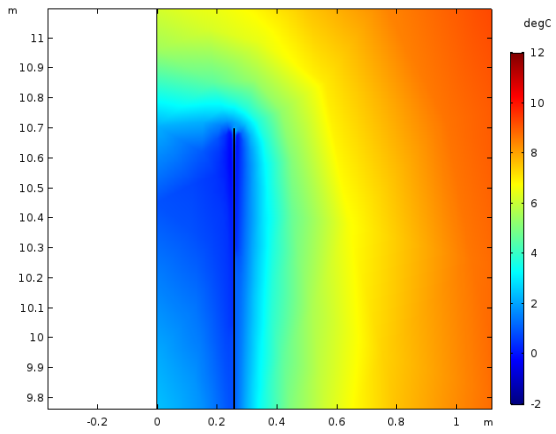
$t = 7$ hours



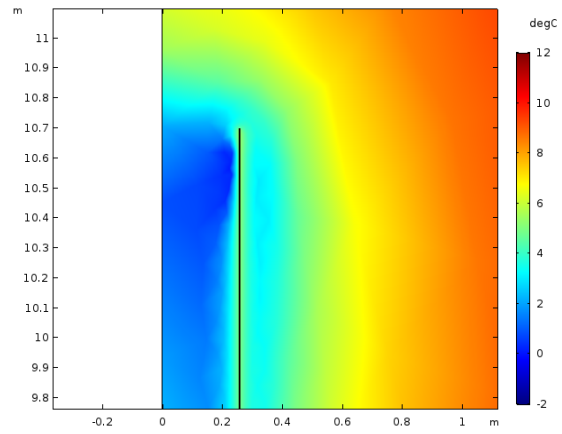
$t = 8$ hours



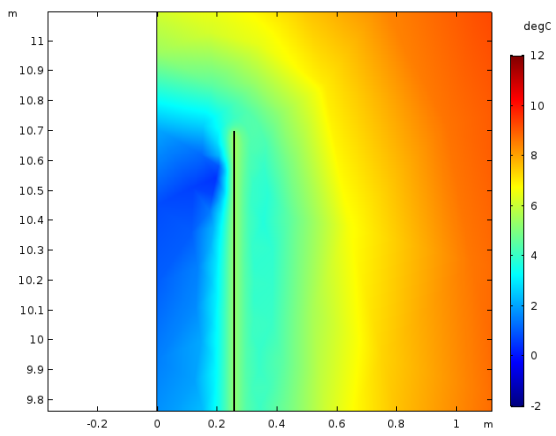
$t = 9$ hours



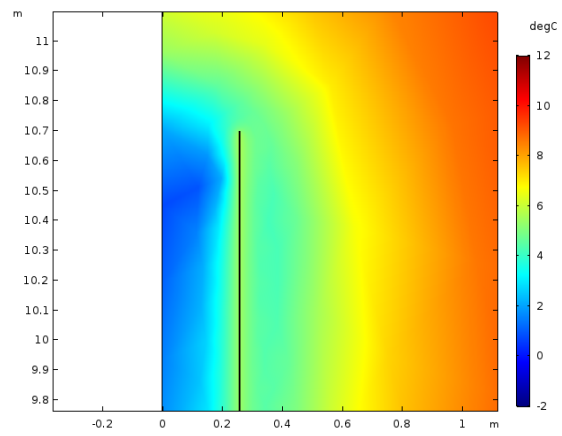
t = 10 hours



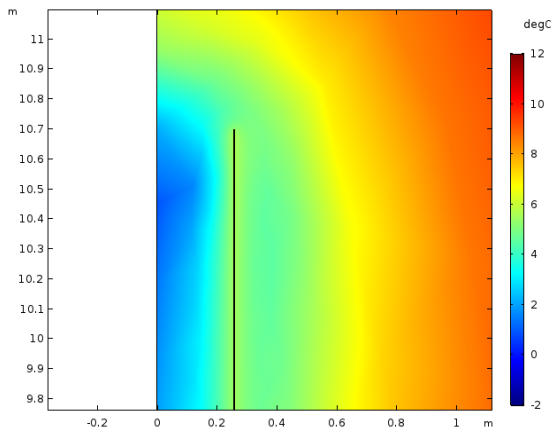
t = 11 hours



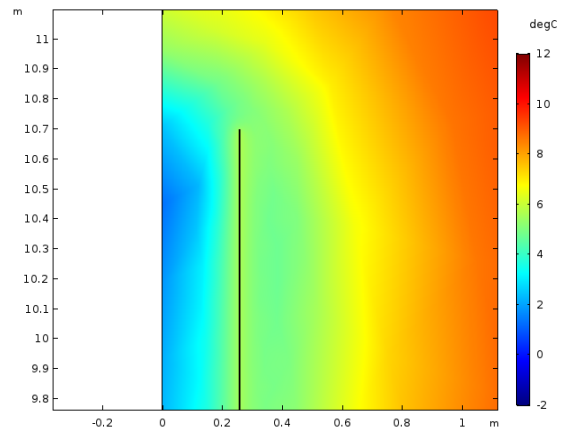
t = 12 hours



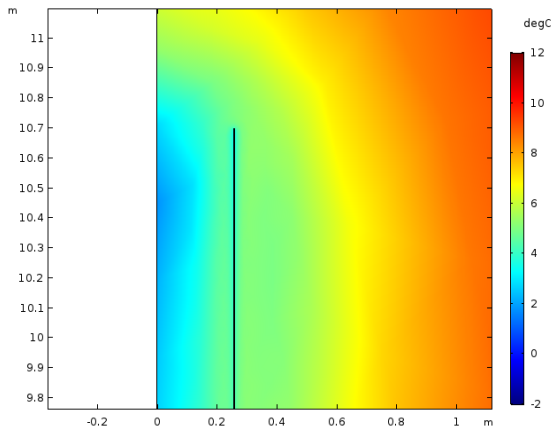
t = 13 hours



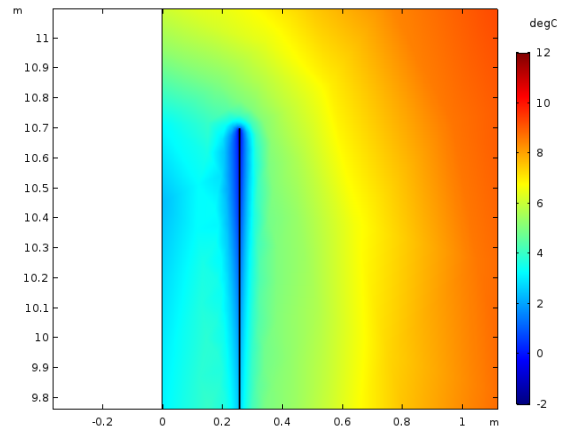
t = 14 hours



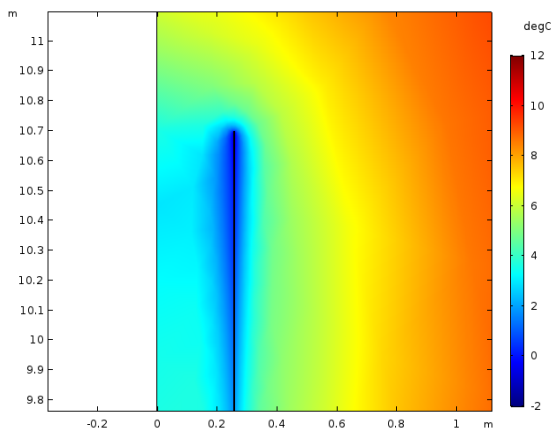
t = 15 hours



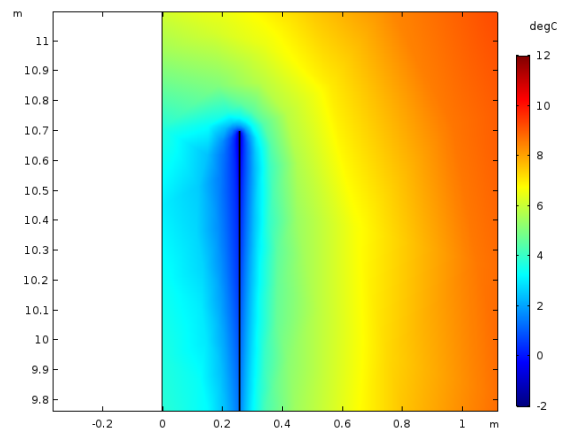
t = 16 hours



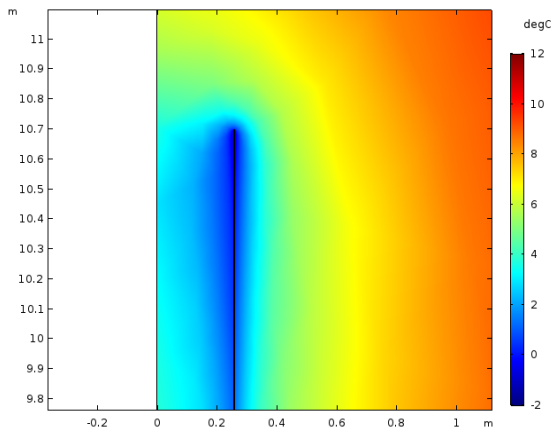
t = 17 hours



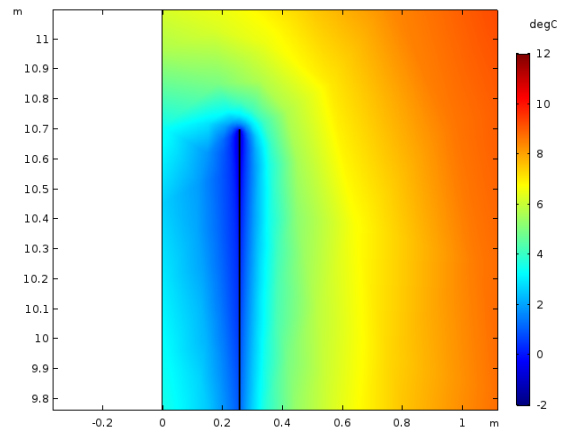
t = 18 hours



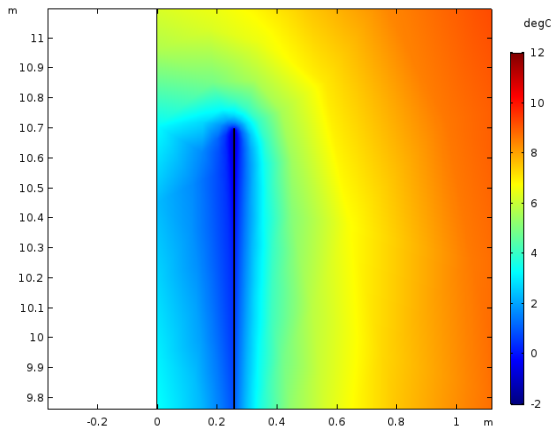
t = 19 hours



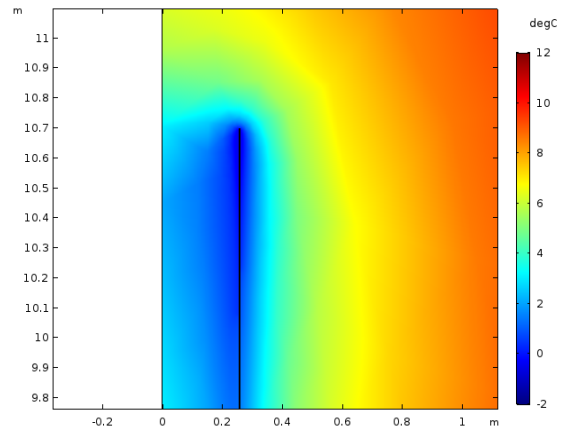
t = 20 hours



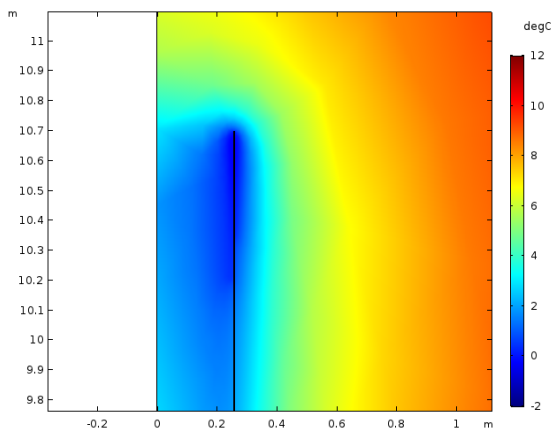
t = 21 hours



$t = 22$ hours



$t = 23$ hours



$t = 24$ hours

Appendix L

Derivation cylinder height

In Equation (8.9) on Page 59 it is assumed that the frozen ground layer at the top is the maximum ice thickness layer and the ice decreases linear. When deriving the volume of the frozen ground layer, this can be expressed as function of the height and the radius. A schematic representation of this problem can be found in Figure L.1. The derivation for calculating the volume of a geometric shape is:

$$V = \int \int \int r dz d\varphi dr$$

$\begin{aligned} \varphi = 0 &\rightarrow 2\pi \\ r = r_{out} &\rightarrow R \\ z = 0 &\rightarrow \frac{r-R}{r_{out}-R}h \end{aligned}$ $V = \int_{r_{out}}^R \int_0^{2\pi} \int_0^{\frac{r-R}{r_{out}-R}h} r dz d\varphi dr$ $V = \int_{r_{out}}^R \int_0^{2\pi} [rz]_0^{\frac{r-R}{r_{out}-R}h} d\varphi dr$ $V = \int_{r_{out}}^R \int_0^{2\pi} r \frac{r-R}{r_{out}-R} h d\varphi dr$ $V = \int_{r_{out}}^R [r \frac{r-R}{r_{out}-R} h \varphi]_0^{2\pi} dr$ $V = \int_{r_{out}}^R 2\pi h r \frac{r-R}{r_{out}-R} dr$ $V = \frac{2\pi h}{r_{out}-R} \int_{r_{out}}^R (r^2 - Rr) dr$ $V = \frac{2\pi h}{r_{out}-R} [\frac{r^3}{3} - \frac{Rr^2}{2}]_{r_{out}}^R$ $V = \frac{2\pi h}{r_{out}-R} (\frac{R^3}{3} - \frac{R^3}{2} - \frac{r_{out}^3}{3} + \frac{Rr_{out}^2}{2})$ $V = \frac{1}{3}\pi h (R - r_{out})(R + 2r_{out})$	$\begin{aligned} \varphi = 0 &\rightarrow 2\pi \\ r = R' &\rightarrow r_{in} \\ z = 0 &\rightarrow \frac{r-R'}{r_{in}-R'}h \end{aligned}$ $V = \int_{R'}^{r_{in}} \int_0^{2\pi} \int_0^{\frac{r-R'}{r_{in}-R'}h} r dz d\varphi dr$ $V = \int_{R'}^{r_{in}} \int_0^{2\pi} [rz]_0^{\frac{r-R'}{r_{in}-R'}h} d\varphi dr$ $V = \int_{R'}^{r_{in}} \int_0^{2\pi} r \frac{r-R'}{r_{in}-R'} h d\varphi dr$ $V = \int_{R'}^{r_{in}} [r \frac{r-R'}{r_{in}-R'} h \varphi]_0^{2\pi} dr$ $V = \int_{R'}^{r_{in}} 2\pi h r \frac{r-R'}{r_{in}-R'} dr$ $V = \frac{2\pi h}{r_{in}-R'} \int_{R'}^{r_{in}} (r^2 - R'r) dr$ $V = \frac{2\pi h}{r_{in}-R'} [\frac{r^3}{3} - \frac{R'r^2}{2}]_{R'}^{r_{in}}$ $V = \frac{2\pi h}{r_{in}-R'} (\frac{r_{in}^3}{3} - \frac{R'r_{in}^2}{2} - \frac{R'^3}{3} + \frac{R'R'^2}{2})$ $V = \frac{1}{3}\pi h (r_{in} - R')(2r_{in} + R')$
$V_{total} = V_{out} + V_{in}$ $V_{total} = \frac{1}{3}\pi h ((R - r_{out})(R + 2r_{out}) + (r_{in} - R')(2r_{in} + R'))$ $h = \frac{3V_{total}}{\pi((R - r_{out})(R + 2r_{out}) + (r_{in} - R')(2r_{in} + R'))}$	

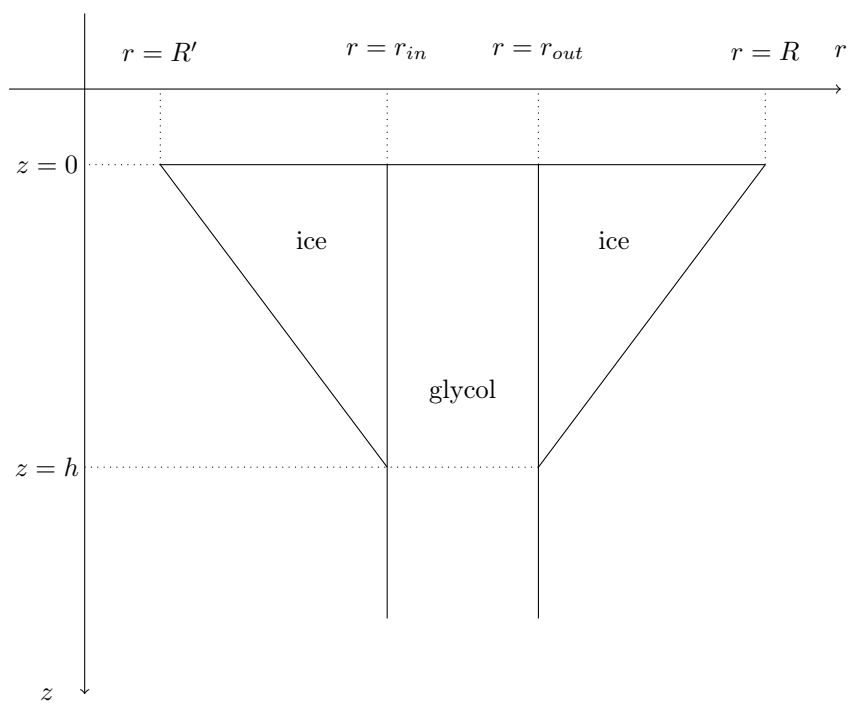


Figure L.1: Schematic representation of ice forming